KTH Engineering Sciences

Modeling and Data Analysis in Cellular Biophysics

Jacob Kowalewski

Doctoral Thesis
Cell Physics, Department of Applied Physics
Royal Institute of Technology
Stockholm, Sweden 2009

TRITA-FYS 2009:60
ISSN 0280-316X
ISRN KTH/FYS/--09:60--SE
ISBN 978-91-7415-492-4

KTH AlbaNova University Center
Cell Physics
SE-106 91 Stockholm
SWEDEN

Akademisk avhandling som med tillstånd av Kungl Tekniska högskolan framlägges till offentlig granskning för avläggande av teknologie doktorsexamen i biologisk fysik fredagen den 20 november 2009 klockan 13.00 i FD5, AlbaNova Universitetscentrum, Roslagstullsbacken 21, Stockholm.

Tryck: Universitetsservice US AB

Abstract

Cellular biophysics deals with the physical aspects of cell biology. This thesis presents a number of studies where mathematical models and data analysis can increase our understanding of this field.

During recent years development in experimental methods and mathematical modeling have driven the amount of data and complexity in our understanding of cellular biology to a new level. This development has made it possible to describe cellular systems quantitatively where only qualitative descriptions were previously possible. To deal with the complex data and models that arise in this kind of research a combination of tools from physics and cell biology has to be applied; this constitutes a field we call cellular biophysics. The aim of this doctoral thesis is to develop novel approaches in this field. I present eight studies where quantitative modeling and analysis are involved.

The first two studies concern cells interacting with their surrounding environment in the kidney. These cells sense fluid flow and respond with calcium (Ca^{2+}) signals. The interaction between fluid and cells in renal tubular epithelium can be described by biomechanical models. This thesis describes a mathematical model of flow sensing by cilia with focus on the flow frequency response and time delay between the mechanical stress and the Ca^{2+} signaling response.

Intracellular Ca^{2+} is kept at a very low level compared to the extracellular environment, while several intracellular compartments have higher Ca^{2+} concentration than the cytoplasm. This makes Ca^{2+} an efficient messenger for intracellular signaling, the process whereby signals are transduced from an extracellular stimulus to an intracellular activity such as gene expression. An important type of Ca^{2+} signaling is oscillations in intracellular Ca^{2+} concentration which occur due to the concerted interplay between different transport mechanisms within a cell. A study in this thesis examines ways to explain these mechanisms in terms of a mathematical model. Another study in the thesis reports that erythropoietin can regulate the water permeability of astrocytes and that it alters the pattern of Ca^{2+} oscillations in astrocytes. In this thesis the analysis of this Ca^{2+} signaling is described.

Simulations described in one of the studies show how different geometries can affect the fluorescence recovery and that geometrically constrained reactions can trap diffusing receptors in dendritic spines. When separate time scales are present in a fluorescence revovery after photobleaching (FRAP) experiment the reaction and diffusion components can be studied separately.

Applying single particle tracking methods to the migration trajectories of natural killer cells shows that there is a correlation between the formation of conjugates and transient confinement zones (TCZs) in these trajectories in vitro. TCZs are also present in *in vivo* experiments where they show strong similarities with the *in vitro* situation. This approach is a novel concept in data analysis methods for tracking immune cells.

Sammanfattning (in Swedish)

Cellens biologiska fysik behandlar de fysikaliska aspekterna av cellbiologi. Denna avhandling presenterar ett antal studier där matematiska modeller och dataanalys kan öka vår förståelse av detta område.

Under senare år har utvecklingen av experimentella metoder och matematisk modellering drivit mängden data och komplexiteten i vår förståelse av cellbiologi till en ny nivå. Denna utveckling har gjort det möjligt att beskriva cellulära system kvantitativt där endast kvalitativa beskrivningar tidigare var möjliga. För att hantera de komplexa data och modeller som uppstår i denna typ av forskning krävs en kombination av verktyg från fysik och cellbiologi; detta utgör ett område vi kallar cellens biologiska fysik. Syftet med denna avhandling är att utveckla nya metoder inom detta område. Jag presenterar åtta studier där kvantitativ modellering och analys ingår.

De första två studierna behandlar hur celler interagerar med sin omgivning i njurarna. Dessa celler känner av ett vätskeflöde och svarar med kalcium (Ca^{2+})-signaler. Samspelet mellan vätska och celler i tubulärt njurepitel kan beskrivas med biomekaniska modeller. Denna avhandling beskriver en matematisk modell för flödeskänslighet hos cilier med fokus på flödesfrekvenssvar och tidsfördröjningen mellan den mekaniska påverkan och Ca^{2+}-signaleringssvaret.

Intracellulärt Ca^{2+} hålls på en mycket låg nivå jämfört med den extracellulära miljön, samtidigt som flera intracellulära delar har högre Ca^{2+}-koncentrationen än cytoplasman. Detta gör Ca^{2+} till en effektiv bärare för intracellulär signalering, den process där signaler överförs från ett extracellulärt stimuli till en intracellulär händelse, exempelvis genuttryck. En viktig typ av Ca^{2+}-signalering är de oscillationer i intracellulär Ca^{2+}-koncentration som uppstår på grund av det ordnade samspelet mellan olika transportmekanismer i en cell. En studie i denna avhandling undersöker olika sätt att förklara dessa mekanismer i form av en matematisk modell. En annan studie i avhandlingen rapporterar att erytropoietin kan reglera vattenpermeabilitet av astrocyter och att det ändrar mönstret av Ca^{2+}-oscillationer i astrocyter. I denna avhandling beskrivs analysen av denna Ca^{2+}-signalering.

Simuleringar som beskrivs i en av studierna visar hur olika geometrier kan påverka fluorescensåterhämtning och att geometriskt begränsade reaktioner kan fånga in receptorer in i dendrittaggar. När separata tidsskalor förekommer i ett *fluorescence revovery after photobleaching* (FRAP)-experiment kan reaktions- och diffusionskomponenter studeras separat.

Tillämpande av *single particle tracking*-metoder på naturliga mördarceller visar att det finns ett samband mellan bildandet av konjugat och *transient confinement zones* (TCZs) i dessa trajektorier *in vitro*. TCZs förekommer också i *in vivo-experiment* där de visar stora likheter med *in vitro*-situationen. Denna strategi är ett nytt grepp inom dataanalys-metoder för att spåra immunceller.

Contents

Papers

This thesis is based on the following publications that will be referred to by their roman numerals:

I. Rydholm, S., T. Frisk, J. M. Kowalewski, H. Andersson Svahn, G. Stemme, and H. Brismar. 2008. *Microfluidic devices for studies of primary cilium mediated cellular response to dynamic flow conditions*. Biomed Microdevices **10**(4): p. 555-60.

II. Rydholm, S., G. Zwartz, J M. Kowalewski, P. Kamali-Zare, T. Frisk, and H. Brismar. *Mechanical Properties of Primary Cilia Regulate the Response to Fluid Flow.* **Manuscript**.

III. Kowalewski, J. M., P. Uhlén,., H. Kitano, and H. Brismar, *Modeling the impact of store-operated Ca^{2+} entry on intracellular Ca^{2+} oscillations.* Mathematical Biosciences, 2006. **204**(2): p. 232–249.

IV. Gunnarson, E., Y. Song, J. M. Kowalewski, H. Brismar, M. Brines, A. Cerami, U. Andersson, M. Zelenina, and A. Aperia. *Erythropoietin modulation of astrocyte water permeability as a component of neuroprotection*. PNAS, 2009. **106**(5): p. 1602−1607.

V. Kamali-Zare, P., J. M. Kowalewski, M. Zelenina, B. Önfelt, A. Aperia, and H. Brismar. *Role of diffusion limited space on water and salt homeostasis.* **Manuscript.**

VI. Scott, L., S. Zelenin., S. Malmersjö, J. M. Kowalewski,, E. Z. Markus., A. C. Nairn, P. Greengard, H. Brismar and A. Aperia. *Allosteric changes of the NMDA receptor trap diffusible dopamine 1 receptors in spines.* PNAS, 2006. **103**(3): p. 762–767.

VII. Li, Z., J. Lock, H. Olofsson, G. Nurani, B. Kull, J. M. Kowalewski, S. Teller, Y. Liu, E. Manser, H. Zhang, and S. Strömblad. *PAK4 is activated by cell-matrix attachment and modulates integrin clustering, turn-over, and actin connectivity.* **Submitted manuscript.**

VIII. Vanherberghen, B.*, J. M. Kowalewski*, K. Garrod, H. Brismar, S. Lindström, H. Andersson Svahn, M. Cahalan and B. Önfelt. *Single Cell Tracking of Natural Killer Cell Migration in vivo and in vitro reveals Transient Migration Arrest Periods.* **Manuscript.**

Additional publications not included in this thesis

Fu, Y., H. Ågren, J. M. Kowalewski, H. Brismar, J. Wu, Y. Yue, N. Dai and L. Thylén *Radiative and nonradiative recombination of photoexcited excitons in multi-shell-coated CdSe/CdS/ZnS quantum dots.* EPL (Europhysics Letters), **86**(3):37003 (6pp), 2009.

*These authors contributed equally.

Summary and contributions by the author

Below is a brief summary of the papers that this thesis is based on. It also lists the contributions by the author of this thesis, below called the respondent.

Paper I describes microfluidic devices used to study flow induced cellular responses in living cultured cells using confocal microscopy imaging. To assess the performance of the channel geometries of these devices the respondent performed the fluid mechanical simulations presented in Figure 3.

Paper II presents experimental data and a computational model, using a finite element method, which explains the role of membrane properties in this signaling process and how mechanical stress is built up in the plasmamembrane by a fluid drag force that bends cilia. It includes a novel application of planar flow to study the bending of primary cilia and the Ca^{2+} response of cultured kidney epithelial cells using confocal microscopy. The respondent designed the model together with P. Kamali-Zare and implemented the finite element method simulations.

Paper III describes a general model of Ca^{2+} signaling including active and passive transport of Ca^{2+} in between the cytosol, endoplasmic reticulum and the extracellular environment. The paper explores the effects of different models of the inostitol-trisphosphate receptor and the inclusion of store-operated Ca^{2+} entry of Ca^{2+} oscillations. The model was designed by the respondent together with H. Brismar and P. Uhlén. The manuscript was written by the respondent, P. Uhlén and H. Brismar. For this paper, a MATLAB® toolbox, described in Appendix A of this thesis, was created by the respondent who implemented the model and ran the computer simulations.

Paper IV explains the impact of erythropoietin on water permeability in astrocytes and suggests a neuroprotective role for this substance. A signaling pathway through a metabotropic glutamate receptor is explored as a source of this modulation. This exploration is done by studying Ca^{2+} signaling induced by the receptor. The respondent analyzed the data from the Ca^{2+} signaling measurements and developed a tool for semi-automatic classification of Ca^{2+} responses as described in the paper and its supplementary text.

Paper V presents a novel concept in geometrical modeling as it tests how K^+ and water transport in kidney principal cells is affected by cellular and subcellular geometry. In particular it explores extracellular diffusion limited spaces where the local concentration can differ from the rest of the extracellular environment. The respondent developed the model together with P. Kamali-Zare and took part in the implementation of the geometrical model and the effect of water on K^+ conductance of channels.

Paper VI introduces a novel mechanism for localizing dopamine 1 receptors to spines in the neuronal plasmamembrane. A confocal microscopy method used in this study is fluorescence recovery after photobleaching (FRAP). The paper includes experimental data showing the recovery of fluorescently tagged proteins and a mathematical model explaining this recovery in terms of

diffusion. The respondent contributed to the paper by creating the model together with H. Brismar. The respondent performed the calculations presented in the paper and its supplementary material. The respondent also performed part of the data analysis.

Paper VII finds new roles for p21-activated kinase 4 in integrin dynamics and its roles in cell migration. One of the methods in this study is FRAP resulting in the data fitted to a model of protein dynamics that was developed by the respondent and J. Lock. The respondent developed the model, optimized it and performed the analysis of the FRAP data in terms of recovery rate as presented in Figure 6.

Paper VIII explores a novel method to characterize experimental trajectories of migrating natural killer cells in culture and in animal studies. The method uses statistical properties of trajectories based on the assumption of unrestricted diffusion and identifies transient confinement zones in space and time where this assumption does not hold. For this paper the respondent developed the tools for analyzing the trajectories that were recorded and detected by B. Vanherberghen. The respondent also wrote the manuscript together with B. Vanherberghen and B. Önfelt.

1 Introduction

A cell is in many aspects the smallest living unit, characterized by a living interior separated from the rest of the world by a membrane. The membrane has a hydrophobic interior that acts as a barrier between the hydrophilic inside of a cell and its external environment. The cell has a whole architecture of possibilities to communicate with its external environment in a controlled manner; cilia sense motion in the fluid surrounding the cell [1], gases, such as oxygen, can diffuse freely across the membrane while ions and water have to pass via specialized proteins in the membrane [2].

During recent years development in experimental methods and mathematical modeling has driven the amount of data and complexity in our understanding of cellular biology to a new level [3]. This development has made it possible to describe cellular systems quantitatively where only qualitative descriptions were previously possible. To deal with the complex data and models that arise in this kind of research a combination of tools from physics and cell biology has to be applied; this constitutes a field we call cellular biophysics. The aim of this doctoral thesis is to develop novel approaches in this field. I present eight studies where quantitative modeling and analysis are involved.

The first two studies concern cells interacting with their surrounding environment in the kidney. Renal tubular epithelial cells are believed to sense fluid flow as a shear and bending stress on the primary cilium. This stimulus generates Ca^{2+} signals via two proteins called polycystin-1 and polycystin-2. Dysfunction in this signaling system can lead to polycystic kidney disease and kidney failure [4]. The interaction between fluid and cells in renal tubular epithelium can be described by biomechanical models [5, 6]. In this thesis I describe a mathematical model of flow sensing by cilia with focus on the flow frequency response and time delay between the mechanical stress and the Ca^{2+} signaling response, presented in Papers I and II.

Mathematical modeling is a valuable tool, helping us to understand the mechanisms involved in biological systems. This has especially been the case within the field of Ca^{2+} dynamics. One reason for this is that modern, experimental methods in fluorescent and confocal microscopy provide accurate measures of spatiotemporal Ca^{2+} distribution in cells, making it possible to test mathematical models and biological theories. Also, the high number of coupled mechanisms regulating the Ca^{2+} level makes Ca^{2+} dynamics a field that is too complex for simple intuitive models.

Intracellular Ca^{2+} is kept at a very low level compared to the extracellular environment, while several intracellular compartments have higher Ca^{2+} concentration than the cytoplasm. This makes Ca^{2+} an efficient messenger for intracellular signaling, the process whereby signals are transduced from an extracellular stimulus to an intracellular activity such as gene expression [7-9]. An important type of Ca^{2+} signaling is oscillations in intracellular Ca^{2+} concentration which occur due to the concerted interplay between different transport mechanisms within a cell. Paper III examines ways to explain these mechanisms in terms of a mathematical model.

Astrocytes belong to a type of cells, known as glia cells which constitute about 90 % of the total number of cells in the central nervous system [10]. Their name is derived from the Greek word for glue as they glue together and support neurons. Astrocytes are known to express the water channel protein aquaporin-4 and can easily change their volume [11]. Astrocytes are also known to express metabotropic glutamate receptors which can induce Ca^{2+} signaling [12]. The Ca^{2+} signals induced by these receptors are often seen as oscillations. In Paper IV we report that erythropoietin can regulate the water permeability of astrocytes and that it alters the pattern of Ca^{2+} oscillations in astrocytes. In this thesis the analysis of this Ca^{2+} signaling is described.

An important aspect of Ca^{2+} signaling is that Ca^{2+} can have a transient positive feedback on the conductance of Ca^{2+} channels which leads to a phenomenon known as Ca^{2+} induced Ca^{2+} release. Through this phenomenon Ca^{2+} signals can form geometrical patterns as they move in cells [13]. Similar mechanisms are the basis of electrical signaling in the nervous system where Na^{+} and K^{+} currents form electrical signals in neurons [10]. This neural activity increases the extracellular K^{+} concentration in the brain which can interfere with continued neuronal activity. One role for astrocytes is to regulate this K^{+} level by conducting it to other areas of the brain, such as perivascular regions, where neuronal activity cannot be affected. Similar types of K^{+} regulation appear in the kidney. A common aspect of these types of Ca^{2+} signals and K^{+} regulation is the effect of geometry [14-16]. To model the influence of geometry we set up spatial models that use partial differential equations to describe both spatial and temporal patterns of ion and water dynamics. Paper V describes how the geometry of cells and subcellular structures can influence the dynamics of K^{+} and water.

Mathematical modeling has also been very successful in computational neuroscience and network modeling [2, 8, 17, 18]. Previously investigators in our group have proposed diffusion as a mechanism for lateral transport of dopamine 1-receptors within the membranes of neurons, and as a way for these receptors to be trapped in dendritic spines [19]. Paper V in this thesis describes experimental studies using confocal microscopy and mathematical modeling to examine and describe the mobility of these receptors. The physical concepts in this study are lateral diffusion and chemical reactions between protein molecules. In this thesis, analytical and numerical methods to solve reaction diffusion equations that describe this system are explained.

In case the diffusion and reaction components of the system are on different time scales, they can be treated independently. In the case of integrin dynamics the diffusion dominated the initial part of the fluorescence recovery in a focal adhesion. After two minutes the diffusion reached its final level and a slower reaction took over. In Paper VII we describe how reaction rates can be extracted from this data.

Integrins and focal adhesions are important components in cell migration. In Paper VIII we have tracked migration of human natural killer (NK) cells and applied Transient Confinement Zone analysis [20] as a way to characterize their trajectories. The goal of this project is to use mathematical methods to automatically detect features such as cell-cell interaction and immunoresponses by studying *in vitro* and *in vivo* systems.

2 Background

Biological systems are characterized by being open systems that interact with their environment but maintain a state far from thermodynamic equilibrium. This state is achieved by the biochemical systems that convert molecules with a high content of chemical energy to stable ones such as CO_2 and water. The chemical energy in these reactions drives active processes which are responsible for phenomena ranging from steep ion gradients across cellular membranes to movement of cells and organisms. Active processes are counteracted by passive ones that drive the system towards equilibrium [2, 13].

Life cleverly combines active and passive processes on different time and length scales to create signaling systems such as action potentials, where the slowly built up electrochemical gradients of Na^+ and K^+ are utilized to transmit fast electrical signals on scales ranging from μm to meters [10]. The smallest systems that can be considered living, in the sense of combining active and passive dynamical phenomena, are cells. A characteristic feature of cells is that they are surrounded by a membrane that selectively permeates certain molecules and thereby separates the intracellular environment from its surroundings.

2.1 Quantification and modeling in biology

Compared to physics, biology has often been a qualitative rather than quantitative branch of science. One explanation to this is that questions in biology often only have qualitative answers e.g. dead or alive? In many cases qualitative answers are an oversimplification. These questions include: response or no response, sick or healthy? Here of course a quantitative measure can give the investigator more details, when it comes to strength of a response or severity of sickness.

Modern methods in biology have the strength to give quantitative rather than qualitative measures, also allowing for mathematical descriptions of the systems [3, 13]. The combination of quantitative measurements and mathematics has the potential to strengthen biology and strongly deepen our understanding in this field.

2.1.1 Quantitative methods in biology

During the last decades a large number of experimental methods to quantify biological processes in living cells have evolved. These methods range from ratiometric fluorescent dyes allowing for calibrated measurements of ionic concentrations to atomic force microscopy that makes it possible to measure mechanical properties of the cytoskeleton and individual protein molecules. These quantitative measurements often require a mathematical model for their interpretation; this combines the modeling and data analysis which have given this thesis its title.

2.1.2 Biophysical modeling and computational biology

Biological systems are characterized by a complex and often also symbiotic nature where several mechanisms act in concert and simultaneously in large networks. Cell biological phenomena, such as Ca^{2+} signaling, can be present on time scales ranging from ms to days [3]. To fully understand and describe these systems mathematical tools used to describe dynamical systems are necessary [2].

Differential equations

Dynamical biological systems can be modeled by ordinary differential equations (ODEs) involving time derivatives, describing changes over time in e.g. chemical reactions. Systems of ODEs describe the change over time of several interacting quantities. In simple cases these systems have an exact analytical solution, but often numerical methods have to be used to solve them. When spatial variations are considered, the system is described by both time and spatial derivatives. Such systems are known as partial differential equations (PDEs) and can describe several phenomena such as reaction-diffusion systems, but also non dynamical systems such as stationary fluid flow [2, 3, 13, 18, 21, 22]. Examples of PDEs are Fick's laws of diffusion, see Section 2.4.1 and Navier-Stokes equations, see Section 2.2. In general PDEs involve three spatial dimensions, often making them very complex. However, the use of symmetry and simplifications can reduce the number of considered dimensions and thereby making simulations of the systems feasible; see e.g. Section 3.3.2 and Paper VI.

2.1.3 Levels of biophysical modeling

To make a biological model requires a choice of level, in detail, complexity, and time scale. Detailed studies of the nature of individual molecules in a membrane can be done using molecular dynamics simulations, solving a system of differential equations describing a discrete system of molecular interactions which can require months of computational time to even reach a μs in simulated time [23].

To reach a longer time scale simplifications are done so that individual molecules are not considered, but rather concentrations of substances. These kinds of simplifications describe biological systems as continuous. Rather than being built by individual molecules and ions we can describe reactions in terms of kinetics, changing concentration, and ion fluxes in terms of currents driven by voltages across membranes. [13]

When considering the mechanical properties of cells, membranes and subcellular structures, such as cilia, biomechanical models can be used. In these types of models fluid mechanical and structural mechanical descriptions are used. These types of models also take a continuous approach describing the systems in terms of viscosity, elasticity and damping [24].

2.1.4 Cellular biomodeling

Cells are systems that to a certain extent can be described both as discrete systems when individual genes are considered and as continuous when considering the large number of water molecules or K^+ ions in a cell. This is also the case of mechanical characteristics of membranes and subcellular structures which have been studied both as molecular structures and larger scale systems [25-28].

Cellular biomechanical modeling

Several types of cells interact with and sense their environment. In mammals these include several cell types, among those epithelial cells. These cells often have protruding organelles called cilia that can be divided into subtypes known as primary and motile cilia. The two types of cilia are both supported by an axoneme, a scaffolding structure consisting of a ring of microtubules, see Section 2.2.1. Motile cilia have an active role in transporting material e.g. in our airways while primary cilia have lately been shown to be sensors of flow in the liquid environment surrounding them [29]. In Paper II we present a study of the biomechanical properties of primary cilia and, using a mathematical model, how the mechanical structure of a cilium is related to the fluid flow response in kidney epithelial cells

Mechanical modeling of a cellular structure like a primary cilium requires knowledge about the material properties of both the axoneme and the membrane covering it. These types of materials are soft and have both elastic and viscous properties, often referred to as viscoelastic. Elasticity is a measure relating stress to strain in a material, while viscosity is a measure of resistance to stress in a fluid. These material properties make cells and particularly cilia flexible but also sensitive to time and frequency as the viscous properties of these structures damp any build up of stress [30].

Reaction kinetical modeling

Reaction kinetics relates concentrations to reaction rates [31]. This allows us to put together differential equations and calculate how concentrations vary in time and space. This can for example involve enzymes. An important step in this area was taken by Hill [32] who constructed the first mathematical model for hemoglobin oxygen uptake already in 1910. Hill's equation has since then been applied to several types of cooperative enzyme reactions and can be written as:

$$j = \frac{V_{\max} c^n}{c^n + {K_{1/2}}^n} \tag{2.1}$$

where j is the reaction rate, c is the substrate concentration and $K_{1/2}$ is the half rate of reaction constant, equal to the concentration at which the reaction rate is half of the maximal, $V_{\max}$. n is often referred to as the Hill coefficient and indicates the number of cooperative sites in the enzyme [33]. The Hill equation has also proven to be a good model for ATP-driven ion pumps in cell membranes [34].

A very successful model for passive ion channels was originally presented by Hodgkin and Huxley in 1945 [35] and could explain action potentials in neurons in terms of Na^+ and K^+ currents through voltage gated ion channels. In this thesis a model describing Ca^{2+} signaling is included. Ca^{2+} is characterized by remarkably high concentration gradients across membranes which dominate over the electrical gradients that drive currents of other ions through ion channels [34].

2.2 Cellular signaling and mechanosensitivity

To explore epithelial cells *in vitro* as well as *in vivo* environments their interaction with an external environment has to be understood. Typical length scales of these cells are on the order of 10 μm. In order to model systems on this scale the fundamental properties of

such systems are central. Epithelial cells are characterized by having one side facing a liquid environment with which they interact both chemically and mechanically.

In cell biological applications, unless single molecules are considered, liquids can be viewed as continuous and incompressible. Such liquids are generally known as Newtonian fluids and fully characterized by their density and viscosity [36]. The mechanical properties of an incompressible, Newtonian fluid can in principle be described by the Navier-Stokes equation [37, 38]:

$$\rho\left(\frac{\partial \mathbf{v}}{\partial t}+\mathbf{v}\cdot\nabla\mathbf{v}\right)=-\nabla p+\eta\nabla^2\mathbf{v}+\mathbf{f}\,, \tag{2.2}$$

where $\mathbf{v}$ is the fluid flow velocity, ρ the density, η the viscosity, p the pressure field and $\mathbf{f}$ the external force. It can basically be derived from Newton's second law and the conservation of momentum. The left hand side corresponds to mass density × acceleration and the right hand side to a volume force. In its general form the equation can become highly nonlinear but in many practical cases in microfluidics the inertial effects in the left hand side can be ignored.

To characterize the type of flow that is present in a certain case the Reynolds number, which is the dimensionless ratio between inertial and viscous quantities in a system, can be calculated as [36]:

$$Re=\frac{\rho v R}{\eta}, \tag{2.3}$$

with R being the characteristic length scale of the system. Typically R is the radius of a particle or some other obstruction to the flow. On a cellular level the Reynolds number is almost always low ($Re \leq 1$) meaning that the viscous effects are dominant and that the flow is laminar and non-mixing.

2.2.1 Primary cilia

Motile and primary cilia, introduced above, differ both in function and structure. In motile cilia the axoneme is built up of a ring of doublet microtubules with two singlet microtubules inside the ring and dynein arms connecting the ring with the singlet microtubules in the middle. This is known as a 9+2 structure. The structure of primary cilia is referred to as a 9+0 structure, as they lack the two singlet microtubules and dynein arms. In a number of studies Praetorius et al. [1, 39-41] have shown that the primary cilium acts a flow sensor in kidney epithelial cells. These studies show that this response is manifested as a Ca^{2+} signal which is not seen until at least 20 s after the flow starts.

There are two proteins known to form a mechanosensitive complex. These proteins are named polycystin-1 and polycystin-2. A third protein known as fibrocystin may also be a part of this complex. These proteins are located in primary cilia and mutations in these proteins are known to cause polycystic kidney disease which commonly leads to end stage kidney failure. There are few details known about the exact mechanosensation mechanism in cilia [25, 42-44].

Mathematical modeling of kidney epithelial mechansosensation and Ca^{2+} response dates back to before the role of cilia was known [27, 45]. In these models the mechanosensation is caused by shear stress on the cells without any clear sensing mechanism. Curently, there are a number of models that model the mechanosensation of

cilia [46, 47]. These models predict that the sensitive complex is located near the base of the cilium as that is the location of the highest stress. However, they do not explain the delay between flow onset and Ca^{2+} response.

2.3 Intracellular signaling and ion dynamics

All eukaryotic cells respond to signals originating from chemicals in the extracellular environment [7, 48, 49]. These chemicals can be hormones that bind to receptors in the plasma membrane. Other signaling molecules are neurotransmitters and mediators involved in local cell communication. Some signaling molecules are cell permeable and bind to intracellular receptors [50]. The process in which extracellular signals are translated into the intracellular environment is called signal transduction, which involves second messenger molecules. Common second messengers are ions such as Na^{+} or Ca^{2+} [51]. Both of these ions are present in high extracellular and low intracellular concentrations [9]. In the case of Ca^{2+} the intracellular concentration is around 100 nM, while the extracellular concentration is 10,000 times higher. Ca^{2+} is also stored in intracellular organelles or compartments such as the endoplasmic reticulum (ER), which has a Ca^{2+} concentration several orders of magnitude higher than the cytosol. This organelle has a membrane which constitutes around half of the total membrane area in a eukaryotic cell [52]. Na^{+} and Ca^{2+} ions access the cytosol via ion channels in a process described as passive transport. The process which transports these ions out of the cell or Ca^{2+} into the ER is called active transport.

The study of Ca^{2+} dynamics has grown tremendously as a field over the past years due to the introduction of effective dyes that make it possible to study the dynamics in real time [9]. This has also made it possible to create and test mathematical models of this phenomenon and increase our knowledge in the field [8]. The mechanisms involved in Ca^{2+} dynamics are Ca^{2+} channels in the plasma membrane and ER which can rapidly increase the cytosolic Ca^{2+} concentration and pumps in the plasma membrane and ER that decrease this concentration.

2.3.1 Cellular membranes

The plasma membrane is the main barrier between a living cell and its exterior environment. Intracellular membranes separate organelles from the surrounding cytoplasmic environment in the cell. The concept of cellular membranes originates from the nineteenth century. Charles Ernest Overton studied cellular membranes and discovered that there is a wide variety in permeabilities across cellular membranes for different substances. Overton used this knowledge to propose that membranes are constituted of phospholipids and cholesterol. Overton's theory of a dissolve and diffuse mechanism of solutes across membranes is a simple model of membrane flux [2]. Overton also suggested that there must be an active transport mechanism to concentrate certain solutes in the intracellular environment. Overton summarized his theory in a set of rules for membrane structures [2].

Since then one has discovered that cellular membranes are composed of a phospholipid bi-layer containing large amounts of proteins which are involved in transporting ions, nutrients and other solutes. Proteins called aquaporins transport water across membranes, resulting in cell volume changes [53]. One description of the membrane

structure is the fluid mosaic model which describes cellular membranes as phospholipid bi-layers containing clusters of proteins with hydrophobic interiors [54]. Other studies have reformulated this picture into one where low mobility proteins can bind to different parts of the cytoskeleton and lipid bi-layer. This binding, known as trapping, can result from extracellular signals [55], see also Section 2.4.2.

Passive transport

The simplest possible model for transport across a cellular membrane is a description of different permeabilities for different solutes. This description is called the dissolve and diffuse-model and for a thin membrane can be summarized as:

$$J_n = P_n\left(c_n^i - c_n^o\right), \tag{2.4}$$

where J_n is the flux of a solute n through a membrane in the outward direction, c_n^i is the inside concentration of that solute, c_n^o is the outside concentration of solute n, and P_n is the permeability of that solute. The permeability is given by:

$$P_n = \frac{D_n k_n}{d}, \tag{2.5}$$

where D_n is the diffusion coefficient of solute n in the membrane, d is the thickness of the membrane, and k_n is the partition coefficient, which is the ratio between the membrane and water solubilities of solute n. Equation (2.4) is basically a special case of Fick's first law as described by Equation (2.7) on page 14, with the membrane being in a steady state. Although the dissolve and diffuse model is a very simple description which, while not considering modern concepts of transport proteins, remains a good description of passive transport at moderate solute concentrations. However, there are many solutes that can cross the plasma membrane via pure diffusion; this includes gases such as O_2 and CO_2 as well as hydrophobic substances such as many anesthetic agents.

Passive transport gated by proteins, such as ion channels, can often be described by a modified version of (2.5), where P_n is replaced by an opening probability multiplied by the permeability of an open channel and the number of channels in the considered membrane [2, 13, 48]. Because there is a voltage across the plasma membrane, ion channel permeability will depend both on this voltage and the concentration gradient through a process called electrodiffusion. In the case of Ca^{2+} the concentration gradient is so high that it dominates over the effect of voltage [8, 13], and in this thesis the membrane voltage will not be considered as a contributing factor in Ca^{2+} dynamics.

Active transport

Some of the most energy consuming mechanisms in living cells are involved in maintaining the concentration gradients of ions across intra- and extracellular membranes. These gradients are created by transport against a concentration gradient in a process called active transport. Active transport is performed by carrier proteins that take up free energy from one reaction to lower the entropy by increasing a concentration gradient. The most common source of free energy for active transport is the dephosphorylation of adenosine-triphosphate (ATP). The membrane proteins which are involved in this transport are popularly called pumps. Other types of active transport take up free energy from concentration gradients in processes called exchange and co-

transport [48]. Many carrier proteins exploit the Na^+ gradient across the plasma membrane to actively transport other solutes uphill against their concentration gradient. Examples of this process, called secondary active transport, are the Na^+/Ca^{2+} exchanger and the Na^+-glucose cotransporter [2]. Secondary active transport does not consume ATP.

2.3.2 Calcium channels

Calcium channels are present both in the plasma membrane and the intracellular membranes. They are passive transporters, often with high permeability, that are efficient because of the steep Ca^{2+} concentration gradients across these membranes. Ca^{2+} channels are opened because of a gating variable, which can be either a ligand or voltage across the membrane. An important ligand for Ca^{2+} channels in the ER membrane is inositol 1,4,5-triphosphate (IP_3), which is produced in the plasma membrane from phosphatidylinositol biphosphate (PIP_2) upon extracellular signals. IP_3 diffuses rapidly in the cytosol and binds to the IP_3 receptor (IP_3R), a ligand gated Ca^{2+} channel in the ER membrane, and thereby increases its open probability [10, 56].

In the plasma membrane, voltage operated Ca^{2+} channels (VOCs) as well as other types of Ca^{2+} channels are present. Some of these channels are gated by mechanisms that are not fully known. Polycystin-2 is a protein present in the plasma membrane which is thought to be involved in Ca^{2+} signaling caused by mechanical stimulation [4], while store operated Ca^{2+} channels (SOC) are gated by a decrease in the Ca^{2+} concentration in the ER [57].

Inositol 1,4,5-triphosphate receptor (IP_3-receptor)

IP_3R is a large protein located in the ER membrane of most eukaryotic cell types. It functions as a Ca^{2+} channel with the specific ligand IP_3. This ligand is typically produced through G protein linked receptor signaling [56, 58]. Interestingly Ca^{2+} release through IP_3R is also stimulated by Ca^{2+} itself at low concentrations. This is known as Ca^{2+} induced Ca^{2+} release (CICR), which works as a positive feedback mechanism. At higher concentrations Ca^{2+} instead works as an inhibitor for Ca^{2+} release, resulting in negative feedback. This combination of positive and negative feedback of Ca^{2+} on the IP_3R has been described as a bell shaped response curve [59].

There are three subtypes of the IP_3R, known as types 1, 2 and 3 [60]. It has been shown that these receptors show similar basic properties but have different types of regulation. IP_3R types 2 and 3 in lipid bi-layers are not inhibited by Ca^{2+} [61, 62]. However IP_3R type 3 has been shown to be so in intact cells [63]. Knockdown of specific type 1 and type 3 IP_3Rs have shown that these two receptor types play different roles in Ca^{2+} oscillations [64]. It has been suggested that IP_3R type 1 maintains Ca^{2+} oscillations while IP_3R type 3 can be involved in the activation of Ca^{2+} signaling as it is not as readily inhibited as the IP_3R type 1 receptor.

Miyakawa-Naito et al. [65] have proposed a new mechanism in gating of the IP_3R. Their study showed that ouabain induced Ca^{2+} oscillations in renal proximal tubular cells are not caused by an increased level of IP_3 but by a specific physical interaction between ouabain bound Na,K-ATPase (NKA) and IP_3R. The study also showed a close proximity between ouabain bound NKA and IP_3R using fluorescent energy transfer (FRET).

The complex mechanisms of the IP_3R that control the positive and negative feedback of the IP_3R is a well studied subject by both experimentalists and modelers [59, 61, 66-69]. The modeling of IP_3R was thoroughly reviewed by Sneyd and Falcke [70]. One of the first models was the De Young and Keizer model [67] which assumes that there are three independent subunits in the IP_3R. These subunits have to be in a conducting state to allow for Ca^{2+} flux. Another model is the Mak-McBride-Foskett model that is a phenomenological model in which the open probability has been fitted to measured data from IP_3R types 1 and 3 [66]. In Paper III we have compared these two models and how they are affected by store-operated Ca^{2+} channels.

Store operated calcium channels (SOC channels)

Non-excitable cells often lack voltage operated Ca^{2+} channels, but have other means to let Ca^{2+} into the cytosol. One such way, thought to be involved in Ca^{2+} oscillations, is through store-operated Ca^{2+} (SOC) entry. The exact mechanism involved in this kind of Ca^{2+} influx, as well as the identity of SOC channels, is not known [71]. When Ca^{2+} is released from intracellular stores it is taken up by Ca^{2+} pumps in the ER and plasma membrane of the cell. This may cause a decrease in the total amount of intracellular Ca^{2+}, which must somehow be replenished. This was modeled by Putney [72] and termed capacitative Ca^{2+} entry (CCE). At first it was thought that CCE took place through a direct link between the ER and extracellular space. It has later been shown that Ca^{2+} stores are replenished by a relatively slow increase of cytosolic Ca^{2+}, which can be pumped into the ER [71].

One important discovery was that of Ca^{2+} release activated Ca^{2+} (CRAC) current, which was shown to be highly selective for Ca^{2+} compared to some other divalent cations. This was done by whole-cell patch clamp measurements combined with ratiometric Ca^{2+} imaging that showed Ca^{2+} currents that were activated by depletion of the ER in mast cells. CRAC is today considered to be one of perhaps several SOC pathways [71, 73, 74].

At the time of publishing Paper III it was not how the ER communicates Ca^{2+} depletion to the plasma membrane. At least three different qualitative explanations had been proposed [74]. One of these models describes vesicular transport, according to which SOC channels are transported in vesicles and fused into the plasma membrane. Another model suggests physical interaction between the membranes of the ER and the cell, possibly through the IP_3R. The third possible explanation was first presented by Randriamampita and Tsien [75] and includes a diffusible Ca^{2+} influx factor (CIF) that diffuses through the cytosol and activates SOC in the plasma membrane. In Paper III we have made use of the CIF explanation when modeling SOC and its impact on Ca^{2+} oscillations.

Some studies suggest that that there is a physical interaction between the IP_3R in the ER membrane and SOC channels in the plasma membrane. Mikoshiba, Gill and colleagues [76] have shown that IP_3R is required to activate SOC. These studies have suggested that transient receptor potential (TRP) channels are functionally similar to SOC channels. TRP is a large family of Ca^{2+} channels, first found in *Drosophila*, but several members of this family have also been found in mammalian cells, amongst others, in human embryonic kidney cells [68, 76, 77]. Today there is a general view that a

common view that a type proteins called STIM communicates ER depletion to complexes in the plasma membrane involving the protein Orai or TRP channels [78].

2.3.3 Calcium pumps

The low, cytosolic Ca^{2+} concentration is maintained by active transporters, in non-excitable cells mainly by ATP consuming pumps. These pumps are found in the mitochondria, ER and plasma membranes. A well understood protein for this kind of transport is the Sarco-Endoplasmic Reticulum Ca^{2+} ATPase (SERCA). This pump consumes ATP and transports Ca^{2+} from the cytosol to the ER. A similar pump for active Ca^{2+} transport is the plasma membrane Ca^{2+} ATPase (PMCA) which pumps Ca^{2+} across the plasma membrane, out of the cell.

There are mathematical, well-established models on how the active Ca^{2+} transport works in the ER membrane, see the modeling section. These models are based on measurements of uptake of the radioactive isotope $^{45}Ca^{2+}$ into vesicles prepared from intracellular membranes. The PMCA and SERCA proteins have also been crystallized and their three dimensional molecular structure is known [13, 79].

2.3.4 Calcium oscillations

A high cytosolic Ca^{2+} concentration is toxic to a cell, especially if this level is sustained for a longer period of time. As mentioned above, Ca^{2+} signaling is involved in a large number of cellular processes. Some of these processes, such as neural activity and muscle contraction are triggered by single Ca^{2+} transients, while many complex processes such as gene transcription respond to oscillating Ca^{2+} signals. Ca^{2+} oscillations can have periods ranging from seconds to days. It is believed that this diversity in frequencies, as well as amplitudes, can be an explanation of the large number of mechanisms involving Ca^{2+} signaling [9, 80-83].

The channels and pumps described above serve as ON and OFF mechanisms in Ca^{2+} signaling. One important actor in Ca^{2+} oscillations is IP_3 receptor (IP_3R), with its combination of positive and negative feedback on cytosolic Ca^{2+} levels. It is clear that Ca^{2+} oscillations are driven by a system with inertia. As we show in Paper III stimulation of the IP_3R can create a system where Ca^{2+} is released from the ER and undergoes reuptake by the SERCA pump in a periodic manner.

The most common way to activate the IP_3R is through phospholipase C via G proteins that produce IP_3 and diacylglycerol from PIP_2. IP_3 increases the open probability of the IP_3 receptor which in turn rapidly releases Ca^{2+} into the cytosol. The rate of Ca^{2+} release is at first increased through CICR, and later decreases by negative feedback. At this point the OFF processes, mainly pumps in the plasma and ER membranes begin to dominate and cause a decrease in cytosolic Ca^{2+} [84]. As mentioned above, Miyakawa-Naito et al. [65] have shown that Ca^{2+} oscillations can also be caused by a novel mechanism involving physical interaction between the Na,K-ATPase and IP_3R, without involving IP_3.

The large range of frequencies at which Ca^{2+} oscillations occur in combination with the large number of cellular processes that they are involved in make it plausible that these processes are sensitive to the frequency of Ca^{2+} oscillations. This is generally believed, but there is very little experimental evidence for this view. One important

finding in this area was made by De Koninck and Schulman [85], showing that calmodulin-dependent protein kinase II (CaM kinase II) has an activity which is highly regulated by the Ca^{2+} oscillation frequency. CaM kinase II in turn affects synaptic plasticity in neurons, which is the basic principle for learning and memory, and gene transcription, the main process behind cell differentiation.

2.3.5 Calcium dynamics in astrocytes

The human central nervous system consists of around 10^{11} neurons and ten times as many glial (supporting) cells. One kind of glia are astrocytes, star shaped cells with processes that face neuronal synapses and endfeet that face capillaries in the brain [48, 86]. A key discovery in understaning the physiological role of astrocytes was made as late as 1990 by Cornell-Bell et al. [12] who reported that metabotropic glutamate receptors (mGluRs) in astrocytes can induce Ca^{2+} signals in these cells and are believed to form signaling networks in the brain. Ca^{2+} signaling in astrocytes often occurs as oscillations with periods ranging from seconds to minutes [87, 88]. Ca^{2+} oscillations in astrocytes with a period of a few minutes have also been demonstrated by Liu et al. [89]. They also showed that these oscillations were not caused by the glutamate pathway.

Glutamate has been shown by our group to increase the water permeability of astrocytes [90]. Gunnarson et al. [90] also showed that this effect was dependent on a certain amino acid (Serine 111) in the aquaporin-4 (AQP4) primary structure. They also showed that the mGluR group I agonist dihydroxyphenylglycine (DHPG) had similar effects as glutamate on astrocytes, both increasing water permeability and inducing Ca^{2+} signaling. Finally the authors show that there is a pathway including mGluR1/5 Ca^{2+} signaling and nitric oxide that causes an increase in AQP4 water permeability.

2.3.6 Potassium spatial buffering

One role of astrocytes, originally discovered by Orkand et al. [15] in 1966, is their ability to stabilize the extracellular K^+ concentration. This is accomplished by an electrical effect that makes K^+ currents go from a region of high concentration to regions with lower concentration through selective channels in the astrocytic plasma membrane. A channel present in this membrane is an inward rectifying K^+ (Kir) channel known as Kir4.1 [91, 92]. Kir channels are characterized by a high conductance while the membrane is hyperpolarized, with a strongly negative and thus attractive electrical potential on its inside [10].

Several studies [93-99] have shown that there is enrichment of both Kir4.1 and the water channel AQP4 in the endfoot region of astrocytes. As described below, there are reasons to believe that there is a coupling between the water and K^+ permeabilities of astrocytic endfoot membranes.

2.3.7 Osmotic gradients and water permeability

Water is the most abundant substance in cells. Many cell membranes are highly permeable to water. Two types of water transport across membranes are known. These are water diffusion and osmosis. The driving forces behind these two types of transport are differences in water concentration and osmolarity between the two sides of the membrane. Osmolarity can be seen as a form of pressure built up by the kinetic energy

of solute molecules. By applying the ideal gas law to the concentrations of solutes the osmotic pressure can be calculated as: $\pi = RTc_{\Sigma}$, where R is the molar gas constant, T is the temperature and c_{Σ} is the total solute concentration [2]. The osmotic water flux is proportional to the osmotic pressure difference across the membrane and can be written as:

$$\phi_w = L_V \Delta\pi = P_f \Delta c_{\Sigma} \tag{2.6}$$

where L_V is the hydraulic conductivity and $P_f = L_V RT$ is the osmotic permeability coefficient. In Paper IV P_f is measured by studying the change of fluorescent dye concentration in a small intracellular volume using confocal microscopy as previously described by Zelelnia and Brismar [11] and Gunnarson [86].

Until the discovery of water channel proteins in 1992 [100] there was no explanation for the difference in water permeability between different cells. Since then there has been a whole range of studies suggesting different roles for the family of proteins, later named aquaporins, in many cell types [11, 86, 92, 93, 96, 101-106].

Aquaporin-4 (AQP4) is expressed in mammalian brain and kidney. It is believed to have a role in the brain K^+ regulation [107]. Knock out of AQP4 in mice has been found to reduce brain edema [108]. There are two isoforms of AQP4, known as M1 and M23. M1 has a longer NH_2 terminus than M23. In astrocyte endfeet electron microscopy has revealed that AQP4 forms orthogonal arrays and that there is a higher likelihood for this formation by the M23 isoform [86, 109]. Regulation of AQP4 water permeability has been shown. Unlike other forms of AQP it is unaffected by mercury but lead can increase the water permeability of cells expressing AQP4 [86, 103, 110].

2.3.8 Cellular geometry and ion transport

One of the most abundant intracellular substances is K^+. It is also a substance to which the membrane is highly conductive due to the fact that there are selective K^+ channels in the membrane. K^+ is kept inside the cell by an electrostatic potential which is maintained by electrogenic transporters such as Na^+/K^+-ATPase [10]. The high K^+ concentration and conductance cause it to be an important osmolyte and by that to have an important part in cell volume dynamics.

One question addressed in this thesis is the role of cellular geometry in the transport of ions and water. In brain and retina K^+ and water channels are co-expressed and show enrichment in some subcellular areas, such as astrocytic endfeet. Studies have shown that these channels and their distribution is involved in seizures and edema [97, 107, 108, 111]. Müller cells in retina are believed to clear extracellular space from K^+ in a process known as siphoning, where K^+ is excreted into the vitreous body of the eye [96, 112].

In kidney there are principal cells that actively take up K^+ via Na^+/K^+-ATPase in the basal membrane and secrete it into tubular lumen. Some K^+ is also recycled through the basal membrane. It is believed that this shuttling of K^+ is important for the maintenance of membrane potential [113].

2.4 Cellular transport and migration

Transport processes of solutes and solvents are central in biology. Such processes take place on length scales ranging from nm in subcellular compartments to tens of meters of

water transport from the roots to the tree tops. On a cellular scale membranes act as chemical transport barriers for many substances. A membrane can also regulate its electrical conductance and thereby create an electrical potential difference between each of its sides. In eukaryotic cells membranes also separate subcellular compartments known as organelles [2, 10].

2.4.1 Fick's laws of diffusion

The simplest mechanism for transport on cellular scales is diffusion, the process that transports solvents from regions of high concentration to regions of low concentration. The nature of diffusion is typically irreversible, increasing the entropy of the system. The flux of solute through a given area is given by Fick's first law of diffusion:

$$\mathbf{J} = -D\nabla c\,, \tag{2.7}$$

where ∇c is the concentration gradient. The flux vector $\mathbf{J}$ is measured in mol/(m^2·s), the SI unit of concentration is mol/m^3 or mM, and consequently the diffusion coefficient D is measured in m^2/s [2]. Combining Fick's first law with the continuity equation one obtains:

$$\nabla \cdot \mathbf{J} = -\frac{\partial c}{\partial t}, \tag{2.8}$$

which states that the divergence in the flux is equal to the rate of decrease in concentration. Using Gauss' theorem, this can be expressed as:

$$\iiint_V (\nabla \cdot \mathbf{J})\, dV = \oiint_S \mathbf{J} \cdot d\mathbf{S} = -\iiint_V \frac{\partial c}{\partial t} dV\,, \tag{2.9}$$

where $\mathbf{S}$ is the surface of the volume V. This means that the total flux through the surface of a given closed volume is equal to the rate of concentration decrease in that given volume [2]. Combining (2.7) and (2.8) gives Fick's second law, also known as the diffusion equation:

$$\frac{\partial c}{\partial t} = D\nabla^2 c\,. \tag{2.10}$$

The consequences of the equations above are illustrated in Figure 2.1.

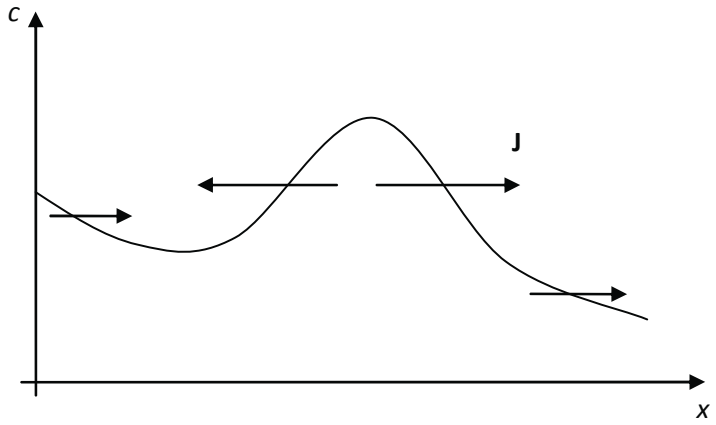

Figure 2.1 The diffusive flux **J**, indicated by the arrows, depends on the concentration *c* according to Equation (2.7). *c* is a function of the spatial coordinate *x*. At extreme points in concentration (maxima and minima) the flux is zero.

The physical explanation of diffusion is that thermal energy induces random collisions between solute and solvent particles [114]. One can show that in the continuous limit, the location of a random walking particle, undergoing the process known as Brownian motion, will have a probability distribution equal to the concentration given by the diffusion equation [2, 21].

In real biological systems diffusion plays an important role in all kinds of passive transport, such as exchange of gases, neurotransmission and Ca^{2+} signaling. The time scale for diffusion over a certain distance is proportional to the square of that distance, making diffusion a fast process over short length scales such as synaptic clefts, but an extremely slow process over longer length scales, such as neuronal axons or the whole human body. As an example of this we can note that a synaptic cleft is approximately 10 nm in distance, this results in a 100 ns diffusion time with $D = 10^{-9}$ m^2/s [2, 115], while the same diffusion coefficient results in a 30 year diffusion time over a distance of 1 m! The concentration gradient is also an important driving force for transport across cellular membranes, and as we shall see further on in this thesis, for localization of receptor proteins in neuronal membranes.

2.4.2 Lateral diffusion in membranes

One of the first studies of lateral diffusion in cellular membranes was performed by Frye and Edidin in the early 1970s [116] and was one of the main motivations of Singer and Nicolson's fluid mosaic model [54]. Frye and Edidin used immunofluorescence to study the mixture of two different proteins in cellular membranes from mouse and human cell cultures that were fused together with the Sendai virus. The two proteins were allowed to mix for 40 min and then were seen to have mixed almost completely. This mixing was proven to be decreased by lowering the temperature below 15 ºC. Also it was not affected by inhibitors of protein synthesis, by adenosine triphosphate (ATP) formation or by glutamine-dependent synthetic pathways. The diffusion coefficient was estimated to be [54]:

$$D = \frac{l^2}{2t} = 0.005\ \mu\text{m}^2/\text{s},$$

where l = 5 μm is the distance of mixing and t = 40 min is the time that the proteins were allowed to mix.

During the mid 1970s, a new experimental method called *Fluorescence Recovery After Photobleaching* (FRAP) was developed to study the mobility of membrane lipids [117]. In this method a small, fluorescent target area is bleached using strong laser light. The bleached fluorophores are thereby no longer visible, but are replaced by mobile molecules from the surrounding area in the studied object. The speed of this recovery can be used to measure the mobility of the fluorophores. Axelrod et al. [117] developed a mathematical method to fit recovery time series to a solution of an equation given by an expanded version of Fick's second law.

Axelrod et al. assume that fluorescent recovery in a region where a small subregion is bleached follows:

$$\frac{\partial c}{\partial t} = D\nabla^2 c - V_0 \frac{\partial c}{\partial x}, \tag{2.11}$$

where D is the diffusion coefficient of the fluorophore whose distribution is given by the concentration c. V_0 is the velocity of a uniform flow of fluorophores in the x-direction. Axelrod et al. provide a solution to the equation given above for a two-dimensional plane where a circular region with radius w is bleached initially. According to their solution, the mean concentration in the bleached region is given by:

$$\bar{c}(t) = C_0 \sum_{n=0}^{\infty} (-K)^n \frac{\exp\left[-\dfrac{2(t/\tau_F)^2 n}{1+n(1+2t/\tau_D)}\right]}{n!\left[1+n(1+2t/\tau_D)\right]}, \tag{2.12}$$

where K is the "amount of bleaching", given as $K \equiv \alpha T I(0)$, with α being the rate of bleaching, T, the time interval during which the bleaching take place, and $I(0)$ the intensity of the bleaching radiation. τ_F and τ_D are time constants of flow and diffusion respectively, defined as $\tau_F \equiv w/V_0$ and $\tau_D \equiv w^2/4D$. Axelrod et al. suggest ways to estimate the diffusion or flow rate for a circular bleaching beam by:

$$D = 0.22\frac{w^2}{\tau_{1/2}}, \quad \text{in case of diffusion,}$$

$$V_0 = 0.81\frac{w}{\tau_{1/2}}, \quad \text{in case of flow,}$$

where $\tau_{1/2}$ is the time at which the recovery has reached half of its final intensity above the initial level.

FRAP was later developed to study protein mobility in excitable membranes of neural and muscle cells, amongst others by Poo [55]. One of the main targets in the studies presented by Poo was acetylcholine (ACh) receptors. Several studies have been conducted showing that the diffusion coefficient can vary between different membrane proteins, and ranges from immobility up to around 0.5 μm^2 /s, 100 times higher than the diffusion coefficient first reported by Singer and Nicolson. The recovery of membrane protein fluorescence is often not complete which suggests that a fraction of the proteins

are immobile. The mechanism behind this immobility is called trapping and can be of various origins, such as extracellular ACh receptors which are strongly concentrated close to nerve terminals in muscle membranes. The nerve terminals are thought to chemically attract the ACh receptors [55].

2.4.3 Cell migration as a random walk

Migrating cells can show different patterns in the directional characteristics of movement. A central role in directing epithelial cell migration is the formation of large protein complexes known as focal adhesions. The complexes form attachments of the actin cytoskeleton and the extracellular matrix through proteins known as integrins. The trafficking and turnover rate of integrins is believed to have a central role in how focal adhesion form and thereby how cells migrate [118].

Immune cells are known to follow a random walk type of trajectory as they move in organs such as lymph nodes [119]. A random walk suggests that there is no preferred direction in the movement and no correlation over time between the directions of the movement of these cells on the time scale at which they are observed. The random walk nature of immune cells can be observed by measuring how their total displacement grows with time [119]. A class of immune cells that have recently received large attention are natural killer (NK) cells [119] currently thought to be parts of both the adaptive and inate immune response [120].

A random walk description is also the basis of diffusion models where the collision time determines the nature of the movement. In most applications the collision time is much smaller than the resolution of the observation system, in which case the total displacement grows as the square root of time [2]. A general term for the technique of observing the nature of diffusing particles is single particle tracking. It has successfully been applied to the tracking of single membrane proteins in neurons, and especially the synaptic region [121-125].

The square root time dependence of the displacement is commonly illustrated by plotting the mean square displacement (MSD) as a function of time lag. The physical laws of diffusion claim that the MSD grows linearly with time lag as $MSD = 2dD\Delta t$, where d is the number of dimensions that the particle is free to move in and D is the diffusion coefficient [20, 124]. In the case of cell trajectories the term motility coefficient is often used instead of diffusion coefficient *(D)*.

2.5 Thesis objective

One aim of this thesis is to mathematically model behavior found experimentally in living cells. A necessary principle in this kind of work is to simplify the biological system in such a way that only a limited number of parameters are present. This simplification is a major part in the creation of a model, introducing a hypothesis that can be compared with experimental results. Using physical laws, a hypothesis can be formulated into a mathematical model, normally describing the studied system by differential equations. Computer simulations can be used to numerically solve these differential equations and make it possible to compare hypothetical model results to actual experiments. Hypotheses that may seem realistic may be excluded if they make predictions that do not agree with the experimental results [13].

The study of cilia requires novel microfluidic devices and models for biomechanical signal transduction. In this thesis finite element methods are used to study the flow profile in microfluidic devices and to simulate bending of membrane surrounded cilia in order to explain the nature of flow induced Ca^{2+} signals.

The discovery of Ca^{2+} oscillations induced by α-haemolysin [81] and ouabain [80] have led to questions concerning the specific mechanisms. Experimental studies have shown that ouabain-induced oscillations are caused by a signaling microdomain with physical protein-protein interactions [65]. This thesis proposes a mathematical model with characteristics resembling the experimental results as well as a novel model for SOC.

Ca^{2+} signals are further studied in astrocyte cultures to understand the role of erythropoietin and its regulation of astrocyte water permeability. Ca^{2+} signals are semi-automatically classified in terms of oscillatory nature and number of peaks. K^+ regulation in the kidney by principal cells has a similar function as K^+ clearance by astrocytes. This thesis presents a novel mechanism for understanding K^+ regulation in the kidney by spatial models of diffusion limited space in subcellular structures of the kidney.

Protein transport is crucial for neuronal function and cell migration as the localization of proteins is in many aspects what drives these types of cell function. The method described in this thesis to study protein mobility is FRAP [55, 117]. A selected fluorescent fusion protein is bleached by intense laser light [19]. The recovery of fluorescence is studied and can be analyzed to measure the transport properties in these systems. To describe the recovery processes mathematical models are developed. Analytical and numerical methods are used in this thesis to fit the experimental data of the FRAP experiments to the models.

Finally this thesis presents methods to study characteristics of migrating cells and suggests ways to characterize trajectories using methods previously used for single particle tracking [20].

3 Modeling and experimental methods

3.1 Biomechanical modeling of cell flow sensitivity

The two studies described in Papers I and II contain computer simulations of fluid mechanics in a microfluidic system and flow induced structural deformation of a membrane covered cilium. The microfluidic device was originally designed for studies of fluid flow induced bending of cilia in living cells. This device later proved to be insufficient as the time dependence of the fluid flow could not be fully controlled. For this reason in Paper II a new device using planar flow is used. The new device has a higher time resolution and can produce strong enough shear forces to show unambiguous flow induced Ca^{2+} responses in cells growing on a cover slip.

3.1.1 Assumptions

The purpose of modeling the channels in the microfluidic device in Paper I was to see the distribution of velocity and pressure in the device and thereby optimize these quantities before fabrication. The aim was to create an environment for the cells with a homogeneous flow profile and by that a reliable set up for flow induced cell signaling experiments. The model was simulated using a finite element method (FEM) in Comsol Multiphysics (Comsol AB, Stockholm).

As further described in Paper II the cilium was modeled as a cylindrical structure with a semi-spherical top loaded by a drag force similarly to the previously published model by Resnick and Hopfer [47]. To be consistent with a FEM description the bending rigidity (EI) previously published by Schwartz et al. [6] and Liu et al. [126] had to be converted to Young's modulus (E) by simply dividing it with the area moment of inertia, which for a cylinder is given by $I = \pi a^4$, where a is the cylinder's radius. The drag force per area is given by:

$$f_{\text{drag}}(z) = \frac{4\pi\eta v(z)}{2a\left[\frac{1}{2} - \gamma - \ln\left(\frac{a\rho v(z)}{8\eta}\right)\right]} \text{ (cylinder) and } \quad f_{\text{drag}}(z) = 3\eta v(z)/(2a) \begin{pmatrix} \text{semi-} \\ \text{spherical top} \end{pmatrix}$$

where z is the distance above the apical cell surface, η, the fluid viscosity and ρ its density. Compared to the equations in Paper II there is a factor of π difference in the spherical top part due to a difference in cross-sectional area.

The cell membrane was modeled using the shell description in the Structural mechanics module in Comsol Multiphysics. Material parameters came from previously published studies [5, 6, 126, 127]. Some of these studies did not use a three dimensional model and therefore their parameters had to be adjusted to the current geometry. These parameters include the membrane spring constant from which Young's modulus was calculated as $E_m = K_m l/A$ and the Rayleigh stiffness damping β_{dK} which relates to the more common damping parameter ξ as $\xi = \alpha_{dM} m + \beta_{dK} k$ [128, p. 199]. The first term in

this expression is the mass damping and can be ignored; k is the material stiffness which is assumed to be proportional to E_m. Other parameters are listed in Paper II.

To study how stress is built up in the membrane Comsol Multiphysics was used through the MATLAB® scripting interface. This allows for integrating the stress over a circular portion of the membrane surrounding the cilium. The time for this integrated stress to rise was compared to the speed of displacement of the distal part of the cilium.

3.1.2 Simulations

For the study presented in Paper I, the fluid flow was set up in the present geometries using Comsol Multiphysics. Boundary conditions were chosen so that the velocity was zero at the walls, known as non slip boundaries, and with inflow and outflow boundaries specified as having a known parabolic velocity profile and known pressure respectively. Sealed inlets and outlets were modeled as walls. Built into the program is a FEM solver which was used to solve Navier-Stokes equation for the incompressible fluid as described in equation (2.2).

The cilium model was constructed using the graphical user interface in Comsol Multiphysics and consists of a three dimensional mesh, built up of tetrahedral elements, describing the structural part of the cilium and a two dimensional mesh, consisting of triangular elements, describing the membrane part. Both meshes are shown in Figure 3.1.

The cilium structure was modeled as an elastic material and covered with a shell model of a strongly damping material, specified by a Rayleigh stiffness damping of

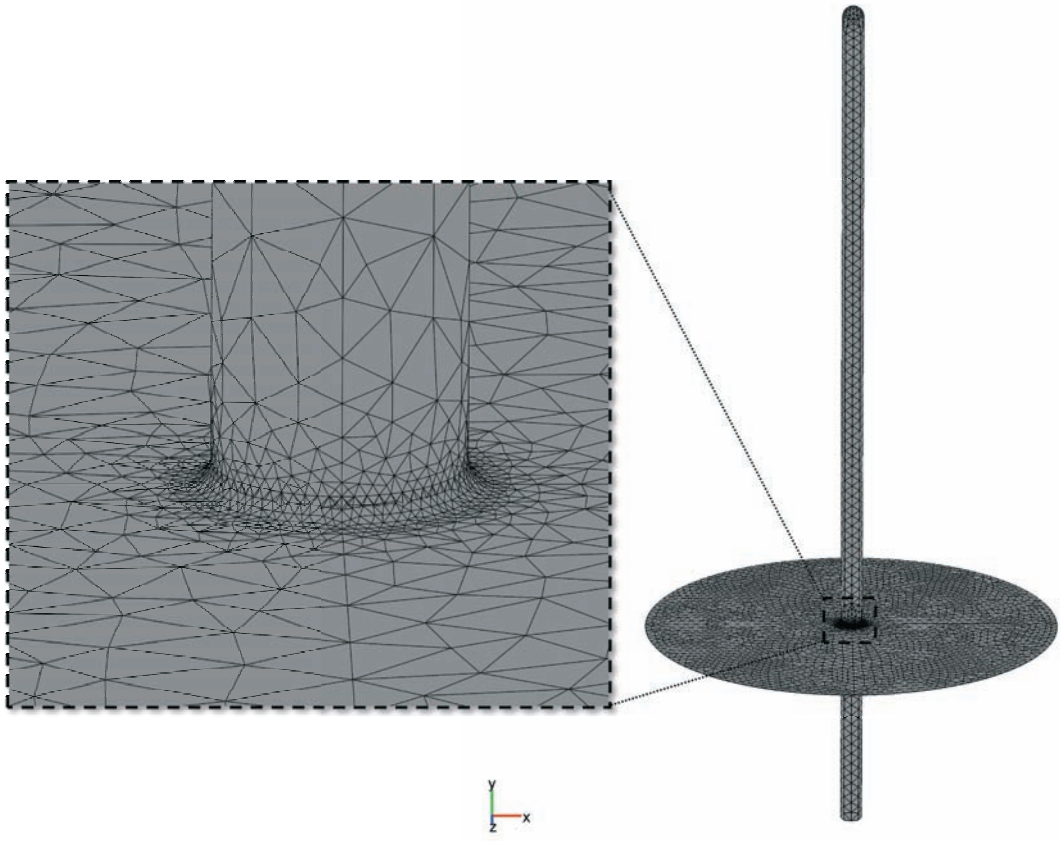

Figure 3.1 Mesh showing the discretization of the cilium model. The magnified portion shows the high resolution of the mesh in the base part of the cilium and the membrane in its close vicinity.

1−10 s as described in Section 3.1.1. The same shell properties were used for the circular, apical part of the membrane. Details of this description are given in Paper II.

3.2 Modeling of calcium signaling

In Paper III we created a compartmental mathematical model of a cell. The model contains a cytosolic compartment, an endoplasmic reticulum (ER) and an extracellular environment. As the extracellular environment is large and has a high Ca^{2+} concentration it can be viewed as a non-emptying source of Ca^{2+}. In the model presented in Paper III the compartments are assumed to be well-stirred with uniform concentrations that are only dependent on time [2, 8, 34, 129]. The model is summarized in Figure 3.2.

A more detailed way to model cellular dynamics is to construct a spatial model where the mixing time is limited by diffusion [130]. In this kind of model, the concentration of a substance n with concentration c_n is described by a modified version of the diffusion equation known as the reaction diffusion equation [131].

$$\frac{\partial c_n}{\partial t} = D\frac{\partial^2 c_n}{\partial x^2} + j(x, y, z, c_n, c_m, \ldots), \tag{3.1}$$

where j is the rate of reactions that consume or produce the substance n. j can depend on a number of different quantities such as c_n, spatial coordinates or the concentration of other substances, for example c_m. A flux, through a membrane, between two different

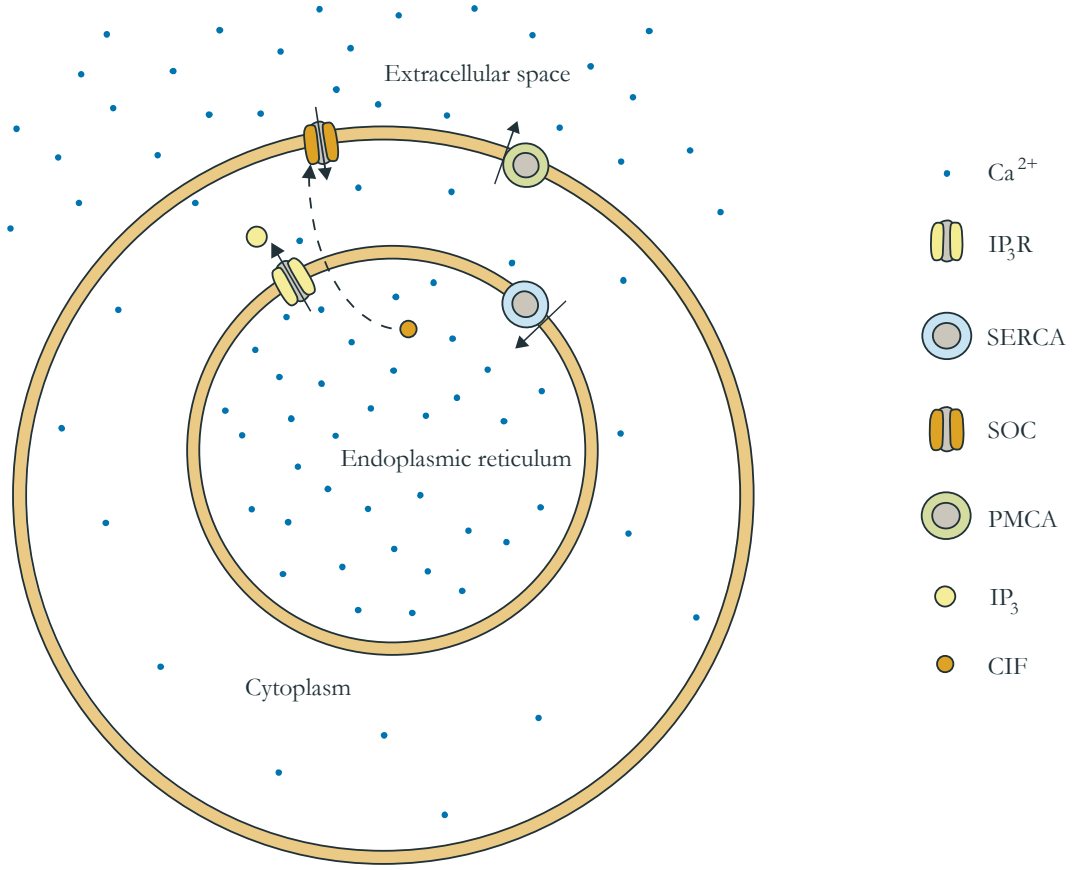

Figure 3.2 A Summary of the Ca^{2+} signaling model shows three compartments that are present in the model. The density of Ca^{2+} ions represents relative differences in Ca^{2+} concentration. Graphics by Linda Westin.

compartments is given as a Neumann boundary condition at the location of that membrane [132]:

$$\hat{\mathbf{n}}_{\text{membrane}} \cdot D_n \nabla c_n = \alpha_{\text{transporter}}(x, y, z) J_n, \tag{3.2}$$

where $\hat{\mathbf{n}}_{\text{membrane}}$ is the unit vector normal to the membrane, $\alpha_{\text{transporter}}$ is the distribution of transporters of substance n and J_n is the flux of that substance n through these transporters. This boundary condition is a special case of Fick's first law given by equation (2.7). A well-stirred or compartmental model can be viewed as a spatial model in the limit where the diffusion coefficients are considered large enough to assume that the time scale of diffusion is much shorter than the time scale of change in concentration by flux of reactions. In a well-stirred compartmental model the equations (3.1) and (3.2) can be summed into [2]:

$$\frac{dc_n}{dt} = j(c_n, c_m, \ldots) + \frac{A_{\text{membrane}}}{V_{\text{compartment}}} J_n, \tag{3.3}$$

where $A_{\text{membrane}}/V_{\text{compartment}}$ is the surface to volume ratio of the compartment where c_n is measured. This description significantly reduces the complexity of the problem.

Ca^{2+} signaling is modeled as a combination of ON and OFF mechanisms working together to create a signal. This signal may be either a steady increase in cytosolic Ca^{2+} concentration, a transient increase, where the cytosolic Ca^{2+} returns to base level after some time or an oscillating signal [9, 82]. In a mathematical model the ON and OFF mechanism are described as terms contributing to the total flux of Ca^{2+}, $J_{Ca^{2+}}$. The three compartments that have been considered in our model are the cytosol, the endoplasmic reticulum (ER) and the extracellular (EC) environment, each one having a certain Ca^{2+} concentration. A compartmental model of this system can be written as a system of ordinary differential equations (ODEs). The model which is described in detail in Appendix A contains eight different concentrations, and ten reactions or fluxes, which can be summed into a system of ODEs using a generalized form of equation (3.3) [133]:

$$\frac{d\mathbf{S}}{dt} = \mathbf{N}\mathbf{j}, \tag{3.4}$$

where **S** is a column vector of all the species in the model, **N** is the 8×10 stoichiometry matrix and **j** is a column vector of all reactions or fluxes in the model. The rows in **j** that contain fluxes have to be multiplied by the surface to volume ratio as described by equation (3.3). This has been done using the *OOR toolbox*, which automatically can calculate the matrix **N**, by specifying the species and reactions between them, as well as the volume of each compartment present in the model. The toolbox was made using MATLAB®, see Appendix A.

To summarize the compartmental model in Paper III: it consists of a species vector:

$$\mathbf{S} = \begin{pmatrix} [Ca^{2+}]_{cyt} \\ [Ca^{2+}]_{ER} \\ [Ca^{2+}]_{EC} \\ [IP_3]_{cyt} \\ [G]_{cyt} \\ [CIF]_{cyt} \\ [CIF]_{ER} \\ [SOC]_{PM} \end{pmatrix}, \tag{3.5}$$

where the first four elements are the concentrations of Ca^{2+} and IP_3 present in the three compartments of the model. The other four species are described below as they take part in the dynamics of IP_3 and the SOC channels. The reaction vector:

$$\mathbf{j} = \left(J_{PMCA}, J_{SERCA}, J_{IP_3R}, J_{SOC}, j_G, j_{IP_3}, j_{CIF\,prod}, j_{SOC\,bindning}, j_{SOC\,deg}, J_{CIF} \right)^T \tag{3.6}$$

contains the ten fluxes and reaction rates that are described below. Figure 3.2 shows a representation of the species and transporters present in the model.

In Equation (3.6) j_G and j_{IP_3} are reaction rates involved in the negative feedback mechanism of Ca^{2+} on the level of IP_3. This mechanism has previously been reported [129, 134, 135]. In our model it has been implemented as a reaction starting at time t_0 which produces IP_3 at a rate:

$$j_{IP_3} = G_{signal} I_{deg} [IP_3]_{max} - I_{deg} [IP_3]_{cyt} . \tag{3.7}$$

G_{signal} depends on a hypothetical substance G which is produced and degraded at a rate:

$$j_G = k_G [Ca^{2+}]_{cyt} - I_G [G]_{cyt} , \tag{3.8}$$

$$G_{signal} = 1 - \frac{[G]_{cyt}{}^n}{[G]_{cyt}{}^n + K_{1/2}{}^n} . \tag{3.9}$$

The parameters in the equations above are defined in Paper III, Table 1.

3.2.1 Calcium channels

Ca^{2+} channels are passive transporters of Ca^{2+} that open and close with certain probabilities. The general form of flux through a Ca^{2+} channel is, as given by (2.4):

$$J_{Ca^{2+}} = P_{Ca^{2+}} \left([Ca^{2+}]_i - [Ca^{2+}]_o \right). \tag{3.10}$$

The permeability of the channels, $P_{Ca^{2+}}$, is given as a product of the permeability of a single open channel, the number of channels in the membrane and the open probability of a single channel.

IP_3-receptors

As described in the background of this thesis there are several models of IP_3R. In our study we have compared two different models. Both of these models obey the general expression:

$$J_{\mathrm{IP_3R}} = \left(V_{\mathrm{IP_3R}} + V_{\mathrm{leak\ ER}}\right)\left([\mathrm{Ca}^{2+}]_{\mathrm{ER}} - [\mathrm{Ca}^{2+}]_{\mathrm{cyt}}\right), \tag{3.11}$$

where $V_{\mathrm{IP_3R}}$ and $V_{\mathrm{leak\ ER}}$ are the permeabilities of the IP_3R by regulated flux and leak, respectively. The De Young and Keizer [67] model is not specific to any subtype of IP_3R and according to this model:

$$V_{\mathrm{IP_3R}} = v_1 \left[\frac{\left[\mathrm{Ca}^{2+}\right]_{\mathrm{cyt}} \left[\mathrm{IP_3}\right]_{\mathrm{cyt}} d_2}{\left(\left[\mathrm{Ca}^{2+}\right]_{\mathrm{cyt}} \left[\mathrm{IP_3}\right]_{\mathrm{cyt}} + \left[\mathrm{IP_3}\right]_{\mathrm{cyt}} d_2 + d_1 d_2 + \left[\mathrm{Ca}^{2+}\right]_{\mathrm{cyt}} d_3\right)\left(\left[\mathrm{Ca}^{2+}\right]_{\mathrm{cyt}} + d_5\right)} \right]^3 . \tag{3.12}$$

The parameters in this model are explained in Paper III, Table 3.

The second IP_3R model was proposed by Mak et al. [66] and is described by the equations:

$$V_{\mathrm{IP_3R}} = v_{IP_3R} \left[1 + \left(\frac{K_{\mathrm{act}}}{\left[\mathrm{Ca}^{2+}\right]_{\mathrm{cyt}}}\right)\right]^{-1} \left[1 + \left(\frac{\left[\mathrm{Ca}^{2+}\right]_{\mathrm{cyt}}}{K_{\mathrm{inh}}}\right)\right]^{-1}, \tag{3.13}$$

where

$$K_{\mathrm{inh}} = \left[1 + \left(\frac{K_{\mathrm{IP_3}}}{[\mathrm{IP_3}]_{\mathrm{cyt}}}\right)^{H_{IP_3}}\right]^{-1} . \tag{3.14}$$

Again, the parameters are described in Paper III, Table 3.

SOC channels

In Paper III we propose a phenomenological model of SOC channel activation. This model involves a diffusible Ca^{2+} influx factor (CIF) which is released from the ER and binds to a channel in the plasma membrane. The model suggests that CIF slowly binds to and opens SOC channels; these channels are in turn deactivated after some time given by the coefficient I_{SOC}. The flux of CIF across the ER membrane is controlled by the Ca^{2+} concentration in the ER lumen. When this concentration falls below a certain value, CIF is released into the cytosol. CIF is regenerated in the ER up to the level $[\mathrm{CIF}]_{\mathrm{max}}$. In Equation (3.6) J_{SOC} is the Ca^{2+} flux through the SOC channels, J_{CIF} is the flux of CIF across the ER membrane, $j_{\mathrm{CIF\ prod}}$ is the production rate of CIF through the regeneration process, $j_{\mathrm{SOC\ binding}}$ is the binding rate of CIF to the SOC channels and $j_{\mathrm{SOC\,deg}}$ the deactivation rate of SOC channels in the plasma membrane. These quantities are coupled through Equation (3.4) as described in detail in Appendix A. The mathematical definition of the Ca^{2+} flux through SOC is given by:

$$J_{\mathrm{SOC}} = (V_{\mathrm{SOC}} + V_{\mathrm{leak\ PM}})\left([\mathrm{Ca}^{2+}]_{\mathrm{EC}} - [\mathrm{Ca}^{2+}]_{\mathrm{cyt}}\right), \quad V_{\mathrm{SOC}} = v_{\mathrm{SOC}}\left[\mathrm{SOC}\right]_{\mathrm{PM}}, \tag{3.15}$$

where V_{SOC} is the SOC channels permeability. The flux of CIF across the ER membrane is given by:

$$J_{\mathrm{CIF}} = \begin{cases} v_{\mathrm{CIF}}\left(\left[\mathrm{CIF}\right]_{\mathrm{ER}} - \left[\mathrm{CIF}\right]_{\mathrm{cyt}}\right), & \text{if } [\mathrm{Ca}^{2+}]_{\mathrm{ER}} < [\mathrm{Ca}^{2+}]_{\mathrm{ER,\,min}}, \\ 0 & \text{otherwise.} \end{cases} \tag{3.16}$$

The reaction rates involved in the regulations of CIF and SOC channels are given by:

$$j_{\text{CIF prod}} = k_{\text{CIF}}\left([\text{CIF}]_{\max} - [\text{CIF}]_{\text{ER}}\right), \tag{3.17}$$

$$j_{\text{SOC binding}} = k_{\text{SOC}}[\text{CIF}]_{\text{cyt}}, \quad j_{\text{SOC deg}} = -I_{\text{SOC}}[\text{SOC}]_{\text{PM}}. \tag{3.18}$$

See Paper III, Table 3 for definitions of the parameters.

3.2.2 Calcium pumps

The activities of the Ca^{2+} pumps were implemented as in Baker et al. [34]. The SERCA and PMCA activities are thus:

$$J_{\text{SERCA}} = \frac{V_{\max,\text{SERCA}}[\text{Ca}^{2+}]_{\text{cyt}}^{\,n_{\text{SERCA}}}}{[\text{Ca}^{2+}]_{\text{cyt}}^{\,n_{\text{SERCA}}} + K_{1/2,\text{SERCA}}^{\,n_{\text{SERCA}}}}, \tag{3.19}$$

$$J_{\text{PMCA}} = \frac{V_{\max,\text{PMCA}}[\text{Ca}^{2+}]_{\text{cyt}}^{\,n_{\text{PMCA}}}}{[\text{Ca}^{2+}]_{\text{cyt}}^{\,n_{\text{PMCA}}} + K_{1/2,\text{PMCA}}^{\,n_{\text{PMCA}}}}. \tag{3.20}$$

The parameters in these expressions are found in Paper III, Table 4.

3.2.3 Calcium oscillation models

To model Ca^{2+} oscillations the parameter $[IP_3]_{\max}$ was varied. This corresponds to a varied degree of stimulation of the IP_3R that has been shown in both experimental and modeling studies to result in Ca^{2+} oscillations [18, 65, 129]. In the present model Ca^{2+} oscillations were induced by increasing the $[IP_3]_{\max}$ after the resting time t_0 which was set to 500 s. The maximum IP_3 concentration was varied in a range between 1 and 80 nM. In the model, other variations that have been implemented were to inhibit SERCA and to remove SOC channels from the model.

3.3 Numerical computation

A system of differential equations can be solved using numerical methods where the problem is discretized in a way where the solution can be described by a limited number of values at different points in space and time [131].

3.3.1 Compartmental models

A compartmental model describes a cell as a system of compartments where the concentration in each compartment is homogeneous at all times. As the concentration of species in the compartments varies in time, but is independent of space, this system can be modeled using ordinary differential equations (ODEs) [131].

As described in Appendix A, the system of ODEs was coupled and solved using the MATLAB® **ode15s** function [136, 137]. This is a variable order, multistep solver that uses numerical differentiation formulas. It can handle stiff problems where the problem contains several different time scales [138]. Physically, the short time scale corresponds to sudden opening of Ca^{2+} channels and the long time scale to the time at which the cell is in nearly steady state.

3.3.2 Spatial models

A computational tool that is specialized in solving a system of reaction diffusion equations is *Virtual Cell* [131, 139]. By using this program, the Ca^{2+} signaling model described by Equations (3.7)–(3.20) was entered and coupled according to Equations (3.1)–(3.2). A geometry based on data from an image of a COS-7 cell taken by a confocal microscope was added to the model, see Section 4.3.2. This resulted in a system of PDEs which was solved using simulations based on the finite volume method. Using this method, the geometry is discretized into two or three dimensional rectangular spaces, or volume elements. Within each element, the change of concentration of a species is the sum of flux and production through reactions in this element. *Virtual Cell* uses a constant time step to numerically integrate the resulting equations [131, 132].

3.4 Characterizing calcium oscillations in astrocytes

To evaluate Ca^{2+} signaling properties of astrocytes ratiometric Ca^{2+} imaging was done on astrocytes treated with dihydroxyphenylglycine (DHPG). A set of measurements involved pre-treatment with erythropoietin (EPO), 10 minutes before Ca^{2+} imaging commenced. The DHPG treatment induced a clear response in most of the cells. To compare the EPO pre-treated and non EPO pretreated groups, Ca^{2+} response was characterized according to a few different criteria.

Power spectra were calculated using spectral analysis software as described by Uhlén [140]. The Ca^{2+} signals were in many cases not sufficiently well resolved to find clear peaks at oscillatory frequencies in the spectra. However, the spectral information proved to contain information which could be used for characterization of whether a Ca^{2+} signal was oscillatory or not. This was done by summing up the total power of the spectrum and determining whether the center of mass was above 10 mHz, meaning oscillatory or below 10 mHz, meaning non-oscillaotory. To exclude weak signals, i.e. non-responding cells a power threshold value was used.

In order to further characterize the Ca^{2+} signals, peaks were manually counted for each responding cell. Peaks were identified if they were clearly above 20 % of the base line Ca^{2+} level.

3.5 Modeling of potassium and water in astrocytes and kidney principal cells

In Paper V we have constructed a spatial model that combines geometry, osmotic water transport and electrodiffusive properties of K^+ channels. The model is constructed using a geometry including subcellular basal invaginations. These invaginations form a diffusion limited space (DLS) in which the K^+ and water concentration can differ from that in the rest of the extracellular space. The model was implemented in *Virtual Cell* [131, 139].

The electrodiffusion was modeled as a K^+ flux given by:

$$J_{\mathrm{K}} = -\frac{G_{\mathrm{K}}}{F}\left(V_{\mathrm{m}} - V_{\mathrm{K}}\right), \text{ where the Nernst potential } V_{\mathrm{K}} = \frac{RT}{F}\ln\left(\frac{[\mathrm{K}^+]_o}{[\mathrm{K}^+]_i}\right), \qquad (3.21)$$

G_K is the local conductance of the membrane, F is Faraday's constant, V_m is the membrane potential, R is the molar gas constant, T is the temperature, and o and i indicate outer and inner K^+ concentration. The membrane potential is considered non-local and thereby calculated as a single number for the whole cell, but is allowed to vary over time. As ions pass the membrane, forming a current I_m the membrane potential changes as:

$$\frac{dV_m}{dt} = \frac{I_m}{C_m}, \tag{3.22}$$

where C_m is the membrane capacitance. To simplify the model, the osmotic difference in (2.6) is calculated for just K^+:

$$\Delta c_\Sigma = ([K^+]_o - [K^+]_{init}^o) - ([K^+]_i - [K^+]_{init}^i). \tag{3.23}$$

The total water flux, including diffusive flux of water and a hydrostatic pressure by the shape of the cell is given by:

$$J_{H_2O} = N_{AQP} P_f \left(\Delta c_\Sigma + \beta([H_2O]_i - [H_2O]_o)\right), \tag{3.24}$$

where N_{AQP} is the number of water channels is the local membrane segment, P_f is the water permeability of a single channel and β is a correction factor relating the included driving forces. The diffusion of K^+ and water is modeled by Fick's second law as presented in Equation (2.10).

3.6 Modeling of diffusion in cells

3.6.1 Reducing the number of dimensions in Fick's laws

In the Background of this thesis diffusion in three dimensions is described. Solving the diffusion equation in three dimensions can be a difficult problem, both analytically and numerically, because of the high number of degrees of freedom. In many problems the number of dimensions can be reduced to two or even one. When studying transmembrane diffusion, the concentration gradient is often one dimensional, in the direction normal to the membrane surface [2]. Lateral membrane diffusion is usually a two dimensional problem, where proteins or other substances can move in any of the dimensions parallel to the membrane surface. Let us consider a diffusion equation as given by (2.10) where a substance is free to move in a d-dimensional space.

To solve a partial differential equation (PDE), like the diffusion equation, two principal methods exist. When the whole space is considered Green's functions can be used. In this method the solution for a point source concentration is calculated to be:

$$c(\mathbf{r}, t) = \frac{1}{(4\pi D t)^{d/2}} e^{-r^2/4Dt}, \tag{3.25}$$

where $r = |\mathbf{r}|$ is the distance from the original point source. The concentration of a diffusing substance with an initial point source is equal to the probability distribution of a random walking particle. For an arbitrary initial concentration $c(\mathbf{r},0)$ the solution is calculated as a convolution between $c(\mathbf{r},0)$ and the Green's function given by (3.25) [21]:

$$c(\mathbf{r},t) = \int_{\mathbf{R}^d} c(\mathbf{r}',0) \frac{1}{(4\pi D t)^{d/2}} e^{-(r-r')^2/4Dt} d^d\mathbf{r}' . \tag{3.26}$$

When a confined region of space is considered, the Green's function method is often not practical. The boundary conditions around a confined region in space make it possible to solve a PDE using the product method instead. This method reduces a PDE to a set of ordinary differential equations, which together with the boundary conditions form a set of eigenfunctions whose product can be shown to be a solution to the original PDE. The number of factors in the solution is equal to the number of degrees of freedom in the PDE. A sum of an infinite number of eigenfunctions can fulfill the initial conditions of the PDE, and thus solve the problem. This kind of method is used in Paper VI to solve the FRAP problem in a dendritic spine (see below). In general the solution to the diffusion equation is given by:

$$c(\mathbf{r},t) = \sum_{n=0}^{\infty} c_n f(k_n \mathbf{r}) e^{-Dk_n^2 t} , \tag{3.27}$$

where k_n and f depend on the geometry and boundary conditions of the problem, and c_n is a series expansion of the initial concentration. For one-dimensional problems $f(k_n x)$ is a periodic function and c_n is given by the corresponding series expansion [21].

3.6.2 Solving the theoretical FRAP problem

Fluorescence recovery after photobleaching (FRAP) is a microscopy method further described in Section 3.9.3. It can be used to study the mobility of intracellular molecules. To understand the relation between this mobility and experimental data a mathematical model is described below.

Diffusion in dendrite

In Paper VI we model the dendrite as a long cylinder. A piece of the dendrite is bleached, leading to diffusion of unbleached and bleached fluorescent molecules independently of each other. To simulate the fluorescent intensity in this system we consider the concentration of fluorescent material and assume that the fluorescent intensity is proportional to this concentration. Because the diffusion only takes place along the dimension of the symmetry axis of the cylindrical dendrite, we can view this problem as one-dimensional. We assume that the bleached area is centered on the origin and has a length of $2l$, Fick's second law can thus be written as:

$$\frac{\partial c}{\partial t} = D \frac{\partial^2 c}{\partial x^2} , \tag{3.28}$$

with the initial condition:

$$c(x,0) = \begin{cases} C_0, & |x| \geq l \\ 0, & |x| < l \end{cases} \tag{3.29}$$

as shown in Figure 3.3a. This PDE can be solved analytically using Green's functions [2, 21] and has the solution:

$$c(x,t) = C_0\left(1 - \int_{-l}^{l} \frac{1}{\sqrt{4\pi Dt}} e^{-(x-x')^2/4Dt} dx'\right) = \frac{C_0}{2}\left[\mathrm{erfc}\left(\frac{x+l}{2\sqrt{Dt}}\right) + \mathrm{erfc}\left(\frac{-x+l}{2\sqrt{Dt}}\right)\right], \quad (3.30)$$

where erfc is the complementary error function defined as:

$$\mathrm{erfc}(x) = 1 - \frac{2}{\sqrt{\pi}} \int_0^x e^{-\xi^2} d\xi .$$

The solution is shown in Figure 3.3b.

When doing FRAP studies the mean fluorescence intensity in the bleached area as a function of time is measured. Under the assumption that fluorescence intensity is proportional to concentration, using the substitution $a = D/l^2$, this quantity can be calculated as:

$$\bar{c}(t) = \frac{1}{2l}\int_{-l}^{l} c(x,t)dx = C_0\left(\sqrt{\frac{at}{\pi}}\left(1 - e^{-1/at}\right) + \mathrm{erfc}\left(1/\sqrt{at}\right)\right). \quad (3.31)$$

This expression could be fitted to a measured recovery curve using nonlinear least-square optimization. However, the measured recovery curve is influenced by focus drift caused by small movements of the dendrite. Because the study is done in a confocal microscope, focus drift has a large impact on the recovery curve. It is often not possible to fit the data well to the expression given by Equation (3.31). A quantity which is less influenced by focus drift is the half time of the recovery, $t_{1/2}$. This is the time from the beginning of the recovery until the intensity has reached half of its final recovery value. This intensity is given by $I_{1/2} = I_i + (I_e - I_i)/2$, where I_i is the intensity after photobleaching and I_e is the intensity at the end of the recovery as shown in Supporting Figure 9 in Paper I. To calculate $t_{1/2}$ we identify $\bar{c}(t)$ given by (3.31) as a function of at and numerically solve the equation:

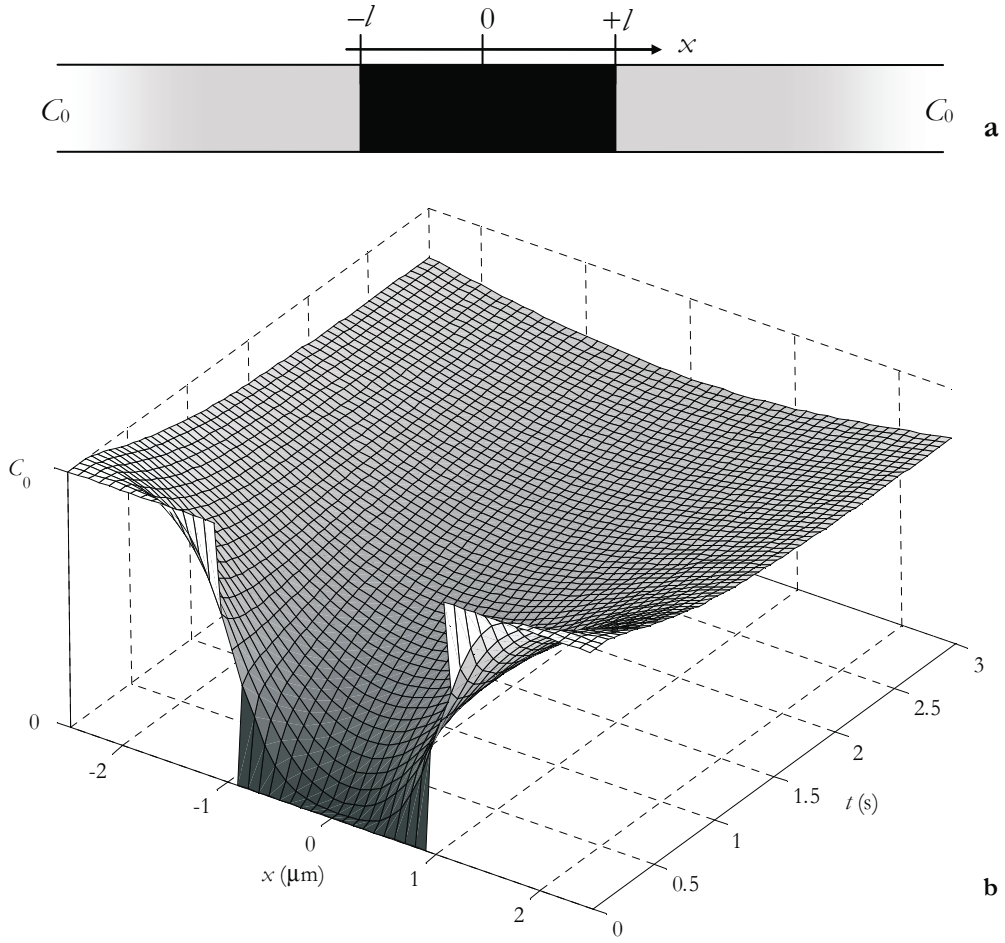

Figure 3.3 (a) The initial condition and (b) analytical solution for the FRAP problem of a dendrite as given by Equation (3.30). The parameters in the solution are D = 1 μm²/s and l = 1 μm

$$\frac{1}{2} = \sqrt{\frac{at_{1/2}}{\pi}}\left(1 - e^{-1/at_{1/2}}\right) + erfc\left(1/\sqrt{at_{1/2}}\right),$$

which gives the result: $at_{1/2} \approx 0.925$. Thereby the diffusion coefficient can be calculated as:

$$D = 0.925\frac{l^2}{t_{1/2}}. \tag{3.32}$$

Diffusion in spines

A FRAP experiment in a dendritic spine can be described as diffusion in a small tube with a closed end, through which the flux of fluorophores is zero. In the other end of the tube is the dendrite, which is much larger than the spine, see Figure 3.4a. The dendrite can thus be viewed as a non-emptying pool. At the connection between the dendrite and the spine the fluorophore concentration is considered to be constantly equal to C_0. These two boundary conditions combined with Fick's second law leads to a one-dimensional diffusion problem in a confined region. Using a series expansion that fulfills the boundary conditions and Equation (3.27), the solution to this problem can be written as:

$$c(x,t) = C_0 - \frac{4C_0}{\pi}\sum_{n=0}^{\infty}\sin\left(\frac{(1+2n)}{4l}\pi x\right)\frac{e^{-D(1+2n)^2\pi^2 t/(16l^2)}}{(1+2n)}, \tag{3.33}$$

where x is the coordinate along the axis of the spine. The length of the spine, and thereby also the bleached region, is $2l$. The solution is shown in Figure 3.4b. When taking the mean concentration over the bleached area in the same way as was done above for the dendrite, the solution becomes:

$$\frac{1}{2l}\int_0^{2l} c(x,t)dx = C_0 - \frac{8C_0}{\pi^2}\sum_{n=0}^{\infty}\left[\frac{1}{(1+2n)^2}e^{-D(1+2n)^2\pi^2 t/(16l^2)}\right]. \tag{3.34}$$

Supporting Figure 8 in Paper VI compares the results of Equations (3.31) and (3.34), showing that the recovery in a spine is faster than in a dendrite.

The time $t_{1/2}$ can be calculated as above by numerically solving the equation:

$$\frac{1}{2} = 1 - \frac{8}{\pi^2}\sum_{n=0}^{10}\left[\frac{1}{(1+2n)^2}e^{-D(1+2n)^2\pi^2 t/(16l^2)}\right]. \tag{3.35}$$

The right hand side of this equation is the first 11 terms of the expression for the mean concentration divided by C_0. This gives the result:

$$D = 0.788\frac{l^2}{t_{1/2}}. \tag{3.36}$$

A more accurate model can be made when assuming that diffusion of the fluorophore into the spine depletes the concentration of fluorophore in the dendrite. This makes the problem two-dimensional and it cannot easily be solved analytically. Therefore Comsol Multiphysics has been used to numerically simulate this problem using a finite element method (FEM). There is no exact, simple relationship between the half time of recovery and the diffusion coefficient in this model, but a first order approximation when l is near 375 nm and $t_{1/2}$ is near 1 s is found to be:

$$D = 1.296\frac{l^2}{t_{1/2}}, \tag{3.37}$$

where l is half the length of the spine.

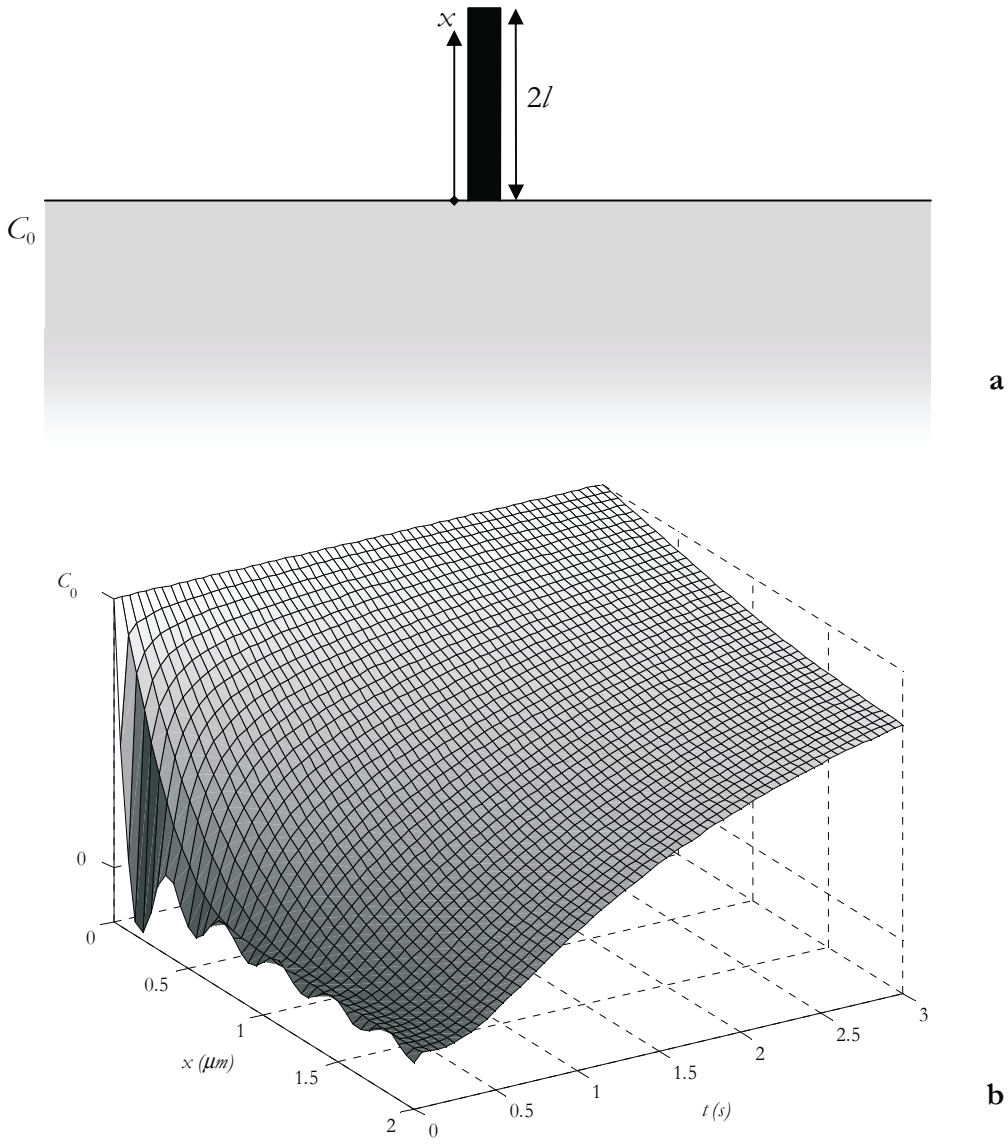

Figure 3.4 The initial condition (a) and analytical solution (b) of the FRAP problem for a spine given by the first 11 terms in Equation (3.33). The limited number of terms gives rise to the oscillatory behavior known as Gibb's phenomenon seen to the left in the picture. The parameters are the same as in Figure 3.3.

3.7 Trapping of dopamine 1 receptors in spines

The trapping of diffusing dopamine 1 receptors (D1R) by N-methyl-D-aspartate (NMDA) receptors can be described by a diffusion reaction equation given by Fick's second law and an additional reaction term, *R*. In two dimensions this reaction diffusion equation is given by:

$$\frac{\partial c}{\partial t} = D\left(\frac{\partial^2 c}{\partial x^2} + \frac{\partial^2 c}{\partial y^2}\right) + R\,, \tag{3.38}$$

where *R* is the reaction rate for a species with concentration *c*. In the current model it has been assumed that there are two diffusing species present. One is the D1R, having a

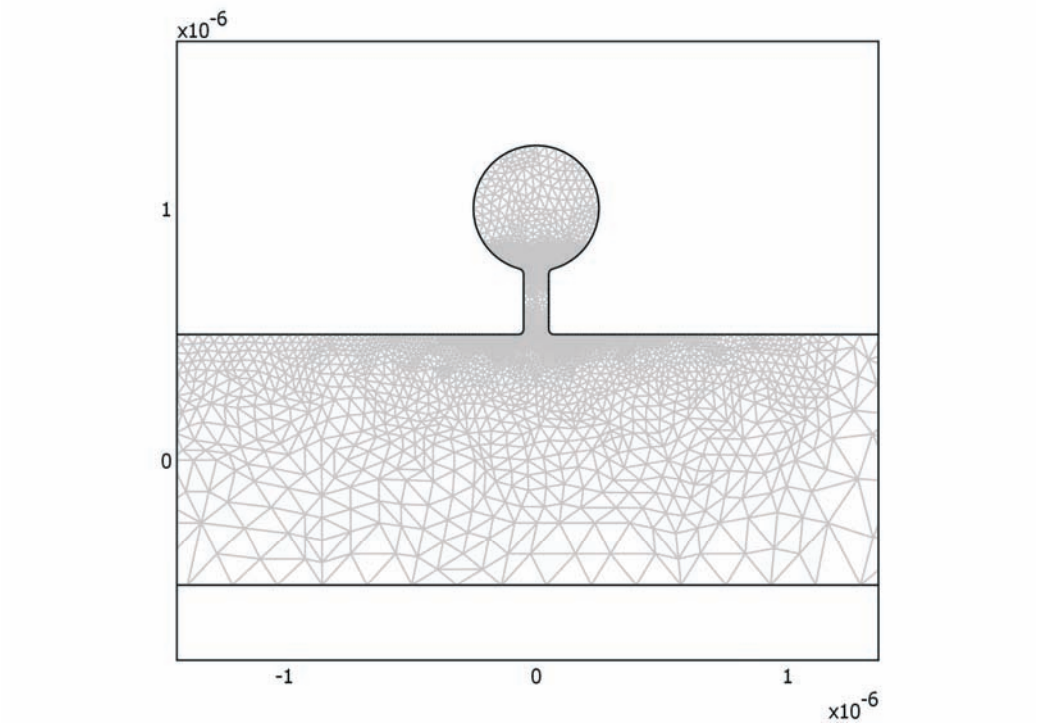

Figure 3.5 The geometry of the FEM model of the spine and the dendrite. The grey mesh shows the discretization used by the FEM solver. The geometry is described by a 1 μm wide, long dendrite with a spine that consists of a 0.10 μm wide and 0.25 μm long tube connected to a circle with a radius of 0.25 μm (the spine head). The spine head is centered at the coordinates (0,1 μm). The scales on the axes are in meters.

concentration c_1, and the other species, with concentration c_2, is D1R bound to the NMDA receptor. This leads to a system of differential equations:

$$\begin{aligned}\frac{\partial c_1}{\partial t} &= D_1\left(\frac{\partial^2 c_1}{\partial x^2}+\frac{\partial^2 c_1}{\partial y^2}\right)+R_1,\\ \frac{\partial c_2}{\partial t} &= D_2\left(\frac{\partial^2 c_2}{\partial x^2}+\frac{\partial^2 c_2}{\partial y^2}\right)+R_2,\end{aligned} \tag{3.39}$$

where $R_1 = -R_2$. This means that the reactions taking place are binding and dissociation between the bound and unbound states. The model of the reactions can be described as:

$$R_2 = -R_1 = \begin{cases} k_a(c_{\max}-c_2)c_1 - k_d c_2, & \text{in the spine head } (y > 0.75\ \mu\text{m}),\\ -k_d c_2, & \text{elsewhere,}\end{cases} \tag{3.40}$$

where k_a is the binding rate and k_d is the dissociation rate in the reactions. The binding only takes place in the head of the spine while the dissociation can occur everywhere in the cell. $c_{\max}$ is the binding site concentration in the spine head. The model has been simulated using FEM in Comsol Multiphysics where it has been mapped onto an analytical geometry, see Figure 3.5.

3.8 Reaction modeling of integrins

In the case of FRAP studies of focal adhesions we study the recovery of fluorescently labeled integrins in these regions. In order to understand this process a turnover rate was calculated by studying the recovery of fluorescence after bleaching as described in Paper VII. The reaction and diffusion system in this case has a strong similarity to the trapping of dopamine 1 receptors in spines; however the dominating mechanism in this system is the reaction that traps integrins in the focal adhesion rather than the diffusion of proteins. The source of integrins being trapped is also to a large extent intracellular rather than in the plasma membrane.

3.8.1 FRAP in a reaction diffusion system

Since the dominating factor in the recruitment of integrins into focal adhesions is a reaction that during the time course of the experiment is dominated by an increase of concentration in the focal adhesion, which is much higher than in the surrounding membrane we can ignore the dissociation and use the simplest form of the reaction diffusion equation:

$$\frac{\partial c}{\partial t} = D\frac{\partial^2 c}{\partial x^2} + R, \tag{3.41}$$

where c is the concentration and R the reaction rate. The time scale of diffusion in this system was seen to be shorter than the time during which the reaction could be observed. By this assumption we can conclude that after a certain time t_D the diffusive term in (3.41) becomes negligible. Thereby the equation for the concentration of integrins in the focal adhesion after the time t_D becomes:

$$\frac{dc}{dt} = R = k(c_{end} - c), \tag{3.42}$$

where k is a reaction rate and c_{end} is the concentration at stationary state. The solution to (3.42), with initial and boundary conditions as described above, is:

$$c(t) = c_{end} - \left(c_{end} - c(t_D)\right)e^{-k(t-t_D)}. \tag{3.43}$$

Curve fitting can determine the parameters c_{end} and k, but this requires a non-linear algorithm. A more statistically reliable method is to do curve fitting for each individual recovery curve and thereby calculate average values of the parameters. This was not possible due to the large amount of noise in the data. By using the estimate of c_{end} from the average for all recovery curves we can calculate $\log\left(c_{end} - c(t)\right)$ and fit this to $-k(t-t_D)+m$, where $m = \log\left(c_{end} - c(t_D)\right)$ and corresponds to the amount of recovery through the described first order reaction. In this case a non-iterative linear curve fit, which is more stable, can be done.

3.9 Fluorescence microscopy

Fluorescence microscopy is a powerful and sensitive technique for real time live cell measurements. Using this method images of cells are recorded by using short wavelength excitation light and detecting longer wavelength emission light with a camera or photomultiplier tube (PMT).

3.9.1 Ratiometric measurements of intracellular calcium

Using fluorescent dyes such as Fura-2, intracellular Ca^{2+} concentrations can be measured. This is done by measuring the ratio of fluorescent intensity at two different excitation wavelengths. In Paper III cells were incubated with Fura-2. During measurements, each image was recorded by exciting sequentially with 340 and 380 nm UV light. The images were detected by a Charge Coupled Device (CCD) camera and 510/45 nm bandpass filter. The absolute intracellular, time dependent Ca^{2+} concentration in such a recording can be calculated by:

$$\left[Ca^{2+}\right] = K_D \frac{R(t) - R_{\min}}{R_{\max} - R(t)} \cdot \frac{F_0}{F_s}, \tag{3.44}$$

where $R(t)$ is the intensity of an image excited by 340 nm at time t pixelwise divided by the image excited by 380 nm at approximately the same time; $R_{\min}$ and $R_{\max}$ are the same ratios calculated at minimum and saturated intracellular Ca^{2+} concentrations, usually taken as average values for a cell. F_0 and F_s are the intensities of images excited by 380 nm at minimum and saturated Ca^{2+} concentrations; K_D is the dissociation constant of Ca^{2+} and Fura-2, approximately equal to 225 nM [9, 81, 140].

3.9.2 Confocal microscopy

A special type of fluorescence microscopes is the laser scanning confocal microscope in which focused laser light is used for excitation; emitted light passes a pinhole and is detected by a PMT. This makes it possible to resolve images in three dimensions. The spatial resolution of a fluorescence microscope is ideally given by the diffraction limit and is approximately equal to half the wavelength of the emission light.

The original idea of confocal microscopy was patented by Minsky in 1961 [141] but it took more than two decades before it was implemented by a research group which today is present at the Applied physics department at KTH [142]. One reason for the long time was the need of laser excitation and computer graphics in order to collect and store the images.

The laser scanning principle, implemented by Carlsson et al. [142], is shown in Figure 3.6. It allows for arbitrary movement of the focus in three dimensions, and thereby for three dimensional volume reconstruction. It is also present in modern, commercially available confocal microscopes [143].

Another confocal technique is two photon microscopy where a nonlinear optical effect allows long wavelength light, usually in the near infrared, to excite fluorophores as if its photon energy was double, that is the wavelength was half. To achieve this nonlinear excitation, highly intense light from a femtosecond laser is used. Two photon microscopy has a higher penetration depth for excitation light than ordinary confocal microscopy and does not require a pinhole [119]. In Paper VIII it is used to record *in vivo* images of NK cells in lymph nodes.

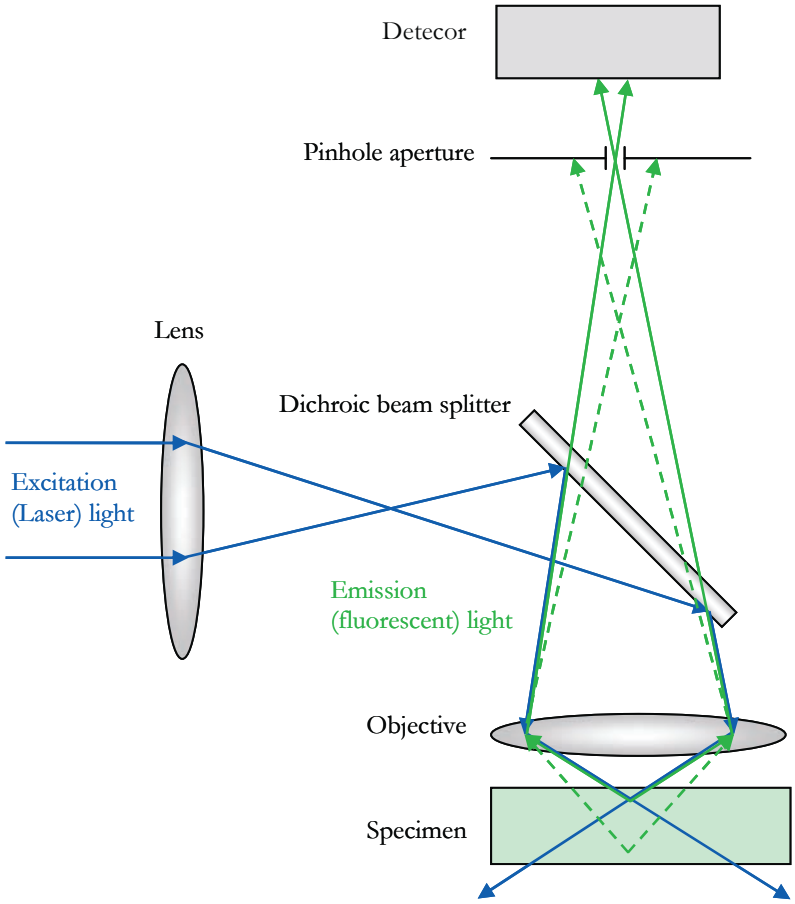

Figure 3.6 This principal drawing of a confocal microscope shows how a laser is focused onto the fluorescent specimen. The short wavelength excitation light is reflected by the beam splitter and focused onto the specimen. In focus emission light (solid line) follows the same path through the objective but passes the beam splitter and is focused onto the pinhole aperture. Out of focus emission light (dashed line) will not pass the pinhole aperture and will therefore not be detected.

3.9.3 Fluorescence recovery after photobleaching

Fluorescence recovery after photobleaching (FRAP) is a method using confocal microscopy to bleach a limited area in the sample. Using this method, the influx of unbleached fluorescent material, known as fluorescence recovery, is studied. In Paper I FRAP has been used to study the movement of dopamine 1 receptors (D1R) in dendrites. Neurons in organotypic striatal cultures were transfected with the fluorescent protein Venus tagged to D1R. An approximately 10 μm long region of the dendrite in a transfected neuron was bleached and the images of the recovery were collected for 5 min by recording a frame every 5 s [19, 144, 145].

The fluorescent signal from the area that had previously been bleached was averaged in each frame and plotted as a function of time. The resulting data is known as the recovery curve and was compared to the theoretical values given by Equation (3.31) as described in Section 3.6.2. From recovery curves the diffusion coefficient was calculated using Equation (3.32).

3.10 Analyzing NK cell migration

To characterize a trajectory of a migrating cell the coordinates in the two dimensional trajectory are given as a discrete series of x and y coordinate pairs separated by a time step Δt. The mean square displacement is then calculated as:

$$\mathrm{MSD}(n\Delta t) = \frac{1}{N-n}\sum_{i=1}^{N-n}\left(\left(x_{i+n}-x_i\right)^2+\left(y_{i+n}-y_i\right)^2\right), \tag{3.45}$$

where N is the number of time steps in the trajectory. By fitting log(MSD) to $\log(n\Delta t)$ an exponent p characterizing the kind of motion can be calculated as $\mathrm{MSD}(n\Delta t) = kt^p$ where the time t is given by $t = n\Delta t$ and $k = 4D$ in the case of random walk in two dimensions. D is the diffusion or migration coefficient. For an ideal random walk $p = 1$ and for straight directed motion $p = 2$, however due to the fluctuating, discrete nature of cell trajectories these numbers show a high variation.

When cells experience an unrestricted random walk their average squared distance from any known location increases linearly with time. Simson et al [20] calculated the probability Ψ for a random walking particle to stay within a region with radius R to be given by:

$$\log\Psi = 0.2048 - 2.5177\frac{Dt}{R^2} \tag{3.46}$$

A probability index L was calculated by

$$L = \begin{cases} -\log\Psi - 1, & \Psi \le 0.1, \\ 0, & \Psi > 0.1 \end{cases} \tag{3.47}$$

and averaged over a varying time window. The total probability index was compared to a threshold level over which it was considered as transiently confined. A transient confinement zone was considered as such when a cell stayed confined over several consecutive time steps. The calculations were implemented in MATLAB®.

4 Results

4.1 Flow profiles in a microchannel

Paper I describes a microstructure device for studying flow induced responses in cells. Here, I will describe the simulations that were done to characterize the flow in the channels of the device. The two geometries, one with two channels crossing each other and one with four channels creating a large opening in the middle of the device, are compared. In the two channel geometry, opening either end of the two channels as an inlet or outlet created the most favorable, uniform profile. Similarly, in the four channels configuration, closing one channel, and having the other three with an inlet and an outlet on each side, created a fairly uniform flow profile.

Additionally to what is presented in Paper I we performed a simulation of convective transport in the device. This allowed us to verify the flow field by performing a similar experiment by adding a fluorescent dye to two of the inlets and taking confocal microscopy images of the device, see Figure 4.1.

4.2 Flow induced build-up of stress

In Paper II we compare the response of Madin-Darby canine kidney (MDCK) cells to fluid flow and how it relates to the bending of cilia and the stress in the membrane surrounding a cilium. To do so a FEM model is compared to an experimental setup where regular step shaped pulses of fluid flow stimulate the ciliated MDCK cells.

The simulations of cilia bending show that the maximum stress in the axoneme occurs where it crosses the plane of the membrane. The stress in the membrane itself is lower than in the axoneme as it is more flexible. As described in Paper II it takes the

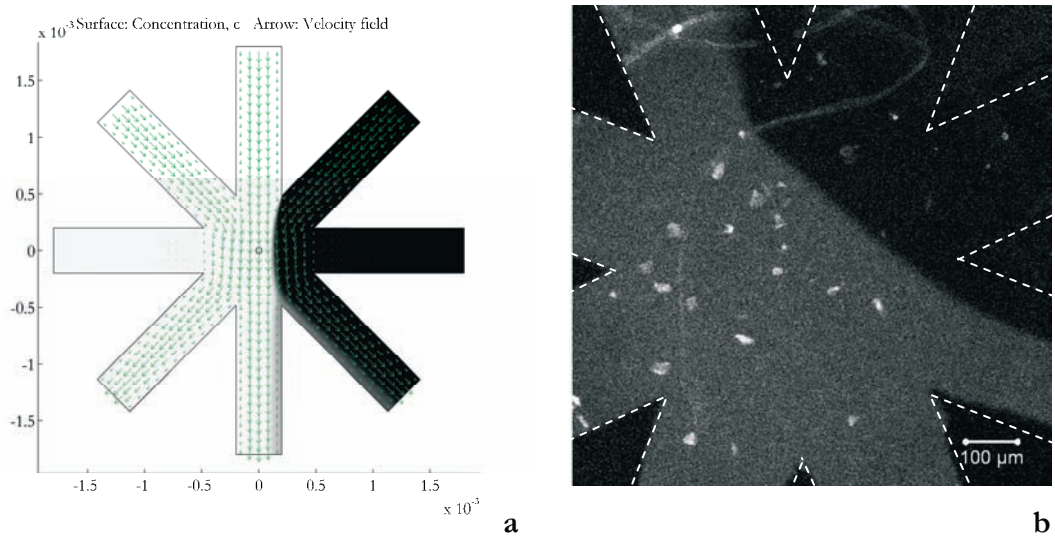

Figure 4.1 Simulated (a) and experimentally verified (b) flow profile in a microfluidic device. The arrows in (a) indicate the magnitude and direction of flow, axes are in metres. The image in (b) is recorded with a 10X/0.3 numerical aperture objective. Dashed lines show overlayed approximate edges of the channels.

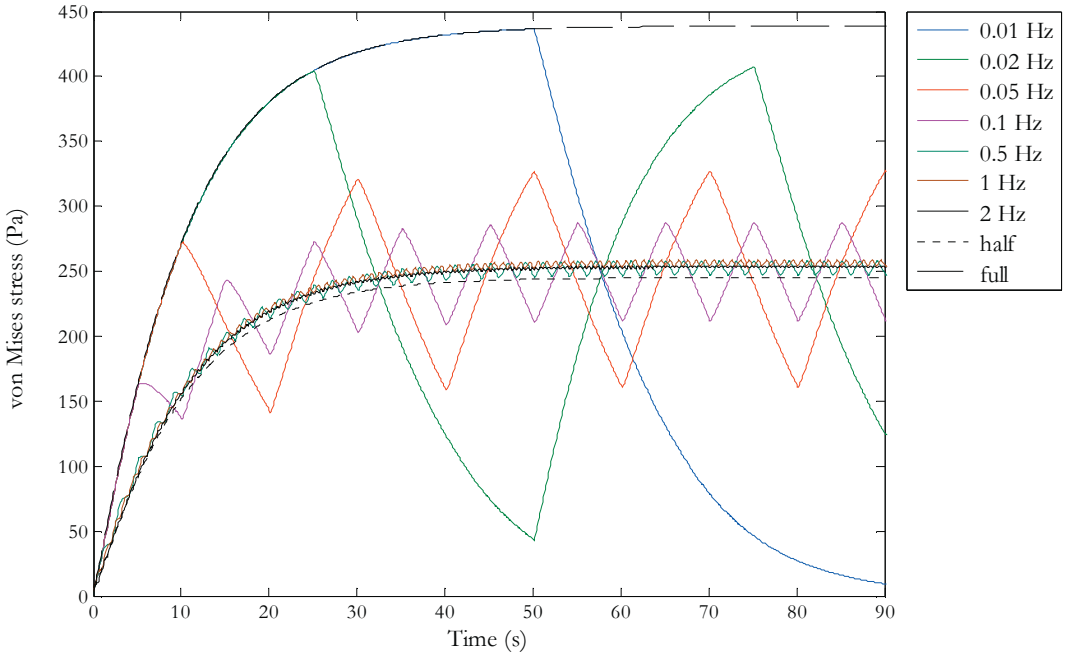

Figure 4.2 Simulated build-up of stress in a small (200 nm) membrane region surrounding the axoneme at different frequencies of pulsed flow and steps functions of full and half strength.

stress in the membrane about 23 s to reach 90% of its maximum while the tip reaches 90% of its displacement in as little as 8 s. This difference corresponds well with our experimental findings that there is a 20-50 s delay between onset of flow and the Ca^{2+} signal.

We also study how single pulses of different duration as well as series of short pulses induce a Ca^{2+} response. The model predicts that the cilium bending and the build-up of stress in the membrane has low pass filter characteristics. We simulate step pulses at different frequencies in time. As the frequency of pulses increases, the stress response approaches that of to a continuous step stimulus with half of the strength of the pulse amplitude. In terms of a low pass filter this means that the ciliated cell only senses the zero-frequency (DC) component of the stimulus. The model's prediction corresponds to the experimental results showing that at half of the flow speed the response is similar to a high frequency (2 Hz) stimulus, see Figure 4.2.

4.3 The impact of store-operated calcium entry on calcium oscillations

In the Ca^{2+} signaling model in Paper III Ca^{2+} oscillations appear mainly as a cyclic exchange of Ca^{2+} between the ER and cytosol. The cause of these oscillations is stimulation of the IP_3R. In the model, this is controlled by changing the parameter $[IP_3]_{max}$. This parameter determines the maximum IP_3 concentration and can be viewed as the strength of an extracellular signal. Figure 4.3 shows the cyclic movement of Ca^{2+} between the two intracellular regions.

4.3.1 Comparing two models of the IP_3 receptor

The two different models of the IP_3R show strikingly different Ca^{2+} oscillations properties, see Fig. 3 and 6 in Paper III. Mainly the DeYoung and Keizer model that is given by Equation (3.12) results in Ca^{2+} oscillations with lower amplitude, but higher frequency than the Mak-McBride-Foskett model of the IP_3R, given by Equations (3.13) and (3.14). Also the DeYoung and Keizer model shows Ca^{2+} oscillations only within a narrow range of IP_3 concentrations, while the Mak-McBride-Foskett model results in Ca^{2+} oscillations for all IP_3 concentrations above 12 nM.

As shown in Figs. 4-6 in Paper III Store-operated Ca^{2+} entry (SOC) has a strong effect on Ca^{2+} oscillations. When SOC, as given by Equations (3.15)-(3.18), is excluded from the model Ca^{2+} oscillations appear in a wider range and with other characteristics using the DeYoung and Keizer description compared to the same model where SOC is included. The effect of excluding SOC from the Mak-McBride-Foskett model is an increase in oscillation frequency above a certain level of IP_3 concentration, where the Ca^{2+} flux out of the ER causes a depletion of ER Ca^{2+} which is sufficient to activate SOC channels.

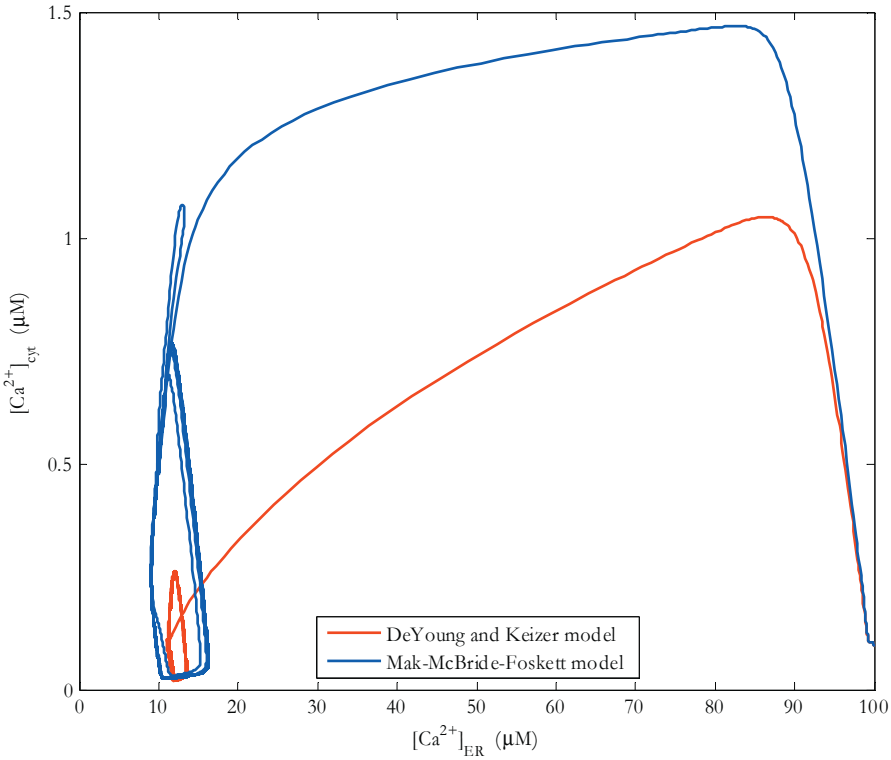

Figure 4.3 Two phase plots showing the cytosolic versus ER Ca^{2+}, corresponding to the two traces in Paper IIIII, Fig. 3. The red curve is based on the De Young and Keizer model of IP_3R and the blue curve on the Mak-McBride-Foskett model. The oscillations appear to the left in the figure, seen as bounded regions where Ca^{2+} is exchanged cyclically between the two compartments. The figure clearly shows the difference in amplitude between the oscillations in the two models, while the period of the oscillations cannot be seen.

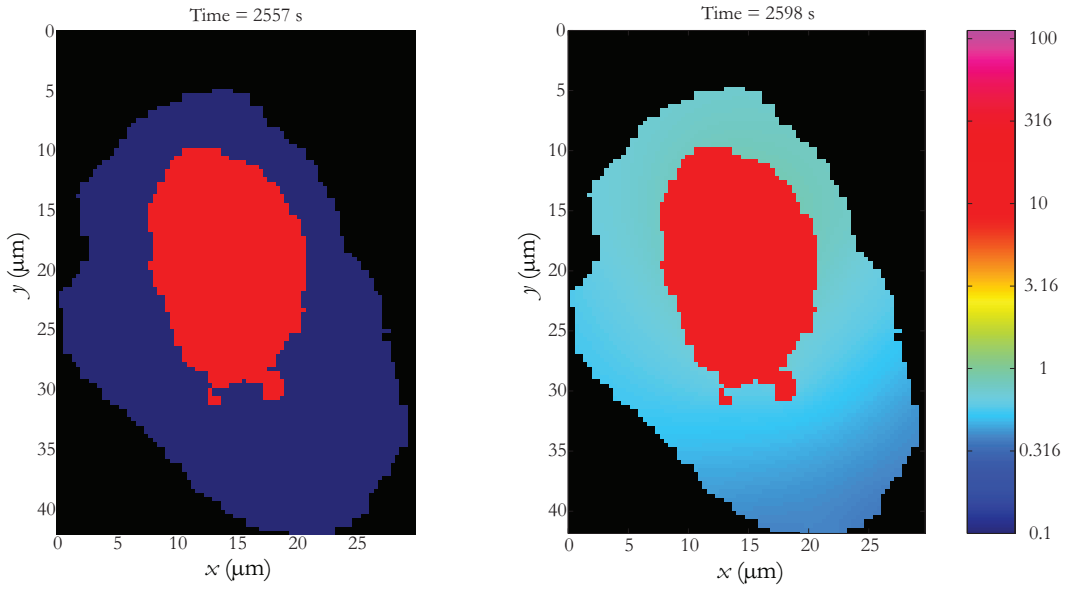

Figure 4.4 The distribution of Ca^{2+} in the modeled cell shown at two points in time. The left panel shows the cells in between two peaks of a Ca^{2+} oscillation while the right panel shows a cell during a peak of cytosolic Ca^{2+} concentration.

4.3.2 Spatial model

In Paper III a compartmental model of Ca^{2+} signaling and oscillations is presented. A similar spatial model has also been constructed using *Virtual Cell*. The IP_3 dynamics model is simplified compared to the compartmental model and does not depend on Ca^{2+}. However, because IP_3 is produced in the plasma membrane and degraded throughout the cytosol, there will be a stationary distribution of IP_3 in the cell. In an irregular geometry this distribution is non uniform. This causes stimulation of IP_3R that is different in different parts of the ER membrane. The results from this model show similar oscillations compared to the model in Paper III. The oscillations in this model show frequencies around 1 mHz. In the current geometry some regions of the cytosol between the ER and plasma membranes are narrow causing large variation in the peak levels of Ca^{2+} concentration within the cytosol. Between peaks the Ca^{2+} concentration is lower and shows a smaller variation, see Figure 4.4.

Figure 4.5a shows the distribution of cytosolic Ca^{2+} concentrations over time and Figure 4.5b shows the distribution of Ca^{2+} concentration in both ER and cytosol integrated over time. To the left in the figure is a darker area showing the oscillations. The wide upper part of this area represents the bursts of Ca^{2+} which are much more distributed than the lower part representing the time in between bursts. As in Figure 4.3 oscillations appear as a closed curve in the lower left part of the panel.

4.3.3 Geometry dependence

As I have shown earlier [18], narrow regions in a geometry can strongly increase the amplitude of Ca^{2+} transients and oscillations. This is a result of geometry and diffusion and can potentially affect reactions in the cell, such as opening of the IP_3R Ca^{2+} channels.

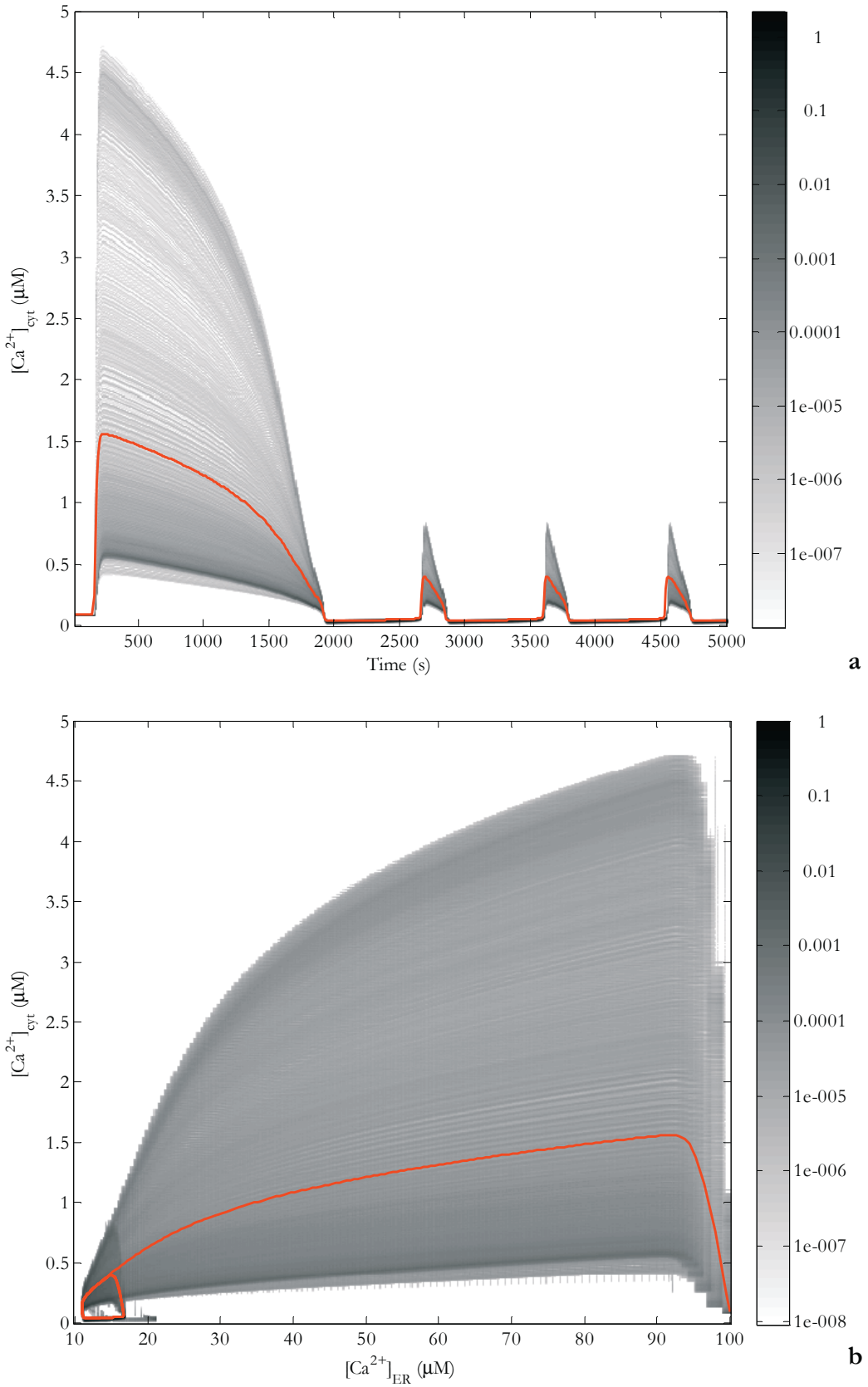

Figure 4.5 (a) Cytosolic Ca^{2+} oscillations in the spatial model. The gray scale shows the distribution of cytosolic Ca^{2+} concentration over time. The red trace shows the mean Ca^{2+} concentration. (b) The same distribution of Ca^{2+} in phase space integrated over time. Dark parts of the diagram indicate that large portions of the cell are in a certain state. Light parts mean that only a small portion of the cell is in that state. The red trace shows the phase plot of the average Ca^{2+} concentration in the two compartments of the cell.

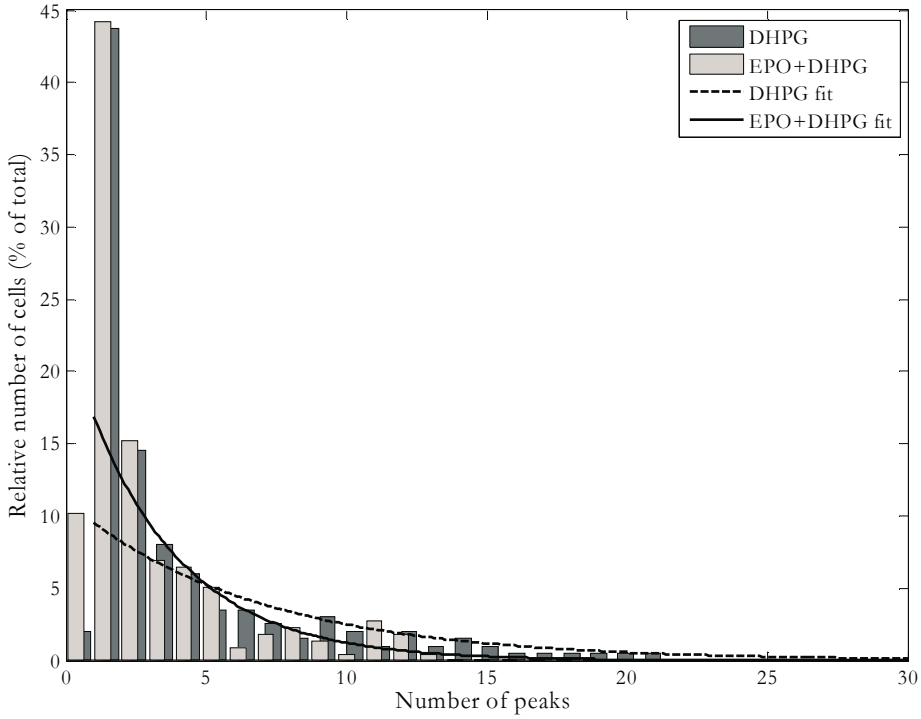

Figure 4.6 The distribution in number of peaks in the Ca^{2+} signal induced by DHPG with and without EPO pre-treatment treatment. The traces show single exponential curve fits to the two distributions excluding the initial bar that shows non-responding cells. The distributions indicate that the pre-treated group has a higher number of non-responding cells and fewer cells having Ca^{2+} signals with many peaks.

4.4 EPO affects calcium signaling in astrocytes

As described in Paper IV the Ca^{2+} signal in the group of astrocytes pre-treated with erythropoietin (EPO) was significantly weaker than in the control group that did not receive pre-treatment. Automatic analysis using spectral analysis showed that 18 % out of the 217 pre-treated cells were oscillating while in the control group 31 % out of the 199 cells were oscillating. Manual analysis of Ca^{2+} peaks showed that 30 % of the cells in the pre-treated group and 40 % of the cells in the control group had at least three peaks. The mean numbers of peaks were 6 in the pretreated group and 8 in the control group. The results also show that 10 % of the pre-treated cells did not respond to DHPG while only 2 % of the control group did not respond. The distribution in number of peaks is shown in Figure 4.6.

4.5 Spatial simulations of K^+ and water in astrocytes and kidney principal cells

Paper V presents a computation model for K^+ regulation and water in kidney principal cells. As mentioned in the discussion of the paper, this can be extended to other asymmetric cells. One such cell type is the astrocyte which has a high non uniform distribution of AQP4 with higher expression in the endfoot region.

Paper V shows that a diffusion limited space (DLS) through its water permeability and small volume can maintain an outward directed driving force for K^+ in a situation where the bulk extracellular space (ECS) has a K^+ concentration which would not allow for this. The dilution of ECS by water maintains a low K^+ concentration in this region and can through the repolarization of the membrane by the outward current drive K^+ in the opposite direction at the part of the basal membrane facing bulk extracellular space. This study also shows that the inclusion of anions such as Cl^-, in the model, has only a weak effect on the dynamics of K^+ and water.

4.6 Trapping of dopamine 1 receptors in neuronal spines

4.6.1 The effective diffusion coefficient of D1R in dendrites

Comparing the analytical solution of the diffusion equation for a dendritic spine with the bleached region given by $2l$ in Equation (3.31) to experimental data shows a strong similarity. Recovery curves from a number of experiments were fitted to the equation using a non-linear least-square regression method by applying the MATLAB® optimization toolbox function **`lsqcurvefit`**, which uses the Levenberg-Marquardt algorithm to fit a curve to the recovery data. The parameters that are calculated by the curve fitting are the diffusion coefficient, the mobile fraction of diffusing receptors and the intensity directly after photobleaching. Because a large fraction of the recovery data curves contained focus drift, which influences the fluorescent intensity in a way completely independent of the diffusion properties of the sample, another method based on the half time of recovery and Equation (3.32) was selected instead. The diffusion coefficient calculated in this way from a large set of recovery data was shown to be 0.80 ± 0.13 $\mu m^2/s$ [19]. Figure 4.7 shows a typical FRAP experiment on a dendrite, with a theoretical recovery curve fitted to the data.

In Paper VI the fluorescence recovery in a dendrite is compared to that of a spine according to the model presented in Section 3.6.2. The recovery of fluorescence in a spine is more rapid than in a dendrite, especially by the end of the recovery curve. Figure 4.8 shows a similar comparison, and also includes the simulated recovery from COMSOL Multiphysics. As can be seen when comparing Equations (3.32), (3.36) and (3.37) the half time of recovery is shortest for the analytical model of the spine, longer for the dendrite, and longest in case of the numerically simulated 2D model of the spine. By the end of the recovery, the 2D model of the spine gains speed compared to the dendrite. This can be understood in terms of fluorescent material being recruited from both directions into the bleached region. In the spine, fluorescent material only enters the region from one direction, but it is not depleted outside of the bleached region to the same extent as in the case of the dendrite. The reason for this is the difference in size between the comparatively large dendrite and the small spine.

4.6.2 Diffusion transports D1R to active spines

The system of combined diffusion and a reaction trapping fluorescent material as given by Equations (3.39) and (3.40) was simulated using COMSOL Multiphysics. Figure 4.9 shows a simulated FRAP experiment on a dendritic spine. The recovery curve is compared to an increase of fluorescent concentration given by the trapping reaction

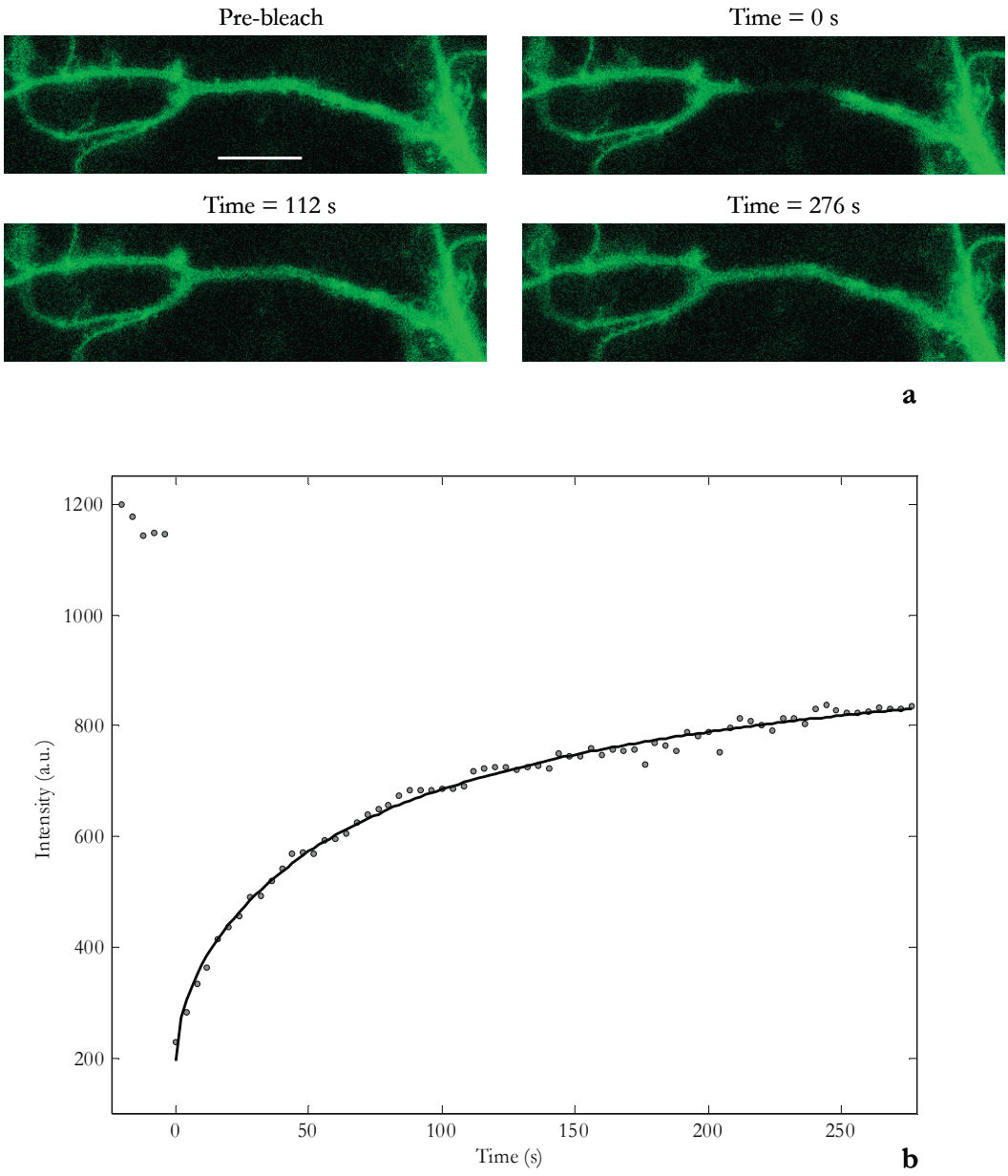

Figure 4.7 (a) Parts of a series of images taken during a FRAP experiment on a dendrite. 0 s is the time directly after bleach and 112 s is the half time of recovery. The scale bar is 10 μm long. (b) The measured FRAP data corresponding to (a) is compared to a fitted, theoretical curve given by Equation (3.31). For this data set, Equation (3.32) and the half time of recovery give a diffusion coefficient of 0.197 $\mu m^2/s$, while curve fitting results in a diffusion coefficient of 0.277 $\mu m^2/s$.

where the initial condition is homogeneous concentration. By varying the diffusion coefficients, D_1 and D_2, the simulations show that when the bound receptor diffuses more slowly than the unbound, the D1R gets trapped in the spine. If D_1 and D_2 instead are equal, then there is no trapping in the spine; the D1R concentration is thus homogeneous.

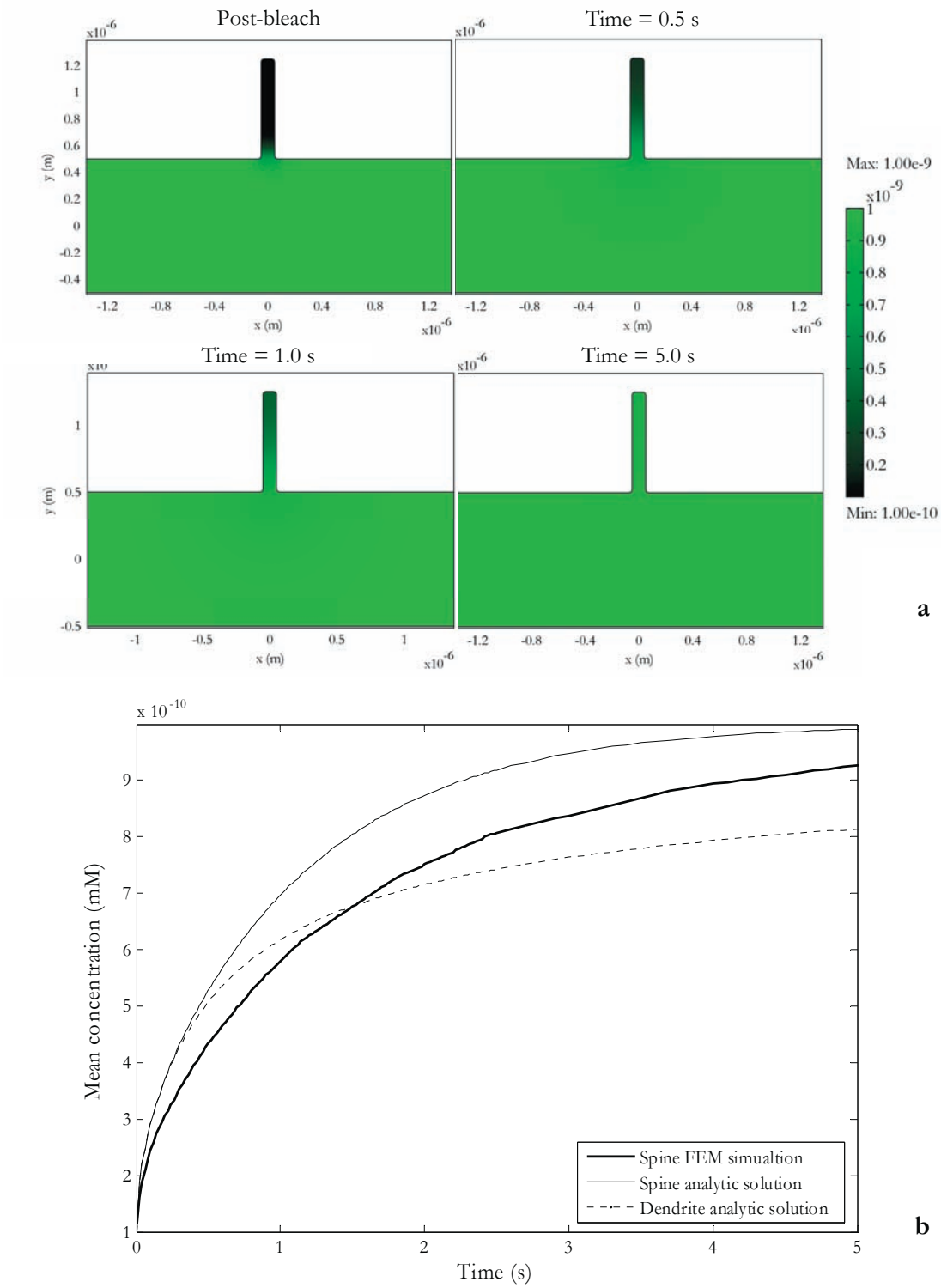

Figure 4.8 (a) Fluorescence recovery in a simulated spine using Comsol Multiphysics. The color scale indicates concentration of fluorophores in mM. (b) The recovery curves of the two models of diffusion in spines. The thick line shows a recovery curve in a simulated FRAP experiment calculated by numerically integrating a FEM solution to the problem. The thin line shows an analytic solution to the one dimensional spine model. The dashed line is the analytical model of a dendrite with a bleached region with the same length as the spine. The parameters are set as $D = 0.2\ \mu m^2/s$ and $l = 0.375\ \mu m$.

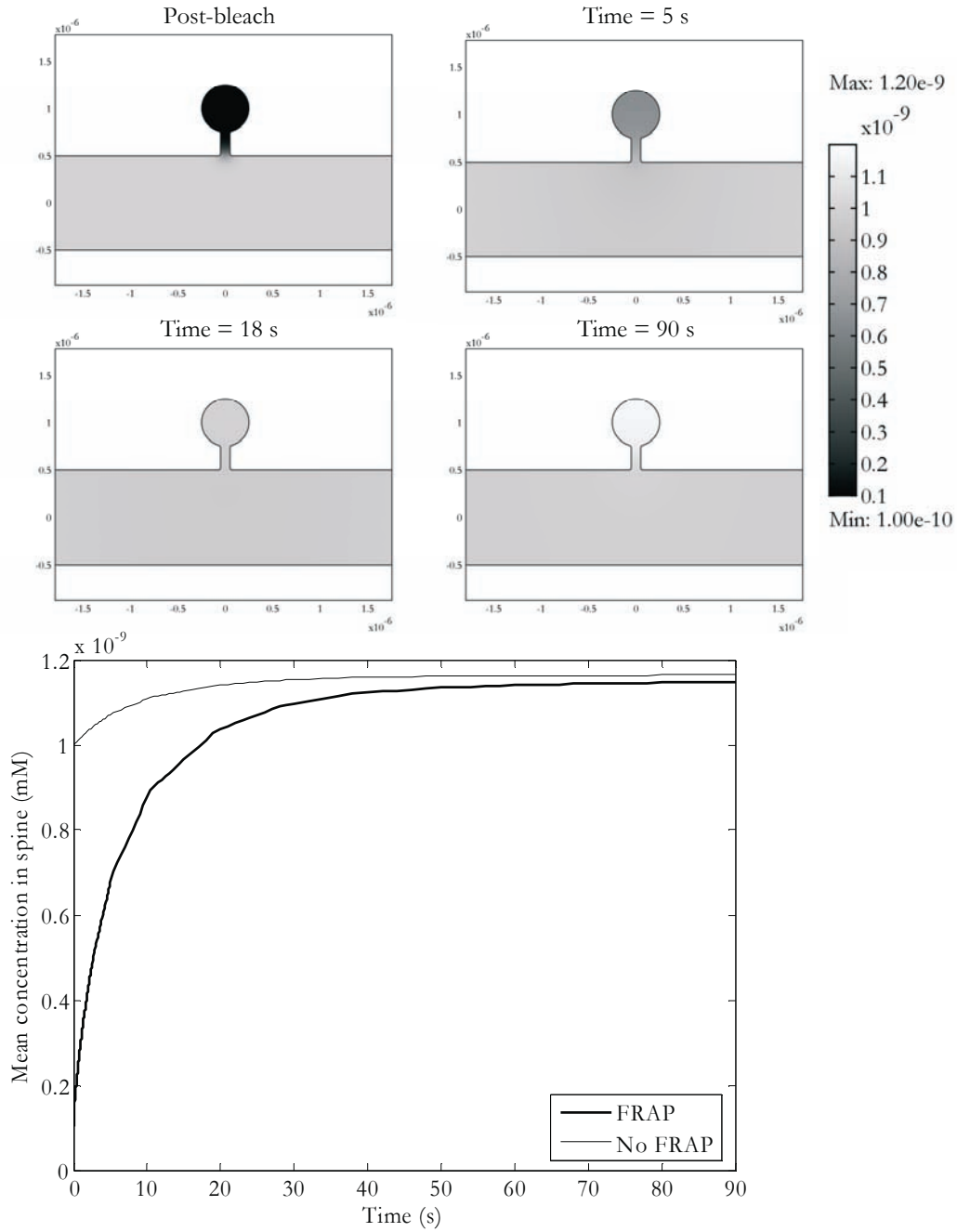

Figure 4.9 A simulated reaction traps diffusing D1R in a spine. The images show a sequence of time frames following initial bleach. After 18 s, fluorescence has recovered fully. The trapping reaction increases the intensity further. The thick curve shows recovery after bleaching while the thin curve shows increase of fluorescence by the trapping reaction alone. The diffusion coefficients are 0.2 $\mu m^2/s$ for the non-trapped substance and five times (0.04 $\mu m^2/s$) smaller for the trapped substance.

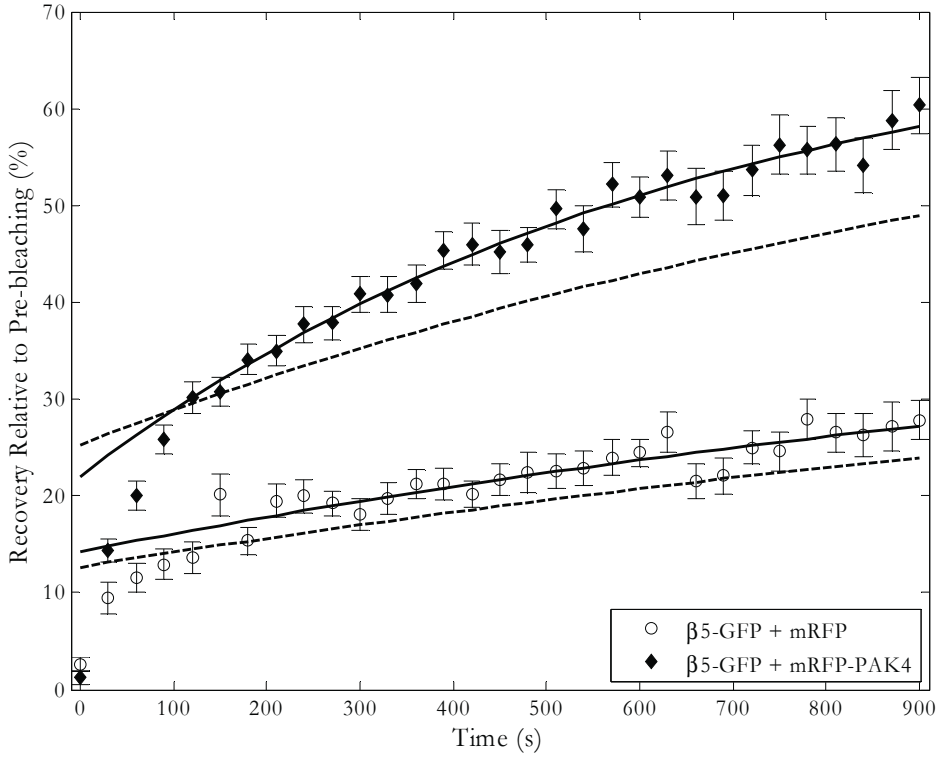

Figure 4.10 FRAP data from bleaching of GFP labeled β5 integrins in focal adhesions with and without PAK4 expression as also presented in Paper VII, Figure 6D. Circles and diamonds indicate average values for each data set and error bars corresponding to standard error. Solid traces show exponential curves fitted to the shown average data starting 2 minutes after bleaching with optimized recovery rates and full recovery values. Dashed lines show the average calculated recovery rates using single exponential functions and curve fitting using a linear algorithm with the same full recovery values as for the solid traces in each case.

4.7 PAK4 modulation of integrin turnover

The results of the calculations described in Section 3.8 show that the rate of recovery with p21-activated kinase 4 (PAK4) is 0.000832 (±0.00010, N = 27) s^{-1} and 0.000511 (±0.000139, N = 25) s^{-1} without PAK4, where the uncertainty is the standard error and N the number of recovery curves. This indicates that the rate of recovery is faster with PAK4 expression than without. The results also show that the amount of recovery through a first order reaction, given by the quantity $c_{\text{end}} - c(t)$ in Equation (3.43), is higher with PAK4 expression than without (44.9±2.8 % compared to 30.7±1.7 % of pre-bleach values).

Figure 4.10 shows the fluorescence recovery of integrins in focal adhesions with and without PAK4 expression. Fitted to the data are curves showing exponential recovery as through first order reactions starting 2 minutes after bleaching as well as curves based on the numbers above. The difference between the two methods is mainly due to the exclusion of recovery curves with data above the final value of recovery. However, the difference is still very clear.

4.8 Transient confinement in NK cell trajectories

In Paper VIII we identify trajectories in the migration pattern of fluorescently labelled NK cells transferred to mice whose lymph nodes were imaged by two-photon microscopy. These are referred to as *in vivo* experiments, while *in vitro* experiments were done by studying 50-100 NK cells in small wells. These cells were studied by recording images once every two minutes for twelve hours. In the *in vitro* setup NK cells could interact with target cells that were fluorescently labelled. This allows for identification of NK cells forming contact with target cells.

4.8.1 Trajectory characteristics

Trajectories of NK cells were characterized by speed of cell migration, characteristics of migration and diffusion (migration) coefficient. MSD curves were calculated as described by Equation (3.45). The exponent of growth for the MSD curves is commonly slightly larger than 1. In the *in vivo* case this was well above 1. This can be interpreted so that there is a certain correlation in direction of migration over time. However, this can also be an effect of short recording times, especially in the *in vivo* case and that the directed movement disappears over a longer time scale.

4.8.2 Transient confinement and conjugate formation

Equations.(3.46)-(3.47) describe a method to identify transient confinement in the trajectory of a random walking particle. For migrating cells these events are commonly referred to as temporary migration arrest periods (TMAP). To identify these periods the probability index was calculated for a time window S_m. The length of this time window as well as the critical probability index (L_c) were varied. As the recording conditions differed for *in vivo* and *in vitro* specimens we could not use the same S_m in both cases. The effect of varying these parameters is summarized in Figure 3 A and D in Paper VIII. For continued analysis $L_c = 3.16$ was used, $S_m = 400$ s was used for *in vivo* and $S_m = 40$ min (2400 s) was used for *in vitro* measurements.

Consecutive time points with a probability index above L_c are considered as belonging to a single TMAP. The time spans and sizes of these TMAPs were calculated by measuring the time between entrance and exit from a TMAP and the radius by calculating the maximal distance from its centre. The radius of a TMAP is typically in the order of 2-5 μm, notably similar to the size of a cell.

The study shows that during a twelve hour recording of NK cells *in vitro* they stop and continue to move several times. The cells normaly had up to four TMAPs during the recording. The *in vivo* recordings are done for a shorter period of time and in that case we almost never see more than two TMAPs for a single trajectory.

5 Discussion

This thesis presents a number of projects where mathematical modeling has been used on cellular systems. The results presented are analytical or numerical solutions to equations that can describe these systems according to physical laws of diffusion and reaction rates.

5.1 Methodological limitations

Biological cells display a complexity which is unparalleled by any other system studied in physics. The large number of interactions in the system requires that any qualitative or quantitative description is greatly simplified. One problem in making quantitative models of biological systems is the lack of good parameter values. In the projects presented in this thesis, parameters have in many occasions been estimated so that steady state occurs in resting systems and that time scales are compatible with experimental results. The complexity in terms of the number of interactions in a system does not necessarily make it unpredictable as the systems are often robust and cooperative [3]. In many cases there exist some key elements which are crucial for the function of a biological system. Identifying these elements may involve both modeling and experiments, calling for an ongoing dialogue between investigators in both these fields.

5.2 Modeling in cellular biophysics

A model always has a limited validity. In the case of biological systems this is perhaps more true than anywhere else, as it is unavoidable to exclude some components (often unknown) from the description. The strategy of simplification has to be done carefully not to exclude important components. In the model of stress build-up for primary cilium, previously overlooked factors were the mechanical properties of the membrane as well as the effect of flow only being present above the surface of the cell. Previous studies had calculated the location of high stress in the cilium [146] in a way that corresponds well with our description. Including the membrane in the model adds the perspective of the actual location of stress sensitive proteins as well as the time scale of the response.

5.2.1 Geometrical influence

The models presented in this thesis work with simplified geometrical descriptions of biological cells and detailed analytical and numerical solutions to reaction-diffusion equations. I believe that this approach is sufficient for drawing conclusions about the importance of some geometrical features present in living cells.

In the Ca^{2+} signaling network model the geometrical description showed qualitatively similar results as the compartmental model, however limited diffusion time results in large spatial variations. It has been suggested that thermal fluctuations, as well as fluctuations in concentration caused simply by a low number of particles taking part in

reactions can be exploited by cells as a way to switch between different states [147]. As the spatial simulations of Ca^{2+} signaling presented in this thesis show, also a deterministic model can have large variations in concentration if the geometry limits diffusion in certain areas. The results also show that the current system is robust enough to maintain its properties, in terms of frequency and shape of the Ca^{2+} peaks, even when there are diffusion limited areas.

One of the studies focuses on dendrites and dendritic spines, where the former case represents an almost ideal system for FRAP studies when the diffusion can be assumed to occur only along one axis. In the later case we have shown that the geometry can have a large influence on the recovery profile as seen in a FRAP experiment. An often overlooked fact when measuring diffusion properties of biological systems is the straight forward scaling law of diffusion, which simply states that the time of diffusion across a volume is proportional to the square of the volume's length scale. I believe this to be an important example where basic ideas of physics and biology can merge.

5.3 Experimental data handling

The large amount of quantitative data produced by today's biological experiments often requires new perspectives when it comes to interpretation and analysis. One of the goals in this thesis is to combine mathematical descriptions and data analysis. The reason for this is that a mathematical model can relate experimental data to a physical phenomenon. In this thesis the trajectories of migrating NK cells are characterized in this manner for us to be able to identify the type of migration that is present.

Large amounts of data need to be analyzed in a more or less automatic way. Except for the obvious reason of time consumption in doing manual data analysis, an automated analysis can be more reliable as it can include strict and controlled criteria rather than risking fuzziness caused by a human observer. This thesis includes methods to automatically characterize Ca^{2+} signals both in MDCK cells where the question is if a response is stronger than the spontaneous background and in astrocytes where we want to know whether a signal is oscillatory or not.

5.4 Conclusions and future perspectives

Mathematical modeling and data analysis are in this thesis applied to different areas in cellular biophysics. The eight studies presented in this thesis all represent various biological questions where a quantitative handling has helped us to identify key parameters and interpret experimental results in more detail than was previously possible.

The flow setup and model of primary cilia in MDCK cells allow us to understand the relevance of mechanical properties of cells and how it affects their biomechanical response to flow at different time scales.

Ca^{2+} signaling and oscillations can be described as a system of contributing channels and pumps leading to slow oscillations in intracellular Ca^{2+}, similar to those observed in experiments. A contributing factor in the oscillating patterns is store-operated Ca^{2+} entry, which affects both qualitative occurrence of oscillations and their characteristics in terms of frequency and amplitude. The system behaves qualitatively similar both when described as a well-stirred compartmental model and as a spatial reaction-diffusion model.

K^+ shunting in the kidney has certain similarities with K^+ spatial buffering by astrocytes. Water following K^+ in this process is considered to cause extracellular shrinkage [16]. As AQP4 is not uniformly distributed in astrocytes [97] there is a possibility for effects similar to those presented in kidney principal cells to also be present in brain

The numerical simulations described in this thesis show how different geometries can affect the fluorescence recovery and that geometrically constrained reactions can trap diffusing receptors in dendritic spines. When separate time scales are present in a FRAP experiment the reaction and diffusion components can be studied separately as presented in Paper VII.

Applying SPT methods to the migration trajectories of NK cells shows that there is a correlation between the formation of conjugates and TCZs in these trajectories *in vitro*. TCZs are also present in the *in vivo* data where they show strong similarities with the *in vitro* situation. This approach represents a novel concept in experimental as well as data analysis methods for tracking immune cells. It is too early to say whether this represents actual cell conjugates *in vivo* as further studies are needed.

Quantum dots are semiconductor particles with a nm scale radius that have a large shift between their conduction and highest valance bands. This property makes them emit light in a new kind of fluorescence that is more stable and has a higher yield than that of organic dyes [148-150]. Previously published [151, 152] as well as ongoing projects in our lab use quantum dots to study single protein molecules and their dynamics in cell membrane and other systems, using SPT. One possible application of this is to use quantum dots to track AQP4 and compare its two different isoforms in terms of single molecule mobility.

The modeling and data analysis tools developed during the work on this thesis partly focus on the spatial and geometrical aspects of cellular biophysics. The characteristics of mathematical modeling are detailed descriptions of dynamic processes. As data from biological experiments increase in resolution and detail, the hypotheses driving the research will have to shift into a more mathematical description.

As a final conclusion I would like to point out that turning biology into physics may risk to change the focus in an unwanted way; an important lesson for someone with a physics or engineering background is that even as methodology is crucial to biology we should not only focus on the methods, as biological questions are not about the methods themselves but about how life functions and about finding its functional key components.

6 Acknowledgements

Many people have been supportive in the work that has lead to the making of this thesis. I would like to give special attention to some of these people:

My encouraging main supervisor Hjalmar Brismar for accepting me as a graduate student, for giving me the opportunity to take part in building a new lab, for believing in my possibilities and for his great ideas.

My two co-supervisors Anita Aperia who is an amazing person with her vast knowledge, understanding, support and inspiration to all people in the lab and Björn Önfelt for his support, encouragement, large engagement and teaching me about the immune system.

My close collaborators in the lab and elsewhere:

Susanna Rydholm for all the fun, hard work and friendship during these years.

Thomas Frisk for all the discussions about tech stuff, ideas and inspiration.

Padideh Kamali-Zare for being my student, co-worker, teacher and close friend and for not forgetting the word *physics* in Cell Physics.

Gordon Zwartz for interesting discussions and collaboration.

Per Uhlén his help, interest, knowledge about Ca^{2+} signaling, sound skepticism and encouragement.

Hiroaki Kitano for inviting me to the Systems biology institute in Tokyo and for his bright ideas.

Eli Gunnarson for her knowledge, great ideas and determinedness that has inspired me not to give up.

Yutong Song for his great ideas and engagement in the aquaporin field.

Marina Zelenina for her great inspiration, skills and knowledge and for always being there when you need her the most.

Lena Scott for her humor, ideas and scientific skills.

Sergey Zelenin for his knowledge, encouragement and inspiration.

Seth Malmersjö for his humor and wide knowledge in both physics and medicine.

Eivor Zettergren-Markus for her expertise and spreading of a good atmosphere around her.

John Lock and Staffan Strömblad for a good collaboration and interesting discussions about focal adhesions, FRAP and modeling.

Bruno Vanherberghen for being a hard working, great biologist who knows everything there is to know about NK cells and for being a very nice person.

Aman Russom for being a great source of inspiration, for his fantastic ideas in microfluidics and always having a piece of advice when I need it.

Linda Csöregh Nord for nice discussions and good collaboration.

Michael D. Cahalan for nice discussion and good collaboration on cell tracking.

Ying Fu and Hans Ågren for a good collaboration and interesting ideas about quantum dots.

Jesper Gantelius for exchanging of ideas about Multiphysics.

Sara Lindström and Helene Andersson Svahn for nice conversations and a good collaboration on the NK cell imaging set up.

Linda Westin for always being nice to talk to and showing a huge interest in science.

Markus Kruusmägi for finally becoming a Mac person and for all the great conversations and exchanging of ideas over the years.

I would also like to thank all other people presently and formerly in the lab: Andreas Sonesson, Gustav Axehult, Kanchana Kankes, Erland Lewin, Victor Akpe, Oleg Aizman, Mark Lal, Xiao-Li Liu, Ann-Christine Eklöf, Juan Li, Ayako Miyakawa, Ulla Holtbäck, Tove Önfelt Tingvall, Mårten Stjernström, Raija Wallenborg, Alexander Bondar, Nina Illarionova, Hans Blom, Karolin Guldevall, Athanasia Christakou, Jovice Boonsing Ng, Sahar Ardbaili, Jonas Hansson, Ali Khorshidi, Hattie Qin, Carolina Fortes Rigos, Georgiy Khodus, Pernilla Grillner, Yanhong Li, Thomas Liebmann, Andreas Ringman Uggla, Nermin Sourial Bassillious, Zuzana Špicarová, Lil-Britt Svensson, Rachel Vieux, Josephine Forsberg, Zachi Horn, Siobhàn Connor and Susanne Crambert for making the days at work a pleasant and inspiring experience.

I would also especially like to thank Rick Rogers for inviting me to his lab in Boston and having great ideas, and Gerald F. DiBona for his help with manuscript reading and being a great source of inspiration.

Thank you also Jerker Widengren, Heike Hevekerl, Gustav Persson, Tor Sandén, Andriy Chmyrov, Johan Strömqvist, Per Thyberg, Lei Xu, Sofia Johansson, Jessica Svennebring and Otto Manneberg in the Experimental Biomolecular Physics and BioX units for nice company and lab sharing.

Gustaf Mårtensson, thank you for patiently discussing basic fluid mechanics with me and for all the other discussion about big and small that we have had.

Other thanks go to my close spare-time friends: Jon and Peter for always being there for me, for coping with me at all times and for helping me with so many practical things.

I would also like to thank my parents, Nina and Jozef, for all support, encouragement, trust and good advice; Ulrica, for always being there for me, for support, comfort, love and understanding; Eva for making me part of your family and being a nice and caring person. Thank you also Inger, Roffe and Wera for your hospitality and generosity; my inspiring and encouraging Polish part of the family: Lesio, Renata, Michał and Ola.

I would finally like to express the loving memory of those who have meant a lot to me but are no longer with us: my courageous and supporting grandparents and the caring and warn-hearted Adi.

7 References

[1] Praetorius, H.A. and K.R. Spring, *The renal cell primary cilium functions as a flow sensor.* Curr Opin Nephrol Hypertens, 2003. **12**(5): p. 517-20.

[2] Weiss, T.F., *Cellular biophysics*. Vol. 1, Transport. 1996: The MIT Press.

[3] Kitano, H., *Computational systems biology.* Nature, 2002. **420**: p. 206-210.

[4] Nauli, S.M. and J. Zhou, *Polycystins and mechanosensation in renal and nodal cilia.* BioEssays, 2004. **26**: p. 844-856.

[5] Han, Y., P. Ganatos, and S. Weinbaum, *Transmission of steady and oscillatory fluid shear stress across epithelial and endothelial surface structures.* Physics of Fluids, 2005. **17**(3): p. 031508.

[6] Schwartz, E.A., M.L. Leonard, R. Bizios, and S.S. Bowser, *Analysis and modeling of the primary cilium bending response to fluid shear.* Am J Physiol Renal Physiol, 1997. **272**(1): p. F132-138.

[7] Hancock, J.T., *Cell signaling.* 1997, Edinburgh Gate, Harlow, Essex, England: Addison Wesley Longman.

[8] Falcke, M., *Reading the patterns in living cells - the physics of Ca2+ signaling.* Adv. Phys., 2004. **53**(3): p. 255-440.

[9] Uhlén, P., *Signal Transduction via Ion Fluxes*, in *Department of Woman and Child Health*. 2002, Karolinska Institutet: Stockholm.

[10] Weiss, T.F., *Cellular biophysics*. Vol. 2, Electrical properties. 1996: The MIT Press.

[11] Zelenina, M. and H. Brismar, *Osmotic water permeability measurements using confocal laser scanning microscopy.* Eur Biophys J, 2000. **29**(3): p. 165-71.

[12] Cornell-Bell, A., S. Finkbeiner, M. Cooper, and S. Smith, *Glutamate induces calcium waves in cultured astrocytes: long-range glial signaling.* Science, 1990. **247**(4941): p. 470-473.

[13] Fall, C.P., E.S. Marland, J.M. Wagner, and J.J. Tyson, eds. *Computational Cell Biology*. 2002, Springer-Verlag: New York.

[14] Connors, N.C., M.E. Adams, S.C. Froehner, and P. Kofuji, *The Potassium Channel Kir4.1 Associates with the Dystrophin-Glycoprotein Complex via α-Syntrophin in Glia.* J. Biol. Chem., 2004. **279**(27): p. 28387-28392.

[15] Orkand, R.K., J.G. Nicholls, and S.W. Kuffler, *Effect of nerve impulses on the membrane potential of glial cells in the central nervous system of amphibia.* J Neurophysiol, 1966. **29**(4): p. 788-806.

[16] Østby, I., et al., *Astrocytic Mechanisms Explaining Neural-Activity-Induced Shrinkage of Extraneuronal Space.* PLoS Comput Biol, 2009. **5**(1): p. e1000272.

[17] Huss, M., *Computational models of lamprey locomotor network neurons*, in *Numerical Analysis and Computer Science*. 2005, KTH.

[18] Kowalewski, J., *Mathematical modelling of intra-cellular Ca^{2+} signalling*, in *Cell physics*. 2003, Royal Institute of Technology: Stockholm.

[19] Scott, L., *Plasticity in the dopamine 1 receptor system : behavior and cell biological studies*, in *Dept. of Woman and Child health*. 2004, Karolinska Institutet: Stockholm. p. 51.

[20] Simson, R., E.D. Sheets, and K. Jacobson, *Detection of temporary lateral confinement of membrane proteins using single-particle tracking analysis*. Biophys. J., 1995. **69**(3): p. 989-993.

[21] Erikson, T. and et al., *Fysikens matematiska metoder*. 1997, Stockholm: Theoretical Physics, KTH.

[22] Kitano, H., ed. *Foundations of Systems Biology*. 2002, The MIT Press: Cambridge, Massachusetts.

[23] Wohlert, J., *Atomistic computer simulations of lipid bilayers*, in *Trita-FYS, 0280-316X ; 2006:82*. 2006, AlbaNova universitetscentrum, Kungliga tekniska högskolan: Stockholm.

[24] Discher, D., et al., *Biomechanics: Cell Research and Applications for the Next Decade*. Annals of Biomedical Engineering, 2009. **37**(5): p. 847-859.

[25] Nauli, S.M., et al., *Polycystins 1 and 2 mediate mechanosensation in the primary cilium of kidney cells*. Nat Genet, 2003. **33**(2): p. 129.

[26] Brannigan, G. and F.L. Brown, *Composition dependence of bilayer elasticity*. J Chem Phys, 2005. **122**(7): p. 074905.

[27] Wiesner, T.F., B.C. Berk, and R.M. Nerem, *A mathematical model of the cytosolic-free calcium response in endothelial cells to fluid shear stress*. PNAS, 1997. **94**(8): p. 3726-3731.

[28] Pänke, O., D.A. Cherepanov, K. Gumbiowski, S. Engelbrecht, and W. Junge, *Viscoelastic Dynamics of Actin Filaments Coupled to Rotary F-ATPase: Angular Torque Profile of the Enzyme*. 2001. **81**(3): p. 1220-1233.

[29] Ainsworth, C., *Cilia: Tails of the unexpected*. Nature, 2007. **448**(7154): p. 638.

[30] Boal, D.H., *Mechanics of the cell*. 2002, Cambridge, UK; New York: Cambridge University Press.

[31] Westermark, P. *Physical biochemistry*. [Study notes] 2002 [cited October 20, 2009]; Available from: http://www.nada.kth.se/kurser/kth/2D1435/2004/forelasnanteckn/F2.pdf.

[32] Hill, A.V., *The possible effects of the aggregation of the molecules of haemoglobin on its dissociation curves*. The Journal of Physiology, 1910. **40**(Suppl): p. iv.

[33] Weiss, J., *The Hill equation revisited: uses and misuses*. FASEB J., 1997. **11**(11): p. 835-841.

[34] Baker, H.L., R.J. Errington, S.C. Davies, and A.K. Campbell, *A Mathematical Model Predicts that Calreticulin Interacts with the Endoplasmic Reticulum Ca2+-ATPase*. Biophys. J., 2002. **82**(2): p. 582-590.

[35] Hodgkin, A.L. and A.F. Huxley, *Resting and action potentials in single nerve fibres*. The Journal of Physiology, 1945. **104**(2): p. 176-195.

[36] Nelson, P., *Biological Physics*. Updated first edition ed. 2008, New York: W. H. Freeman.

[37] Tabeling, P., *Introduction to Microfluidics*. 2005, Oxford: Oxford University press.

[38] Wikipedia, *Navier–Stokes equations*, in *Wikipedia, the Free Encyclopedia*. 2009.

[39] Praetorius, H.A. and K.R. Spring, *Bending the MDCK cell primary cilium increases intracellular calcium*. J Membr Biol, 2001. **184**(1): p. 71-9.

[40] Praetorius, H.A. and K.R. Spring, *A physiological view of the primary cilium*. Annu Rev Physiol, 2005. **67**: p. 515-29.

[41] Praetorius, H.A. and K.R. Spring, *Removal of the MDCK cell primary cilium abolishes flow sensing*. J Membr Biol, 2003. **191**(1): p. 69-76.

[42] Kolb, R.J. and S.M. Nauli, *Ciliary dysfunction in polycystic kidney disease: an emerging model with polarizing potential.* Front Biosci, 2008. **13**: p. 4451-66.

[43] Forman, J.R., S. Qamar, E. Paci, R.N. Sandford, and J. Clarke, *The Remarkable Mechanical Strength of Polycystin-1 Supports a Direct Role in Mechanotransduction.* Journal of Molecular Biology, 2005. **349**(4): p. 861-871.

[44] Yoder, B.K., X. Hou, and L.M. Guay-Woodford, *The Polycystic Kidney Disease Proteins, Polycystin-1, Polycystin-2, Polaris, and Cystin, Are Co-Localized in Renal Cilia.* J Am Soc Nephrol, 2002. **13**(10): p. 2508-2516.

[45] Wiesner, T.F., B.C. Berk, and R.M. Nerem, *A mathematical model of cytosolic calcium dynamics in human umbilical vein endothelial cells.* Am. J. Physiol., Cell Physiol., 1996. **270**(5): p. 1556.

[46] Praetorius, H.A. and K.R. Spring, *A Physiological View of the Primary Cilium.* Annual Review of Physiology, 2005. **67**(1): p. 515-529.

[47] Resnick, A. and U. Hopfer, *Force-response considerations in ciliary mechanosensation.* Biophys J, 2007. **93**(4): p. 1380-90.

[48] Despopoulos, A. and S. Silbernagl, *Color atlas of physiology*. 5th ed. 2003, Stuttgart: Thieme.

[49] Dequidt, C., et al., *Fast Turnover of L1 Adhesions in Neuronal Growth Cones Involving Both Surface Diffusion and Exo/Endocytosis of L1 Molecules.* Mol. Biol. Cell, 2007. **18**(8): p. 3131-3143.

[50] Alberts, B., et al., *Essential cell biology*. 2nd ed. 2004, New York: Galand Science Taylor & Francis Group.

[51] Wikipedia. *Signal transduction - Wikipedia,The Free Encyclopedia*. 2006 [cited March 22nd 2006]; Available from: http://en.wikipedia.org/w/index.php?title=Signal_transduction&oldid=43146521.

[52] Stryer, L., *Biochemistry*. 1999: W. H. Freeman and Company.

[53] Gunnarson, E., et al., *Lead induces increased water permeability in astrocytes expressing aquaporin 4*. Neuroscience, 2005. **136**(1): p. 105.

[54] Singer, S.J. and L. Nicolson, *The Fluid Mosaic Model of the Structure of Cell Membranes.* Science, 1972. **175**: p. 720-731.

[55] Poo, M.-m., *Mobility and Localization of Proteins in Excitable Membranes.* Annual Review of Neuroscience, 1985. **8**(1): p. 369-406.

[56] Nicolau, D.V., Jr., J.F. Hancock, and K. Burrage, *Sources of Anomalous Diffusion on Cell Membranes: A Monte Carlo Study.* Biophys. J., 2007. **92**(6): p. 1975-1987.

[57] Putney, J.W., Jr., ed. *Calcium signaling*. Methods in signal transduction. 2000, CRC Press Boca Raton, Florida.

[58] Berridge, M.J., *Inositol trisphosphate and calcium signalling*. Nature, 1993. **361**(6410): p. 315.

[59] Bezprozvanny, I., J. Watras, and B.E. Ehrlich, *Bell-shaped calcium-response curves of Ins(1,4,5)P3- and calcium-gated channels from endoplasmic reticulum of cerebellum.* Nature, 1991. **351**: p. 751-754.

[60] Taylor, C.W., *Inositol trisphosphate receptors: Ca2+-modulated intracellular Ca2+ channels.* Biochimica et Biophysica Acta (BBA) - Molecular and Cell Biology of Lipids, 1998. **1436**(1-2): p. 19.

[61] Hagar, R.E., A.D. Burgstahler, M.H. Nathanson, and B.E. Ehrlich, *Type III InsP3 receptor channel stays open in the presence of increased calcium.* Nature, 1998. **396**: p. 81-84.

[62] Ramos-Franco, J., M. Fill, and G.A. Mignery, *Isoform-specific function of single inositol 1,4,5-trisphosphate receptor channels.* Biophys. J., 1998. **75**: p. 834-839.

[63] Missiaen, L., et al., *Functional Properties of the Type-3 InsP3 Receptor in 16HBE14o- Bronchial Mucosal Cells.* J. Biol. Chem., 1998. **273**(15): p. 8983-8986.

[64] Hattori, M., et al., *Distinct Roles of Inositol 1,4,5-Trisphosphate Receptor Types 1 and 3 in Ca^{2+} Signaling.* J. Biol. Chem., 2004. **279**(12): p. 11967-11975.

[65] Miyakawa-Naito, A., et al., *Cell signaling microdomain with Na,K-ATPase and inositol 1,4,5-trisphosphate receptor generates calcium oscillations.* J Biol Chem, 2003. **278**(50): p. 50355-61.

[66] Mak, D.-O.D., S. McBride, and J.K. Foskett, *Inositol 1,4,5-tris-phosphate activation of inositol tris-phosphate receptor Ca2+ channel by ligand tuning of Ca2+ inhibition.* PNAS, 1998. **95**(26): p. 15821-15825.

[67] De Young, G.W. and J. Keizer, *A Single-Pool Inositol 1,4,5-Trisphosphate-Receptor-Based Model for Agonist-Stimulated Oscillations in Ca2+ Concentration.* PNAS, 1992. **89**(20): p. 9895-9899.

[68] Mikoshiba, K. and M. Hattori, *IP_3 Receptor-Operated Calcium Entry.* Science's STKE, 2000. **2000**(51): p. 1.

[69] Sneyd, J., J.-F. Dufour, J. Sneyd, and M. Falcke, *A dynamic model of the type-2 inositol trisphosphate receptor.* PNAS, 2002. **99**(4): p. 2398-2403.

[70] Sneyd, J. and M. Falcke, *Models of the inositol trisphosphate receptor.* Progress in Biophysics and Molecular Biology, 2005. **89**(3): p. 207-245.

[71] Parekh, A.B. and J.W. Putney, Jr., *Store-Operated Calcium Channels.* Physiol. Rev., 2005. **85**(2): p. 757-810.

[72] Putney, J.W., Jr, *A model for receptor-regualated calcium entry.* Cell Calcium, 1986. **7**: p. 1-12.

[73] Hoth, M. and R. Penner, *Depletion of intracellular calcium stores activates a calcium current in mast cells.* Nature, 1992. **355**(6358): p. 353.

[74] Parekh, A.B., *Store-operated Ca2+ entry: dynamic interplay between endoplasmic reticulum, mitochondria and plasma membrane.* Journal of Physiology, 2003. **547**(2): p. 333-348.

[75] Randriamampita, C. and R.Y. Tsien, *Emptying of intracellular Ca2+ stores releases a novel small messenger that stimulates Ca2+ influx.* Nature, 1993. **364**(6440): p. 809.

[76] Ma, H.-T., et al., *Requirement of the Inositol Trisphosphate Receptor for Activation of Store-Operated Ca2+ Channels.* Science, 2000. **287**(5458): p. 1647-1651.

[77] Venkatachalam, K., D.B. van Rossum, R.L. Patterson, H.T. Ma, and D.L. Gill, *The cellular and molecular basis of store-operated calcium entry.* Nature Cell Biol., 2002. **4**(11): p. 263-272.

[78] Cahalan, M.D., *STIMulating store-operated Ca2+ entry.* Nat Cell Biol, 2009. **11**(6): p. 669-677.

[79] Alberts, B., et al.,, *Molecular biology of the cell.* 2002: Garland Publising.

[80] Aizman, O., P. Uhlen, M. Lal, H. Brismar, and A. Aperia, *Ouabain, a steroid hormone that signals with slow calcium oscillations.* PNAS, 2001. **98**(23): p. 13420-13424.

[81] Uhlén, P., et al., *α-Haemolysin of uropathogenic E. coli induces Ca2+ oscillations in renal epithelial cells.* Nature, 2000. **405**: p. 694-697.

[82] Berridge, M.J., M.D. Bootman, and P. Lipp, *The versatility and universality of calcium signalling.* Nature Reviews. Molecular Cell Biology, 2000. **1**: p. 11-21.

[83] Tang, Y. and H.G. Othmer, *Frequency encoding in excitable systems with applications to calcium oscillations.* PNAS, 1995. **92**: p. 7869-7873.

[84] Sneyd, J., ed. *Tutorials in mathematical biosciences. 2, Mathematical modeling of calcium dynamics and signal transduction*. Lecture notes in mathematics. Vol. 1867. 2005, Springer: Berlin.

[85] De Koninck, P. and H. Schulman, *Sensitivity of CaM Kinase II to the Frequency of Ca2+ Oscillations*. Science, 1998. **279**(5348): p. 227-230.

[86] Gunnarson, E., *Studies on aquaporin 4, a molecular determinant of brain water homeostasis*, in *Deparment of Woman and Child Health*. 2006, Karolinska Institutet: Stockholm.

[87] Wang, X., T. Takano, and M. Nedergaard, *Astrocytic Calcium Signaling: Mechanism and Implications for Functional Brain Imaging*, in *Dynamic Brain Imaging*. 2009. p. 93-109.

[88] Verkhratsky, A., R.K. Orkand, and H. Kettenmann, *Glial Calcium: Homeostasis and Signaling Function*. Physiol. Rev., 1998. **78**(1): p. 99-141.

[89] Liu, X.L., A. Miyakawa, A. Aperia, and P. Krieger, *Na,K-ATPase generates calcium oscillations in hippocampal astrocytes*. NeuroReport, 2007. **18**(6): p. 597-600.

[90] Gunnarson, E., et al., *Identification of a molecular target for glutamate regulation of astrocyte water permeability*. Glia, 2008. **56**(6): p. 587-96.

[91] Butt, A.M. and A. Kalsi, *Inwardly rectifying potassium channels (Kir) in central nervous system glia: a special role for Kir4.1 in glial functions*. Journal of Cellular and Molecular Medicine, 2006. **10**(1): p. 33-44.

[92] Kofuji, P. and E.A. Newman, *Potassium buffering in the central nervous system*. Neuroscience, 2004. **129**(4): p. 1043.

[93] Amiry-Moghaddam, M., D.S. Frydenlund, and O.P. Ottersen, *Anchoring of aquaporin-4 in brain: Molecular mechanisms and implications for the physiology and pathophysiology of water transport*. Neuroscience, 2004. **129**(4): p. 997.

[94] Amiry-Moghaddam, M., et al., *An α-syntrophin-dependent pool of AQP4 in astroglial end-feet confers bidirectional water flow between blood and brain*. PNAS, 2003. **100**(4): p. 2106-2111.

[95] Amiry-Moghaddam, M., et al., *Delayed K+ clearance associated with aquaporin-4 mislocalization: Phenotypic defects in brains of {alpha}-syntrophin-null mice*. PNAS, 2003. **100**(23): p. 13615-13620.

[96] Nagelhus, E.A., et al., *Immunogold evidence suggests that coupling of K^+ siphoning and water transport in rat retinal Müller cells is mediated by a coenrichment of Kir4.1 and AQP4 in specific membrane domains*. Glia, 1999. **26**(1): p. 47-54.

[97] Nagelhus, E.A., T.M. Mathiisen, and O.P. Ottersen, *Aquaporin-4 in the central nervous system: Cellular and subcellular distribution and coexpression with KIR4.1*. Neuroscience, 2004. **129**(4): p. 905.

[98] Nielsen, S., et al., *Specialized Membrane Domains for Water Transport in Glial Cells: High-Resolution Immunogold Cytochemistry of Aquaporin-4 in Rat Brain*. J. Neurosci., 1997. **17**(1): p. 171-180.

[99] Puwarawuttipanit, W., et al., *Differential effect of α-syntrophin knockout on aquaporin-4 and Kir4.1 expression in retinal macroglial cells in mice*. Neuroscience, 2006. **137**(1): p. 165.

[100] Preston, G.M., T.P. Carroll, W.B. Guggino, and P. Agre, *Appearance of Water Channels in Xenopus Oocytes Expressing Red Cell CHIP28 Protein*. Science, 1992. **256**(5055): p. 385-387.

[101] Agre, P., et al., *Aquaporin CHIP: the archetypal molecular water channel*. Am J Physiol Renal Physiol, 1993. **265**(4): p. F463-476.

[102] Eid, T., et al., *Loss of perivascular aquaporin 4 may underlie deficient water and K+ homeostasis in the human epileptogenic hippocampus.* PNAS, 2005. **102**(4): p. 1193-1198.

[103] Gunnarson, E., et al., *Lead induces increased water permeability in astrocytes expressing aquaporin 4.* Neuroscience, 2005. **136**(1): p. 105-14.

[104] Rodionova, E.A., et al., *Urinary aquaporin-2 in children with acute pyelonephritis.* Pediatr Nephrol, 2006. **21**(3): p. 361-7.

[105] Verkman, A.S., D.K. Binder, O. Bloch, K. Auguste, and M.C. Papadopoulos, *Three distinct roles of aquaporin-4 in brain function revealed by knockout mice.* Biochimica et Biophysica Acta (BBA) - Biomembranes, 2006. **1758**(8): p. 1085.

[106] Zelenina, M., et al., *Urinary aquaporin-2 excretion during early human development.* Pediatr Nephrol, 2006. **21**(7): p. 947-52.

[107] Zador, Z., S. Stiver, V. Wang, and G.T. Manley, *Role of Aquaporin-4 in Cerebral Edema and Stroke.* Handb Exp Pharmacol. , 2009. **190**(Aquaporins): p. 159-170.

[108] Zador, Z., O. Bloch, X. Yao, G.T. Manley, and T.W.a.A.I.R.M. John, *Aquaporins: role in cerebral edema and brain water balance*, in *Progress in Brain Research*. 2007, Elsevier. p. 185.

[109] Furman, C.S., et al., *Aquaporin-4 square array assembly: Opposing actions of M1 and M23 isoforms.* Proceedings of the National Academy of Sciences of the United States of America, 2003. **100**(23): p. 13609-13614.

[110] Gunnarson, E., M. Zelenina, and A. Aperia, *Regulation of brain aquaporins.* Neuroscience, 2004. **129**(4): p. 947-55.

[111] Nagelhus, E.A., et al., *Aquaporin-4 Water Channel Protein in the Rat Retina and Optic Nerve: Polarized Expression in Muller Cells and Fibrous Astrocytes.* J. Neurosci., 1998. **18**(7): p. 2506-2519.

[112] Newman, E.A., D.A. Frambach, and L.L. Odette, *Control of extracellular potassium levels by retinal glial cell K^+ siphoning.* Science, 1984. **225**(4667): p. 1174-1175.

[113] Giebisch, G., S.C. Hebert, and W.-H. Wang, *New aspects of renal potassium transport.* Pflügers Archiv European Journal of Physiology, 2003. **446**(3): p. 289-297.

[114] Sonesson, A., *Lipase diffusion on solid surfaces*, in *Physics*. 2005, Royal Inst. of Technology.

[115] Chudler, E.H. *Brain Facts and Figures.* [cited 2005 November 4, 2005]; Available from: http://www.univ.trieste.it/~brain/NeuroBiol/Neuroscienze%20per%20tutti/facts.html#neuron.

[116] Frye, L.D. and M. Edidin, *The Rapid Intermixing of Cell Surface Antigens After Formation of Mouse-Human Heterokaryons.* J Cell Sci, 1970. **7**(2): p. 319-335.

[117] Axelrod, D., D.E. Koppel, J. Schlessinger, E. Elson, and W.W. Webb, *Mobility measurement by analysis of fluorescence photobleaching recovery kinetics.* Biophys. J., 1976. **16**(9): p. 1055-1069.

[118] Petrie, R.J., A.D. Doyle, and K.M. Yamada, *Random versus directionally persistent cell migration.* Nat Rev Mol Cell Biol, 2009. **10**(8): p. 538-549.

[119] Cahalan, M.D. and I. Parker, *Choreography of Cell Motility and Interaction Dynamics Imaged by Two-Photon Microscopy in Lymphoid Organs.* Annual Review of Immunology. (Free full text manuscript from PubMed Central), 2008. **26**(1): p. 585-626.

[120] Sun, J.C., J.N. Beilke, and L.L. Lanier, *Adaptive immune features of natural killer cells.* Nature, 2009. **457**(7229): p. 557-561.

[121] Choquet, D. and A. Triller, *The role of receptor diffusion in the organization of the postsynaptic membrane*. Nat Rev Neurosci, 2003. **4**(4): p. 251.

[122] Dahan, M., et al., *Diffusion Dynamics of Glycine Receptors Revealed by Single-Quantum Dot Tracking*. Science, 2003. **302**(5644): p. 442-445.

[123] Choquet, D. and A. Triller, *The Role of Receptor Diffusion in the Organization of the Postsynaptic Membrane*. Nat Rev Neurosci, 2003. **4**(4): p. 251-265.

[124] Ribrault, C., A. Triller, and K. Sekimoto, *Diffusion trajectory of an asymmetric object: Information overlooked by the mean square displacement*. Physical Review E (Statistical, Nonlinear, and Soft Matter Physics), 2007. **75**(2): p. 021112.

[125] Holcman, D. and A. Triller, *Modeling Synaptic Dynamics Driven by Receptor Lateral Diffusion*. Biophys. J., 2006. **91**(7): p. 2405-2415.

[126] Liu, W., et al., *Effect of flow and stretch on the $[Ca^{2+}]_i$ response of principal and intercalated cells in cortical collecting duct*. Am J Physiol Renal Physiol, 2003. **285**(5): p. F998-1012.

[127] Marcelli, G., K.H. Parker, and C.P. Winlove, *Thermal Fluctuations of Red Blood Cell Membrane via a Constant-Area Particle-Dynamics Model*. 2005. **89**(4): p. 2473-2480.

[128] *Structural Mechanics Module User's Guide*, in *COMSOL Multiphysics 3.2*. 2005: Stockholm.

[129] Hallén, K., M. Huss, P. Kettunen, A. El Manira, and J. Hellgren Kotaleski, *mGluR-Mediated calcium oscillations in the lamprey: a computational model*. Neurocomputing, 2004. **58-60**: p. 431-435.

[130] Fink, C.C., B. Slepchenko, and L.M. Loew, *Determination of Time-Dependent Inositol-1,4,5-Trisphosphate Concentrations during Calcium Release in a Smooth Muscle Cell*. Biophys. J., 1999. **77**(1): p. 617-628.

[131] Slepchenko, B.M., J.C. Schaff, J.H. Carson, and L.M. Loew, *Computational Cell Biology: Spatiotemporal Simulation of Cellular Events*. Annu. Rev. Biophys. Biomol. Struct., 2002. **31**(1): p. 423-441.

[132] Fink, C.C., et al., *An Image-Based Model of Calcium Waves in Differentiated Neuroblastoma Cells*. Biophys. J., 2000. **79**(1): p. 163-183.

[133] Westermark, P., *Physical biochemistry*. 2002.

[134] Kummer, U., et al., *Switching from Simple to Complex Oscillations in Calcium Signaling*. Biophys. J., 2000. **79**(3): p. 1188-1195.

[135] Goldbeter, A., *Computational approaches to cellular rhythms*. Nature, 2002. **420**(6912): p. 238-245.

[136] *The Matlab documentation*. 2003 [cited 2005 May]; Available from: http://www.mathworks.com/access/helpdesk/help/techdoc/matlab.html.

[137] Shampine, L.F. and M.W. Reichelt. *The Matlab ODE suite*. [cited 2006 February 7]; Available from: http://www.mathworks.com/access/helpdesk/help/pdf_doc/otherdocs/ode_suite.pdf.

[138] Heath, M.T., *Scientific computing: an introductory survey*. Computer science series. 1996, Singapore: McGraw-Hill.

[139] Schaff, J., et al. *The Virtual Cell Portal*. [cited 2005 May]; Available from: http://www.vcell.org.

[140] Uhlén, P., *Spectral analysis of calcium oscillations*. Sci STKE, 2004. **2004**(258): p. pl15.

[141] Minsky, M., *Microscopy apparatus*, in *3013467*. 1961: US patent.

[142] Carlsson, K., et al., *Three-dimensional microscopy using a confocal laser scanning microscope*. Opt. Lett., 1985. **10**(2): p. 53-55.

[143] Pawley, J.B., ed. *Handbook of biological confocal microscopy*. 2006, Springer: New York.

[144] Kruse, M.S., et al., *Recruitment of renal dopamine 1 receptors requires an intact microtubulin network*. Pflugers Arch, 2003. **445**(5): p. 534-9.

[145] Scott, L., et al., *Selective up-regulation of dopamine D1 receptors in dendritic spines by NMDA receptor activation*. Proc Natl Acad Sci U S A, 2002. **99**(3): p. 1661-4.

[146] Resnick, A. and U. Hopfer, *Mechanical stimulation of primary cilia*. Front Biosci, 2008. **13**: p. 1665-80.

[147] Rao, C.V., D.M. Wolf, and A.P. Arkin, *Control, exploitation and tolerance of intracellular noise*. Nature, 2002. **420**(6912): p. 231.

[148] Wikipedia, *Quantum dot*, in *Wikipedia, the Free Encyclopedia*. 2009.

[149] Triller, A. and D. Choquet, *New Concepts in Synaptic Biology Derived from Single-Molecule Imaging*. Neuron, 2008. **59**(3): p. 359-374.

[150] Walling, M., J. Novak, and J.R.E. Shepard, *Quantum Dots for Live Cell and In Vivo Imaging*. International Journal of Molecular Sciences, 2009. **10**(2): p. 441-491.

[151] Fu, Y., et al., *Radiative and nonradiative recombination of photoexcited excitons in multi-shell-coated CdSe/CdS/ZnS quantum dots*. EPL (Europhysics Letters), 2009(3): p. 37003.

[152] Sonesson, A.W., U.M. Elofsson, T.H. Callisen, and H. Brismar, *Tracking Single Lipase Molecules on a Trimyristin Substrate Surface Using Quantum Dots*. Langmuir, 2007. **23**(16): p. 8352-8356.

Appendix A: Object Oriented Reaction toolbox documentation

Object Oriented Reaction toolbox (*OOR toolbox*) is a MATLAB® toolbox for creating and simulating chemical reactions involving one or more compartments. Models are built up by species localized in compartments. Reactions connect the species by describing them as reactants, product or catalysts. *OOR toolbox* is fully integrated, and created in MATLAB®, making it possible to automate changing of model properties such as reaction pathways and parameter values from a MATLAB® script or the command line interface. The structure of models built in *OOR toolbox* is similar to the structure of *The Systems Biology Markup Language* (SBML) [1, 2]. *OOR toolbox* uses MATLAB® m-functions, as well as anonymous and inline functions, to define rules. This makes it possible to construct more general models than are easily created using SBML. At this time *OOR toolbox* is not compatible with SBML. The interested reader may see the SBML toolbox for MATLAB® [3] which can import, manipulate and simulate SBML models in MATLAB®.

A model is created in *OOR toolbox* using the object oriented command line interface in MATLAB®. A model is an object containing several other objects such as compartments, species, and reactions. These objects are created and combined using special m-functions called methods. A method is a function working on an object. Methods are defined for a certain class, a type definition and description of that type of objects [4].

A.1 Object structure

The classes in *OOR toolbox* are **`model, comp`** (compartment), **`species`**, **`reaction`**, **`transport`** (a subtype of reaction), and **`speciesref`** (reference to a species object). The transport object works similarly to flux reactions in *Virtual Cell* [5]. Each class has methods which can be called from within MATLAB® as long as the OOR directory is in the search path. Observe: The class directories do not have to be added to the search path. A special method is the constructor which has the same name as the class; it is used to define a new object of that class.

The most fundamental object in *OOR toolbox* is a **`model`**. In most cases modeling in *OOR toolbox* begins with a call to the **`model`** constructor. Other objects such as compartments, species and reactions are added to a model using the **`add`** method, see below. The model object contains all other objects used in the calculation. Species and reactions added to a model are automatically numbered and can be referred to by number. Compartments are not number, and are only possible to refer to by name. Species can be referred to either by number or hierarchically in the form **`model.compartment.species`**. Reactions describe dynamical properties of the model and connect species by containing references to them either as reactants, products or catalysts. Reactions contain function handles or inline objects that express the rate of conversion from reactants to products as a function of the concentration of each species referred to by the reaction object. Reaction rates can also depend on a number of parameters contained in the model. The structure of an *OOR toolbox* model follows similar principles as those described by the SBML definition [2].

A.1.1 Simulations

A model can in principle describe different kinds of dynamics, not necessarily by compartmental models and ordinary differential equations (ODEs). *OOR toolbox* takes advantage of the flexible type definitions in MATLAB® so that a species concentration can be either a scalar, to express its initial amount, a vector, to express a time series, or an array of any number of dimensions to express e.g. a spatial dependence. Presently the only implemented kind of simulation is an interface to MATLAB®'s ODE solvers. This interface is the **`odesim`** method in the **`model`** class. It simulates the dynamics of a model expressing it as a system of ODEs, see below. The output of **`odesim`** is a new model object containing the same species and reaction objects as before but with species concentrations replaced by the times series corresponding to the numerical solution to the system of ODEs.

A.2 Class definitions

A.1.2 Model class

Constructor

`model(mod)`
constructs a new empty model object or uses the persistent one if it exists. If the argument mod is specified, the new model is a copy.

Methods

`add(mod,comp)`
adds a compartment to a model **`mod`**.

`add(mod,spec)`
adds a species **`spec`** to a model **`mod`**. The species **`spec`** is added to its compartment. If it has not yet been assigned a number, this function does that. An already numbered **`spec`** replaces an old species with that number. A species with a name and compartment already present in **`mod`** replaces the old species with the same name and compartment.

`add(mod,reaction)`
adds a reaction to a model.

`add(mod,params)`
adds parameters to **`mod`** contained in the structure **`params`**.

`str = char(mod)`
converts **`mod`** to string **`str`** containg detailed information about the model.

`N = getcouplings(mod)`
returns the couplings matrix of the model mod. It differs from the stoichiometry matrix in the way that it includes information on compartment sizes in transport reactions.

spec = getspecies(mod,n)
gets species from a model. Returns species **n** (1 or more if **n** is non-scalar) from the model. If **n** is not assigned, all species are returned.

N = getstoich(mod)
returns the stoichiometry matrix of the model **mod**. The size of **N** is (the number of species) × (the number of reactions) in **mod**.

odesim(mod,time,odesolver)
simulates a model during the time span **time**, using **odesolver**. If **time** is scalar and **time** is within the time span of **mod.time**, a model which is equal to **mod** at a time close to **time** will be returned. If **odesolver** is not specified **ode15s** is selected.

h = plot(mod,x,varargin)
plots species concentrations or flux rates in a model. **x** is either a species, a flux or the string **'time'**. The following arguments can be species, species references, or reactions. The returned value **h** is a handle to graphics objects as in the built in **plot** function. If **x** is not specified, all concentrations will be plotted as functions of time.

x = subsref(A,s)
returns a species object when called as **A.<compartmentname>.<speciesname>**. Called as **A.<compartmentname>** this method returns a compartment object. In other cases this method returns any field from a model **A**. E.g. **A.params** returns a structure of parameters and **A.time** returns the time vector of **A**.

A.1.3 Compartment class

Constructor

comp(name,size,outside,dim,varargin)
defines a new **comp** object. **name** is a string, **size** is a number, and **dim** is an integer describing the number of dimension of the new compartment.

Methods

addspec(c,spec)
adds a species to a compartment. The species **spec** is added to **c**. This method is mainly used by the **add(species)** method in the model class.

str = char(c)
returns the name of **c**.

setspecies(c,spec)
sets the species reference vector of a compartment to **spec**.

A.1.4 Species class

Constructor

species(name,comp,conc,charge,unit,varargin)
defines a species object. A species has a name, a compartment, a concentration, a charge and a concentration unit. To have the same species in several compartments, a

list of compartments can be given with corresponding concentrations. The name is compulsory, the rest can be set to default values.

Methods

`str = char(s,format)`
converts the species **`s`** to a charater string **`str`**. If the concentration is an array it will be displayed as the size and type of data. **`format`** can be one of **`'long'`**, **`'short'`** **`'context'`** and **`'conc'`**. **`'long'`** is the default.

`display(s)`
prints **`char(s)`** in the command window.

`n = getnumber(spec)`
returns the numbers of spec as a vector.

`[mtimes] specref = n*species`
returns a speciesref **`specref`** where the stoichiometry is multiplied by **`n`**.

`[plus] specref = s1 +s2`
creates a speciesref merged from **`spec1`** and **`spec2`**. Equal references are summed. This is a kind of algebraic sum intended for stoichiometry modeling.

`setconc(s,c)`
sets the concentration of a species **`s`** to **`c`**.

`setnumber(s,n)`
sets the number of a species **`s`** to **`n`**.

A.1.5 Species reference class

Constructor

`speciesref(s,n)`
constructs a **`speciesref`** object. **`s`** can be a species vector, **`speciesref`** or a $N\times2$ matrix containing species numbers in the first and stoichiometries in the second column. The stoichiometry vector **`n`** is set to 1 by default and may be excluded.

Methods

`str = char(s,format,mod)`
converts **`s`** to string **`str`** using format. See also **`species/char`**.

`[mtimes] specref = n*spesref`
creates a species reference where the stoichiometry is multiplied by **`n`**.

`[plus] specref = specref1 + specref2`
creates **`specref`** merged from **`specref1`** and **`specref2`**. Equal references are summed. This is a kind of algebraic sum intended for stoichiometry modeling.

A.1.6 Reaction class

Constructor

`reaction(rule,reactants,products,catalysts,varargin)`
constructs a reaction object that can be added to a model. **`rule`** is a function handle, **`reactants`**, **`products`** and **`catalysts`** are species or species references. Additional arguments should be strings containing names of the parameters for the reaction object.

Methods

`str = char(r)`
returns the name of **`r`**.

`str = char(r,mod)`
converts **`r`** to a longer string containing information about the references from **`r`** to the model **`mod`**.

`display(r)`
prints **`char(r)`** in the command window.

`setnumber(r,n)`
sets the number of a reaction **`r`** to **`n`**.

`setrule(r,rule)`
sets the rule of a reaction **`r`** to **`rule`**.

`subsref(r,x)`
returns a vector **`rate`** containing the flux by **`r`** at every time in **`x.time`** when called as **`rate = r(x),`** where **`x`** is a **`model`**. Otherwise this is a general **`subsref`** method which returns any field name **`x`** from the reaction **`r`**.

A.1.7 Transport class

Constructor: `transport(rule,comp1,comp2,specs,varargin)`

creates a transport reaction involving species **`specs`** going from compartment **`comp1`** to **`comp2`**. **`transport`** is a subclass of **`reaction`**. Additional arguments are strings containing names of the parameters for the transport object.

Method: `setcomps(t,comp1,comp2)`

sets the compartments of **`t`** to **`comp1`** and **`comp2`**.

A.3 Example: Ca^{2+} signaling model

Below follows a MATLAB® script and some functions that together use the *OOR toolbox* to create the Ca^{2+} signaling model presented in Paper II.

A.1.8 Script

```
% CA_SIGNALING script defines the model object.
% Creates a model and runs a Matlab simulation of intracellular
% Ca-signaling.
%
% Jacob Kowalewski 2006

clear setmodel params SOCt Cell
Cell_ID = length(dir('Cell*.mat'))+1

OORpath = pwd;
OORpath = [OORpath(1:length(OORpath)-6) 'OOR']
addpath(OORpath);

tic
params.X=0.4;
params.Y=0.6;
params.r1=0.185;

params.v2=0.002;
params.V_IP3R=0.7*0.1;
params.K_inf=52;
params.IP3R_actCa=210E-3;
params.K_IP3=50E-3;

params.d1=0.13;
params.d2=0.5;
params.d3=9.4E-3;
params.d5=82.34E-3;
params.v1=10;

params.VmaxPMCA=0.245*0.6;
params.VmaxSERCA=0.95*2;
params.K05=0.2;
params.K05_SERCA=0.5;
params.V_SOC=5E-3;
params.leak_PM=1.2E-5;

params.I_deg=0.01;
params.I_R=0.01;
params.period_IP3=5000;
params.T_IP3prod=3000;
params.IP3max= 40E-3

params.k_G=0.2;
params.G_max=1;
params.G_deg=0.5;

params.kZ=2e-4;
params.Zmax=0.1;
params.kSOC=1.7;
params.I_SOC=0.002;
params.Ca_ER_min=10;
params.vZ=1

Cell = model;
Cell = add(Cell,params);
```

```
Cell = add(Cell,comp('EC',inf));
Cell = add(Cell,comp('PM',1/params.r1,'EC'));
Cell = add(Cell,comp('cyt',1/params.r1,'PM'));
Cell = add(Cell,comp('ER',1,'cyt'));

% Initial conditions

Cell = add(Cell,species('Ca',{'cyt','ER','EC'},{0.095,100,10000*0.095},2));
Cell = add(Cell,species('IP_3',Cell.cyt,1E-9,0));
Cell = add(Cell,species('G',Cell.cyt,0));
Cell = add(Cell,species('Z',{'cyt','ER'},{0,0.1}));
Cell = add(Cell,species('SOC','PM',0));

% Reactions
r_SERCA =
transport(@SERCA,Cell.cyt.Ca,Cell.ER.Ca,[],'VmaxSERCA','K05_SERCA','Y');

r_PMCA = transport(@PMCA,Cell.EC.Ca,Cell.cyt.Ca,[],'VmaxPMCA','X','K05');

r_IP3RMak = transport(@IP3RMak,Cell.cyt.Ca,Cell.ER.Ca,Cell.cyt.IP_3,'v2',
...
                     'V_IP3R','K_inf','IP3R_actCa','K_IP3');
r_IP3R = transport(@IP3R,Cell.cyt.Ca,Cell.ER.Ca,Cell.cyt.IP_3, ...
                'v2','d1','d2','d3','d5','v1');
r_SOC = transport(@SOC,Cell.EC,Cell.cyt,'Ca',Cell.PM.SOC, ...
                     'V_SOC','leak_PM');
r_RyR = transport(@RyR,Cell.ER.Ca,Cell.cyt.Ca,[],'vRyR','Ka','Kb', ...
               'Kc');

Grule = inline('k_G*Ca - G_deg*G','G','Ca','k_G','G_deg','t')
IP3rule = inline('G_signal_loop(t,G,G_max).*IP3max*I_deg -
I_deg*IP3','IP3','G','IP3max','I_deg','G_max','t')

Cell = add(Cell,r_PMCA);
Cell = add(Cell,r_SERCA);
Cell = add(Cell,r_IP3R);
%Cell = add(Cell,r_IP3RMak);
Cell = add(Cell,r_SOC);

Cell = add(Cell,reaction(Grule,[],Cell.cyt.G,Cell.cyt.Ca,'k_G','G_deg'));
Cell =
add(Cell,reaction(IP3rule,[],Cell.cyt.IP_3,Cell.cyt.G,'IP3max','I_deg','G_ma
x'));

Cell = add(Cell,reaction(@Zprod,[],Cell.ER.Z,[],'kZ','Zmax'));
Cell = add(Cell,transport(@SOCbind,Cell.cyt.Z,Cell.PM.SOC,[],'kSOC'));
Cell = add(Cell,reaction(@SOCdegrad,Cell.PM.SOC,[],[],'I_SOC'));
Cell = add(Cell,transport(@Ztransp,Cell.ER,Cell.cyt,'Z', ...
                     Cell.ER.Ca,'Ca_ER_min','vZ'));

% Simulate the whole thing
Cell = setmodel(Cell);
spec=getSpecies(model)

Cell=odesim(Cell,[0 7000],@ode15s)
filename = ['Cell_' num2str(Cell_ID)]
figure(1)
plot(Cell,'t',Cell.cyt.Ca,Cell.cyt.IP_3)
save(filename,'Cell');
```

A.1.9 Functions describing the transporters

```
function signal=G_signal_loop(t,G,G_max)
n=1;
signal=(t>500)*G_max*(1-Hill(G,n,G_max/2));

function flux=Hill(c,n,c_05)
% Hill-type flux equation

flux=c.^n./(c.^n + c_05^n);
function J=IP3R(CaCyt,CaER,IP3,v2,d1,d2,d3,d5,v1,t)
%global v2 V_IP3R K_inf IP3R_actCa K_IP3 d1 d2 d3 d5 v1;
%J=-(CaER-CaCyt)*(v2+v1*(d2*IP3*exp(-((CaCyt-0.6)/0.2)^2)));

%H_inh=4;
%H_act=2;
%H_IP3=4;
%IP3R_inhCa=K_inf./(1 + (K_IP3./IP3).^H_IP3);
%J=-(CaER-CaCyt).*(v2 + V_IP3R./((1 + (IP3R_actCa./CaCyt).^H_act) .* ...
%                          (1 + (CaCyt./IP3R_inhCa).^H_inh)));
J=-(CaER-CaCyt).*(v1*(CaCyt.*IP3*d2./((CaCyt.*IP3 + IP3*d2+d1*d2 +
CaCyt*d3).*(CaCyt+d5))).^3+v2);

function J=PMCA(CaEC,CaCyt,VmaxPMCA,X,K05,t)
n=2;
J=-X*VmaxPMCA.*CaCyt.^n./(CaCyt.^n+K05^n);

function J=SERCA(CaCyt,CaER,VmaxSERCA,K05_SERCA,Y,t)
n=1;
blocked_range = (t<100000|t>200000);
J=Y*VmaxSERCA*(0+1*blocked_range).*CaCyt.^n./(CaCyt.^n+K05_SERCA^n);

function J=SOC(CaEC,CaCyt,SOC,V_SOC,leak_PM,t)

J = (V_SOC*SOC + leak_PM) .* (CaEC-CaCyt);
%SOC_flag=~isempty(indexOn);
%tSOC=[tSOC;t];
%JSOC=[JSOC;J];


function J = SOCbind(Z_cyt,SOC_PM,kSOC,t)
J= kSOC*Z_cyt;

function J = SOCdegrad(SOC_PM,I_SOC,t)
J= I_SOC*SOC_PM;

function J = Zprod(Z_ER,kZ,Zmax,t)
J= kZ*(Zmax-Z_ER);

function J = Ztransp(Z_ER,Z_cyt,Ca_ER,Ca_ER_min,vZ,t)
J= (Ca_ER<Ca_ER_min)*vZ.*(Z_ER - Z_cyt);
```

Time = 0
Species:
$[Ca^{2+}]_{cyt}$ = 0.095µM (1)
$[Ca^{2+}]_{ER}$ = 100µM (2)
$[Ca^{2+}]_{EC}$ = 950µM (3)
$[IP_3]_{cyt}$ = 1e−09µM (4)
$[G]_{cyt}$ = 0µM (5)
$[Z]_{cyt}$ = 0µM (6)
$[Z]_{ER}$ = 0.1µM (7)
$[SOC]_{PM}$ = 0µM (8)

Reactions:
$Ca^{2+}_{cyt} \rightarrow Ca^{2+}_{EC}$ (VmaxPMCA,X,K05): PMCA (1)
$Ca^{2+}_{cyt} \rightarrow Ca^{2+}_{ER}$ (VmaxSERCA,K05_SERCA,Y): SERCA (2)
$Ca^{2+}_{cyt} \rightarrow Ca^{2+}_{ER}$ (IP_{3cyt},v2,V_IP3R,$K_i$nf,IP3R_ctCa,K_IP3): IP3RMak (3)
$Ca^{2+}_{EC} \rightarrow Ca^{2+}_{cyt}$ (SOC_{PM},V_SOC,$leak_P$M): SOC (4)
$\rightarrow G_{cyt}$ (Ca^{2+}_{cyt},k_G,$G_d$eg): Grule (5)
$\rightarrow IP_{3cyt}$ (G_{cyt},IP3max,$I_d$eg,$G_m$ax): IP3rule (6)
$\rightarrow Z_{ER}$ (kZ,Zmax): Zprod (7)
$Z_{cyt} \rightarrow SOC_{PM}$ (kSOC): SOCbind (8)
$SOC_{PM} \rightarrow$ (I_SOC): SOCdegrad (9)
$Z_{ER} \rightarrow Z_{cyt}$ (Ca^{2+}_{ER},Ca_ER$_m$in,vZ): Ztransp (10)

X = 0.4
Y = 0.6
r1 = 0.185
v2 = 0.002
V_IP3R = 0.07
$K_i$nf = 52
IP3R_ctCa = 0.21
K_IP3 = 0.05
d1 = 0.13
d2 = 0.5
d3 = 0.0094
d5 = 0.08234
v1 = 10
VmaxPMCA = 0.147
VmaxSERCA = 1.9
K05 = 0.2
K05_SERCA = 0.5
V_SOC = 0.005
$leak_P$M = 1.2e−05
$I_d$eg = 0.01
I_R = 0.01
period$_I$P3 = 5000
T_IP3prod = 3000
IP3max = 4e−05
k_G = 0.2
$G_m$ax = 1
$G_d$eg = 0.5
kZ = 0.0002
Zmax = 0.1
kSOC = 1.7
I_SOC = 0.002
Ca_ER$_m$in = 10
vZ = 1

Figure A.1 Example of output from `char(Cell)` in a Matlab® figure. This shows a summary of the model made by the MATLAB® script.

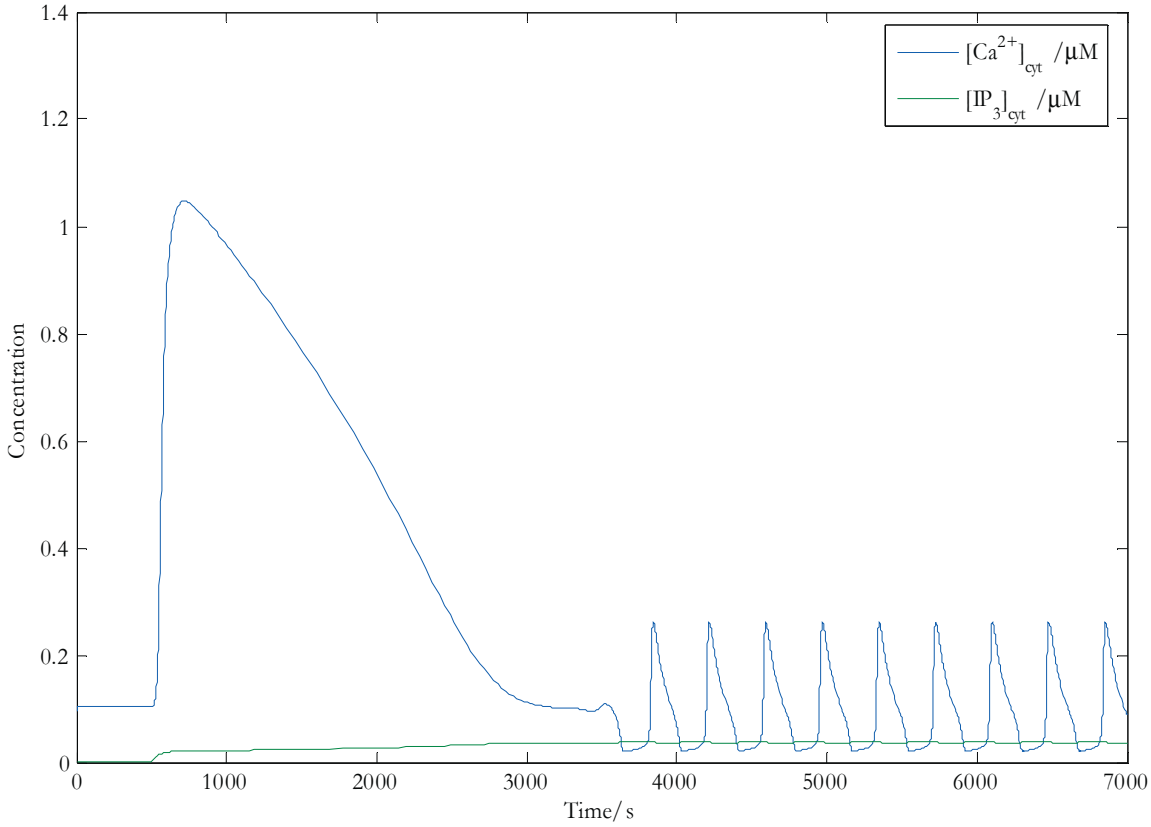

Figure A.2 The figure created by the script is presented here.

A.4 References

1. Hucka, M., et al., *The systems biology markup language (SBML): a medium for representation and exchange of biochemical network models*. Bioinformatics, 2003. **19**(4): p. 524-531.
2. Finney, A. and M. Hucka. *Systems Biology Markup Language (SBML) Level 2: Structures and facilities for Model Definitions*. 2003 [cited 2005 June 8]; Available from: http://www.sbml.org.
3. Keating, S.M. *SBML Toolbox User's manual*. [cited 2005 June 8]; Available from: http://www.sbml.org.
4. *The Matlab documentation*. 2003 [cited 2005 May]; Available from: http://www.mathworks.com/access/helpdesk/help/techdoc/matlab.html.
5. Schaff, J., et al. *The Virtual Cell Portal*. [cited 2005 May]; Available from: http://www.vcell.org.